# REPORT DOCUMENTATION PAGE



AFRL-SR-AR-TR-02-

0783

| 1. AGENCY USE ONLY (*Leave Blank*) | 2. REPORT DATE | 3. REPORT TYPE AND DATES COVERED |
|---|---|---|
| | May 13, 2002 | Final Technical - December 1, 1997 through May 31, 2001 |

4. TITLE AND SUBTITLE
Theoretical Studies of Self-Trapped Optical Beams in Photorefractive Media

5. FUNDING NUMBERS
F49620-98-1-0080

6. AUTHORS
Demetrios N. Christodoulides

7. PERFORMING ORGANIZATION NAME(S) AND ADDRESS(ES)
Lehigh University
526 Brodhead Avenue
Bethlehem, PA 18015

8. PERFORMING ORGANIZATION REPORT NUMBER
533047

9. SPONSORING / MONITORING AGENCY NAME(S) AND ADDRESS(ES)
USAF, AFRL
AF Office of Scientific Research
801 N. Randolph St. Room 732
Arlington, VA 22203-1977

10. SPONSORING / MONITORING AGENCY REPORT NUMBER

11. SUPPLEMENTARY NOTES

12a. DISTRIBUTION / AVAILABILITY STATEMENT
Approved for public release,
distribution unlimited

12b. DISTRIBUTION CODE

13. ABSTRACT *(Maximum 200 words)*

The objective of this research project is to theoretically study self-trapping phenomena of incoherent and coherent optical beams in photorefractive media. Particular emphasis is given to the newly discovered class of incoherent solitons. We study their dynamics, modal composition and coherence properties. Other topics targeted in this research effort include theory of higher-order dark solitons, stability issues of incoherent and coherent photorefractive spatial solitons and interactions among photorefractive optical solitons.

20020614 161

14. SUBJECT TERMS

15. NUMBER OF PAGES
194

16. PRICE CODE

| 17. SECURITY CLASSIFICATION OF REPORT | 18. SECURITY CLASSIFICATION OF THIS PAGE | 19. SECURITY CLASSIFICATION OF ABSTRACT | 20. LIMITATION OF ABSTRACT |
|---|---|---|---|

# 1. Summary of the significant work accomplished

## Bright Incoherent Solitons

### Self-consistent modal theory

The self-consistent modal, theory was developed by our group as an alternative way to describe incoherent solitons in non-instantaneous nonlinear media (Phys. Rev. Lett., vol. 79, pp. 4990, 1997). Unlike the coherent density approach which is by nature more appropriate for dynamical evolution (under arbitrary initial conditions), the modal theory is better suited in identifying incoherent solitons, their range of existence, and coherence properties. This method relies on the idea that every incoherent spatial soliton must be a combination of the modes of its own self-induced waveguide. The total intensity of this soliton is the sum of all the modal intensities. The range of existence of incoherent solitons in saturable media such as photorefractives was also obtained. For bright incoherent solitons we found that the coherence increases at the low intensity tails. Similar results were obtained numerically using the coherent density method (Opt. Lett., vol. 23. pp. 418, 1998).

### Incoherent solitons in Log nonlinear saturable systems

Theoretically, incoherent spatial solitons were first identified in Log saturable nonlinear media using the coherent density approach (Christodoulides et al, Opt. Lett. vol. 22, pp. 1080, 1997). The incoherent bright solitons allowed in this system exhibit a Gaussian intensity profile and they exist below a certain cut-off. It was thus natural to ask whether the self-consistent modal theory could also apply in this system. We have found that the modes of these incoherent Gaussian solitons can be obtained in terms of Gauss-Hermite polynomials as long as the mode-occupancy function is Poissonian. Gaussian soliton solutions were also obtained in two dimensions. Unlike their coherent counterparts, they could also be elliptical depending on their 2-D coherence characteristics. This implies to some extent that incoherent spatial solitons may be more versatile in terms of shape as long as their coherence properties are tailored. Above all, this result demonstrated that the two methods give the same results (in the Log case) and thus they are equivalent. Their equivalence was later formally established on the basis of Mercer's theorem and the associated Karhunen-Loeve expansions. In fact the modal theory is also dynamic (it can be used for dynamic evolution) unlike what we thought in the very beginning.

### Coherence properies of incoherent spatial solitons in non-instantaneous Kerr media

In this part of our research, we have investigated the coherence properties of multimode incoherent spatial solitons in non-instantaneous Kerr nonlinear media (Physical Review E, vol. 59, pp. 1193, 1999). In doing so we employed the self-consistent multimode description first developed by our group (Phys. Rev. Lett., vol. 79, pp. 4990, 1997). In general we have found that the intensity profile of these incoherent Kerr states is of the $\mathrm{sech}^2(x/x_0)$ type. The modal constituents or modes of these solitons were found in terms of associated Legendre polynomial functions. The spatial width of these incoherent states was explicitly obtained as function of the total number of modes supported and the amount of nonlinearity provided by the system. Even more importantly, the complex coherence factor associated with these Kerr incoherent solitons was also obtained in closed form. Our results were in excellent agreement with previous semi-analytical results (Phys. Rev. Lett., vol. 79, pp. 4990, 1997). One interesting aspect that emerged from this study is the fact that the coherence manifolds of such

multimoded states are "topologically" the same depending on whether the number of modes involved is odd or even.

### Elliptic incoherent solitons in saturable nonlinear media

In Optics Letters, vol. 25, pp. 972 (2000), we identified elliptic incoherent solitons in isotropic saturable nonlinear media. We were able to do this by employing a two-dimensional version of the coherent density approach and by assuming that the material nonlinearity depends on the optical intensity, $I$, in a way similar to that in photorefractives. We also found that, even in this case, elliptic solitary states exist, provided that their mutual coherence function is anisotropic. Therefore these soliton states can possibly be excited from anisotropic incoherent sources such as edge-emitting LED's or lasers operated below threshold. The propagation dynamics of this new class of solitons were further studied by use of numerical simulations. Collisions between two such elliptic incoherent solitons were also investigated. In particular, we showed that in certain collision regimes the intensity ellipse for the two solitons rotates, whereas at the same time their centers of gravity tend to revolve around each other. This interaction behavior is possible even though these states are launched parallel to the propagation axis.

### Coherence enhancement of spatially incoherent light beams through soliton interactions

We have shown that it is possible to enhance the spatial coherence length of a bright partially incoherent signal beam through interactions with a coherent (or an incoherent) dark spatial soliton. We have demonstrated that during this interaction part of the incoherent bright beam is trapped within the dark or gray notch of the controlling soliton, thus forming a sharp intensity spike. In this region, the correlation length increases by at least 2 orders of magnitude. Therefore, incoherent light can be effectively cooled (its entropy being reduced) at any arbitrarily chosen point upon a partially incoherent wave front by use of a dark spatial soliton. This is the only passive system that we know of that exhibits an increase in both the local intensity and the local correlation distance simultaneously. These results were presented in Optics Letters, vol. 25, pp. 826 (2000).

## Incoherent dark solitons

### Theory of incoherent dark solitons

The theory of incoherent dark solitons was developed soon after their observation (Phys. Rev. Lett., vol. 80, pp. 5113, 1998). To do so we used the self-consistent modal theory (Phys. Rev. Lett., vol. 79, pp. 4990, 1997). We have found that these dark incoherent solitons are comprised from a belt (a continuum) of radiation modes as well as bound states. Unlike coherent dark solitons which involve only an odd radiation mode at cut-off, the radiation belt contains both odd and even modes. Similarly, the bound states can be odd or even. The presence of even radiation modes and even bound states explains why the incoherent dark solitons are in fact gray. On the other hand, close inspection of their modal structure reveals that in the dark notch, the odd modes dominate which in turn explains the 'phase-memory effect". The coherence properties found theoretically were in agreement with those obtained earlier numerically (Opt. Lett., vol. 23. pp. 418, 1998). Another interesting outcome of this study was the fact that these solutions are by no means unique. Instead they depend on the choice

of the radiation mode distribution function. This problem is equivalent to Manakov system of infinite dimensions.

### Incoherent dark solitons-phase memory effects

The dynamics of incoherent solitons in non-instantaneous nonlinear media were investigated using the so-called coherent density approach, first developed by our group (Phys. Rev. Lett., vol. 78, pp. 646, 1997). In this approach, we assume that the input can be modeled as a continuum of sources, which are mutually incoherent with respect to each other. We further assumme, that at the origin, the source-fluctuations are stationary which is typically the case in statistical optics. This method was augmented with a version of the Van Cittert-Zernike theorem in order to monitor the evolution of the coherence during propagation. This particular version is better suited for multi-Fourier split method techniques, used in our numerical computations. In Opt. Lett., vol. 23. pp. 418, 1998 we have simulated the dynamics of incoherent solitons in biased photorefractive crystals. Surprisingly enough we have found that dark incoherent quasi-solitons can form after a certain distance of propagation. In addition, these incoherent dark solitons were found to be in fact gray. What was even more interesting was the fact that the nonlinear system could exhibit phase memory effects in spite of the incoherency. At higher biased voltages (higher nonlinearities), an even field depression was found to lead to doublets whereas an odd one to triplets, pretty much the same way one would have expected from a coherent system. It was thus natural to ask the following: (i) why are the fundamental incoherent dark solitons gray? (ii) how can the imposed phase be remembered in the midst of random phase fluctuations? Subsequently this behavior was observed experimentally in SBN crystals (Science, vol. 280, pp. 889, 1998). In this experiment 1-D stripe dark (gray) solitons as well as 2-D gray vortex solitons (of topological charge 1) were observed.

### Incoherent dark solitons Y-splitting and "phase memory" effects

The properties of these incoherent dark Y-soliton doublets were further investigated in a subsequent paper of ours (Physical Review E, vol. 59, pp. R4777, 1999) where we have also provided the first experimental observation of this very intriguing behavior. In this paper we have shown that the dynamics of these self-trapped entities are associated with strong "phase-memory" effects that are otherwise absent in the linear regime (i.e., during diffraction). The numerical simulations carried out using the coherent density theory (developed by our group, Phys. Rev. Lett., vol. 78, pp. 646, 1997) revealed that the Y-splitting process is rather insensitive to the degree of spatial coherence. More specifically we found that over a wide range of parameters, the Y-splitting is approximately the same irrespective of the degree of spatial coherence. These conclusions were successfully validated in the experimental part of our study.

### Waveguides formed by incoherent dark solitons

We have demonstrated experimentally optical guidance of coherent light beams using incoherent light (Optics Letters, vol. 24, pp. 1160, 1999). This was made possible using either dark incoherent solitons (previously predicted and verified by our group, Opt. Lett., vol. 23. pp. 418, 1998; Science, vol. 280, pp. 889, 1998) as well as Y-dark soliton doublets as described in the first section of this report. In all cases, the waveguides were probed at higher wavelengths and it was found that they were in fact single-moded. This is in agreement with our earlier predictions concerning the modal structure of

incoherent dark solitons (Phys. Rev. Lett., vol. 80, pp. 5113, 1998). These experiments suggest that it is possible to control high-power laser beams with low-power incoherent light sources such as LEDs.

## Vector solitons

### Multi-component vector solitons

It has been previously shown that saturable Manakov systems can be implemented in photorefractive crystals (Christodoulides et al, Appl. Phys. Lett., vol. 68, 1763, 1996). In principle these Manakov-like systems can involve an arbitrary number of components as long as they are mutually incoherent. It was also known for some time (at least in the Kerr regime) that bimodal vector solitons should also be possible (multi-component, multi-humped), Christodoulides and Joseph, Opt. Lett. 13, pp. 53, 1988, Tratnik and Sipe, Phys. Rev. A 38, pp. 2001, 1988. These soliton states were observed for the first time in saturable nonlinear crystals (Phys. Rev. Lett., vol. 80, pp. 4657, 1998). Their theory was also formulated. Among other things, it was found that double and triple hump solitons are possible. Solitons which can contain no ground state were also identified and observed.

### Multi-component two-dimensional solitons carrying topological charge

In Optics Letters, vol. 25, pp. 61 (2000) we have proposed for the first time two-dimensional vector-solitons for which each component carries a different topological charge (or "spin"). We have found that this family is characterized by a unique triple-point phase diagram, which is completely absent in the two-component case. Moreover, we have shown that these higher-dimensional vector structures are composed of lower-dimensional building blocks. With soliton collisions in mind, it is clear that the spin, the multimode nature, and the multihump structure offer new opportunities for interactions between two-dimensional vector solitons. In this work we employed the thresholding nonlinearity and made use of the self-consistency principle. The core ideas and findings presented are expected to be universal. These composite solitons can provide insight into ways to realize these interactions in materials with saturable nonlinearities. In addition, we have suggested (Physical Review Letters, vol. 84, pp. 1164, 2000) composite solitons that carry topological charge: multicomponent two-dimensional [2+1D] vector (Manakov-like) solitons for which at least one component carries topological charge. These multimode solitons can have a single hump or exhibit a multihump structure. The "spin" carried by these multimode composite solitons suggests 2-D soliton interactions in which the particlelike behavior includes spin, in addition to effective mass, linear, and angular momenta.

### Observation of two-dimensional multimode solitons

In Optics Letters, vol 25, pp. 1113 (2000), we presented the first experimental observation of (2+1)-dimensional multimode (composite) solitons. A single-hump component and a double-hump (dipole-type) component are jointly self-trapped as a composite soliton in a biased photorefractive crystal. We observe that the two modes self-trap when they are launched together, forming the composite soliton. However, the stand-alone components do not trap on their own for the given value of the nonlinearity that supports the composite soliton. This self-trapping of multimode (2+1) D solitons opens up the possibility of distortionless image transmission through highly nonlinear self-focusing media. If the envelope of a highly multimode soliton is modulated to contain an image (superimposed on the intensity profile of the soliton), then this image can be transmitted through the self-focusing

medium and remain unchanged through propagation. This method is in contradistinction to image transmission through a multimode fiber, for which the fiber modes are coherent with each other, yet they propagate at different velocities (intermodal dispersion) and thus destroy the image.

## Modulation instability

### Modulation instability of incoherent beams in noninstantaneous nonlinear media

In Physical Review Letters, vol. 84, pp. 467 (2000), we demonstrated, analytically and numerically, the existence of incoherent MI, that is, modulation instability of incoherent wave packets. Incoherent modulation instability exists when the nonlinear index change exceeds a well-defined threshold that is determined by the amount of incoherence. This is in a marked difference with coherent MI, since there does not exist a similar threshold for coherent MI. The nonlinear index change is determined by the spatial degree of coherence (angular power spectrum of the source). We used analytical and numerical methods to study the properties of incoherent MI in a general self-focusing noninstantaneous medium. Assuming the input beams have Lorentzian angular power spectra, we were able to find closed form solution for incoherent MI when the nonlinearity is either of the Kerr or saturable type. We confirmed our results with numerical simulations.

### Bright spatial solitons on a partially incoherent background

We have demonstrated, both theoretically and experimentally, that stable partially coherent antidark solitons can exist in noninstantaneous nonlinear media. We have analyzed the modal structure of these antidark states in the case where the nonlinearity is of the Kerr type. Our analysis indicates that these solitons always involve a set of discrete bound states as well as a continuum of odd and even radiation modes. Experimental results and computer simulations indicate that the instability affecting an antidark soliton can be totally eliminated by properly increasing the incoherence of its background beam above the threshold of incoherent MI. These antidark solitons are the only known solitons that have nonzero intensity everywhere in space yet they propagate in a stable fashion in a self-focusing medium. We published these findings in Physical Review Letters, vol. 84, pp. 2374 (2000).

## Stimulated Raman Scattering

### Stimulated Raman interactions in massive wavelength-division-multiplexed systems

In addition to our work in photorefractive crystals, we have explored stimulated Raman interactions (SRS) in massive wavelength-division-multiplexed (WDM) systems. This technology shows considerable promise in terms of exploiting the large spectral window offered by today's low loss optical fibers. In general, the SRS power exchange among WDM channels is described by a rather involved system of differential equations of the Lotka-Volterra type. This problem is of considerable complexity since its interconnectivity increases with the square of the number of channels involved. For example, in a 100-channel system, the number of SRS cross-talk flow streams is approximately 5000! Yet, this rather involved problem can exhibit a closed form solution as demonstrated by our group (Optics Letters, vol. 24, pp. 735, 1999). In this paper we found that solitary-like Raman states are possible in such massive wavelength-division-multiplexed systems. These self-similar states can propagate undistorted among channels at constant velocity. The evolution of these states under the action of noise and during

collisions was also investigated. In another study (to be published in IEEE Photonics Technology Letters, October issue, 1999), we have proved that spectral inversion techniques can totally eliminate SRS cross-talk effects which are known to severely limit the performance of high capacity WDM systems. The result was obtained by exploiting the reflection symmetries of the underlying evolution equations and it is therefore general. This work was done in collaboration with Lucent Technologies and Tyco Submarine Systems.

# References


[1] D. N. Christodoulides, T. H. Coskun, M. Mitchell, Z. Chen, and M. Segev, "Theory of incoherent dark solitons", Physical Review Letters, vol. 80, pp. 5113, 1998.

[2] M. Mitchell, Z. Chen, M. Segev, T. H. Coskun, and D. N. Christodoulides, "Self-trapping of incoherent bright and dark beams", Asian Journal of Physics, invited paper,October, 1998.

[3] Z. Chen, M. Mitchell, M. Segev, T. H. Coskun, and D. N. Christodoulides, "Self-trapping of dark incoherent light beams", Science, vol. 280, pp. 889, 1998.

[4] T. H. Coskun, D. N. Christodoulides, M. Mitchell, Z. Chen, and M. Segev, "Dynamics of incoherent bright and dark self-trapped beams and their coherence properties in photorefractive crystals", Optics Letters, vol. 23, pp. 418, 1998.

[5] M. Mitchell, M. Segev, and D. N. Christodoulides, "Observation of multi-hump multi-mode solitons", Physical Review Letters, vol. 80, pp. 4657, 1998.

[6] D. N. Christodoulides, T. H. Coskun, M. Mitchell, and M. Segev, "Multimode incoherent spatial solitons in logarithmically saturable nonlinear media", Physical Review Letters, vol. 80, pp. 2310, 1998.

[7] Z. Chen, M. Segev, T. H. Coskun, D. N. Christodoulides, and Y. S. Kivshar, "Coupled photorefractive spatial soliton pairs", Journal of the Optical Society of America B, vol. 14, pp. 3066, 1997.

[8] M. Mitchell, M. Segev, T. H. Coskun, and D. N. Christodoulides, "Theory of self-trapped spatially incoherent light beams", Physical Review Letters, vol. 79, pp. 4990, 1997.

[9] M. Segev and G. Stegeman, "Self-trapping of optical beams: spatial solitons", Physics Today, August issue, 1998, pp. 42.

[10] Z. Chen, M. Mitchell, M. Segev, T. H. Coskun, and D. N. Christodoulides, "Self-trapping of incoherent dark beams", Optics and Photonics News, vol. 9, no. 12, pp. 48, 1998.

[11] M. I. Carvalho, T. H. Coskun, D. N. Christodoulides, M. Mitchell, and M. Segev, "Coherence properties of multimode incoherent spatial solitons in non-instantaneous Kerr media", Physical Review E, vol. 59, pp. 1193, 1999.

[12] T. H. Coskun, D. N. Christodoulides, Z. Chen, and M. Segev, "Dark incoherent soliton splitting and "phase-memory" effects: theory and experiment", Physical Review E, vol. 59, pp. R4777, 1999.

[13] Z. Chen, M. Segev, D. N. Christodoulides, and R. S. Feigelson, "Waveguides formed by incoherent dark solitons", Optics Letters, vol. 24, pp. 1160, 1999.

[14] D. N. Christodoulides, A. G. Grandpierre, M. Mitchell, and B. R. Jander, "Solitary-like Raman states in massive wavelength-division-multiplexed systems", Optics Letters, vol. 24, pp. 735, 1999.

[15] A. G. Grandpierre, D. N. Christodoulides, and J. Toulouse, "Theory of stimulated Raman cancellation in wavelenth-division-multiplexed systems via spectral inversion", IEEE Photonics Technology Letters, vol. 11, October issue 1999.

[16] Z. H. Musslimani, M. Segev, and D. N. Christodoulides, "Multi-component two-dimensional solitons carrying topological charge", Optics Letters, vol. 25, pp. 61, 2000.

[17] M. Soljacic, M. Segev, T. H. Coskun, D. N. Christodoulides, and A. Vishwanath, "Modulation instability of incoherent beams in non-instantaneous nonlinear media", Physical Review Letters, vol. 84, pp. 467, 2000.

[18] Z. H. Musslimani, M. Segev, and D. N. Christodoulides, "Composite multi-hump vector solitons carrying topological charge", Physical Review Letters, vol. 84, pp. 1164, 2000.

[19] T. H. Coskun, D. N. Christodoulides, Y. R. Kim, Z. Chen, M. Soljacic and M. Segev, "Bright spatial solitons on a partially incoherent background", Physical Review Letters, vol. 84, pp. 2374, 2000.

[20] T. H. Coskun, A. G. Grandpierre, D. N. Christodoulides, and M. Segev, "Coherence enhancement of spatially incoherent light beams using interactions with incoherent and coherent dark solitons", Optics Letters, vol. 25, pp. 826, 2000.

[21] E. D. Eugenieva, D. N. Christodoulides, and M. Segev, "Elliptic incoherent solitons in saturable nonlinear media", Optics Letters, vol. 25, pp. 972, 2000.

[22] T. Carmon, C. Anastassiou, S. Lan, D. Kip, Z. H. Musslimani, M. Segev, and D. N. Christodoulides, "Observation of two-dimensional multimode solitons", Optics Letters, vol. 25, pp. 1113, 2000.

## 2. Computational methodology/algorithms

The equation describing light propagation in nonlinear media is obtained by the solution of Maxwell's equations. By the solution of the Maxwell set the evolution of incoherent light inside a nonlinear medium is governed by

$$i\left(\frac{\partial U_j}{\partial z}+\theta_{x,j}\frac{\partial U_j}{\partial x}+\theta_{y,j}\frac{\partial U_j}{\partial y}\right)+\frac{1}{2}\left(\frac{\partial^2 U_j}{\partial x^2}+\frac{\partial^2 U_j}{\partial y^2}\right)+F(I)U_j=0, \tag{1}$$

where $U_j$ are the so-called coherent density components, and $\theta_{x,j}$, $\theta_{y,j}$ are the direction angles of each component with respect to the propagation $z$ axis. The total intensity of the beam is obtained from $I=\sum_{j=1}^{N}|U_j|^2$, where $N$ is the number of coherent components. $F(I)$ determines the change in the refractive index caused by the material nonlinearity. For a Kerr medium $F(I)=I$, whereas for saturable nonlinearities (as is the case for photorefractive crystals) $F(I)=-1/(1+I)$. The

initial contribution of each component to the total intensity is given by the normalized angular power spectrum $G_N(\theta_x, \theta_y)$ of the incoherent source. Most often $G_N(\theta_x, \theta_y)$ is assumed to have a Gaussian or Lorentzian distribution.

In order to solve Eqs. (1), we first discretize the $(x, y)$ domain. We then use the split-step Fourier method to solve the corresponding discretized equations. To demonstrate the split-step Fourier technique, we write the equation describing each coherent component as:

$$\frac{\partial U}{\partial z} = (L + N)U, \tag{2}$$

where $L$ is a linear differential operator given by

$$L = -\theta_{x,j}\frac{\partial}{\partial x} - \theta_{y,j}\frac{\partial}{\partial y} + \frac{i}{2}\left(\frac{\partial^2}{\partial x^2} + \frac{\partial^2}{\partial y^2}\right)$$

and $N$ is the nonlinear operator

$$N = iF(I).$$

The exact solution of eq. (2) can be found, by integrating with respect to $z$

$$U(z + h, x, y) = \exp[h(L + N)]U(z, x, y). \tag{3}$$

where $h$ is the step size. According to the Cambel-Baker-Hausdorff formula, the operator on the right hand side of this equation satisfies the following relation

$$\exp(hL)\exp(hN) = \exp\left(h(L + N) + \frac{h^2}{2}[L, N] + \frac{h^3}{12}[L - N, [L, N]] + \cdots\right),$$

where the commutation operator is defined as $[a, b] = ab - ba$. Although in principle the operators $L$ and $N$ do not commute, when the step $h$ is small enough the higher order terms, i.e., $\mathcal{O}(h^2)$, are small perturbations in this expansion. Then, eq. (3) can be approximated by

$$U(z + h, x, y) = \exp(hL)\exp(hN)U(z, x, y). \tag{4}$$

Now these two operators can be applied separately into $U(z, x, y)$ in order to propagate a single step in $z$. The action of the nonlinear operator, $N$, in Eq. (4) is straightforward, i.e.,

$$U_1(z, x, y) = \exp(hN)U(z, x, y).$$

On the other hand, the linear, differential part of Eq. (4) can be solved using a two-dimensional discrete Fourier transform

$$U(z + h, x, y) = \exp(hL)U(z) = F^{-1}\{\exp[hL(iq_x, iq_y)]F[U_1(z, x, y)]\}, \tag{5}$$

where $L(iq_x, iq_y)$ is the Fourier transform of operator $L$, and $F$, $F^{-1}$ denote the operators of the forward and the inverse Fourier transform, respectively. This method is implemented on the CRAY T3E at the Pittsburgh Supercomputer center. A sample code copy can be found in Appendix A.

# A Sample code

```
!             2D Incoherent bright solitons

!             Fourier definitions and main arrays
        parameter(Np=101)
        parameter(NRA=1024)
        parameter(Pi=3.141593)
        complex SIG(NRA,Np), B(NRA)
        real ak(NRA)
        real Pow(NRA),B1(NRA),AU(NRA)
        real WFFTC(4*NRA+15), CPY(2*NRA)
c
c     /Program Definitions/
        integer StepNum, SaveNum
        integer Nx, Npp
c
        real IntX,IntY,beta,h
        real Theta0, Strech, rt
        real alpha2
        real xw, xf
c
c     /Loop counters /
        integer st, jj, ECL
c
c   /Save definitions /
        integer*4 sh5, sh6, first_r
        character*1 sheet5, sheet6,list3
        integer grid_ste, dat_ste
c
        external fftcf, fftcb
c
c     /Common blocks/
        common /discr/ nx
        common/components/Npp
        common/discr2/IntX
        common /nonl/beta
        common/ArbUnits/ Theta0, Strech
        common/TotInt/rt
        common/steps/h,dz
        common/LogPar/alpha2
        common/widths/xw,xf
        common/outr/sh5,sh6,first_r,sheet5,sheet6,list3
c
c      /Constants/
c
```

```
c  :-) IntX and IntY are the WHOLE interval lengths.  :-)
c
        Npp=Np
        Nx=NRA
        IntX=200.e0
!
        call InitParam
         print*, 'alpha2 =', alpha2
!!
        print*,'t= ',  h
c
        stepNum=95000
        grid_ste=1900
        dat_ste=200
        SaveNum=stepNum/grid_ste
        list3='e'
c
        pow(:)=0.
        B1=0.
        call fftci(NRA,WFFTC)
        call store_init           ! Initializing the storage parameters
c
         call getBigSignal(SIG)      ! ... and getting the signal - new version
         call getPower(SIG,Pow)
!
           B=Pow
           call fftcf(NRA,B,B)
           B=B/sqrt(real(Nx))
           B1=abs(B)
            AU=0.
            AU(1:nx/2)=B1(Nx/2+1:nx)
            AU(nx/2+1:nx)=B1(1:nx/2)
!
         call fillreal(Pow, AU,IntX,0,dz)
         call getak(ak)
c
                                write(*,*) 'Initializing FFT...'
                                Print*, 'Good Luck !!!'
!
!       The external loop using the (E)xternal (C)ounter (L)oop   SaveNum
!
       do 105 ECL = 1,SaveNum
c                               :-)   The first half step
!
        do 45 jj=1,Np
!
         call fftcf(NRA,SIG(:,jj),SIG(:,jj),WFFTC,CPY)
```

```
         call dispersion(SIG(:,jj),h/2.,ak)
!
         call fftcb(NRA,SIG(:,jj),SIG(:,jj),WFFTC,CPY)
45       continue
         call Power(SIG,Pow)
         call nonlinearity(SIG,h,Pow,Np)
!
        do  65 st=2,grid_ste
! /Action / The main portion of the Difr.- Nonl. loop, grid_ste
!
         do 85 jj= 1, Np              !  The component loop
!
          call fftcf(NRA,SIG(:,jj),SIG(:,jj),WFFTC,CPY)
          call dispersion(SIG(:,jj),h,ak)
!
          call fftcb(NRA,SIG(:,jj),SIG(:,jj),WFFTC,CPY)
85       continue
!
         call Power(SIG,Pow)
         call nonlinearity(SIG,h,Pow,Np)
!
65      continue
!                                          The last half step
!
         do 35 jj=1,Np                     ! the component loop
!
          call fftcf(NRA,SIG(:,jj),SIG(:,jj),WFFTC,CPY)
          call dispersion(SIG(:,jj),h/2.,ak)
          call fftcb(NRA,SIG(:,jj),SIG(:,jj),WFFTC,CPY)
35        continue
          call Power(SIG, Pow)
          B=Pow
           call fftcf(NRA,B,B)
           B=B/sqrt(real(Nx))
           B1=abs(B)
            AU=0.
            AU(1:nx/2)=B1(Nx/2+1:nx)
            AU(nx/2+1:nx)=B1(1:nx/2)
          call fillreal(Pow,AU,IntX,ECL*grid_ste,dz)
!
105      continue
         stop
         end
c
c :-)   :-)   :-)   :-)   :-)   :-)   :-)   :-)   :-)
c                    P R O C E D U R E S
c :-)   :-)   :-)   :-)   :-)   :-)   :-)   :-)   :-)
```

```
c
c :-) ================================================= (-:
        subroutine dispersion(b,d,ak)
c
c :-) ================================================= (-:
c
c ---- Variable declarations ------
c
        common /discr/ nx
        integer nx
        complex b(nx)
        real ak(nx)
        complex c
        real d                  ! d is the step size
!
        c=cmplx(0.,1.)
c
c ---  calculation of the dispersion
             b=(b/sqrt(real(nx)))*cexp(c*d*ak)
        return
        end
c :-) ================================================= (-:
        subroutine getak(ak)
c
c :-) ================================================= (-:
c
c ---- Variable declarations ------
c
        parameter(Pi=3.141593)
        common /discr/ nx
        common/discr2/IntX
        integer nx
        real IntX
        real ak(nx)

        real dkx
        real kx
        integer nx2,i
        integer kx2c
c
        nx2=nx/2+1
        dkx=2.e0*Pi/IntX
c
c --- Begin nested loops to calculate the frequency distribution
c
        do 67 i=1,nx
           if (i <= nx2) kx2 = (i-1)
```

```
            if (i > nx2) kx2 = (-nx - 1 + i)
            kx=real(kx2)*dkx
            ak(i)=((-5.e-1)*(kx**2 ))
67        continue
          return
          end
c
c ================================================================
          subroutine nonlinearity(b,d,pow,Npp)
          common /discr/ nx
          integer nx,Npp
          common /nonl/beta
          real beta
          common /TotInt/rt
          real rt
          complex b(nx,Npp)
          real pow(nx)
          real d
          real  nonlin(nx)
          integer i
          complex c
c ================================================================
c
          c=cmplx(0.,1.)
!
            nonlin=(beta)*(1.+rt)/(pow+1.)
            nonlin=nonlin*d
           do 60 i=1, Npp
            b(:,i)=b(:,i)*cexp(c*nonlin(:))
60         continue
          return
          end
c ================================================================
          subroutine fillreal (a,B1,IntX,rec,step)
          common/discr/nx
          integer nx,rec
          real a(nx), B1(nx),IntX
          common/outr/sh5,sh6,first_r,sheet5,sheet6,list3
          common/TotInt/rt
          integer*4 first_r, sh5, sh6
          character*1 sheet5,sheet6,list3
          character*10 alfabet
          character*8 filename
          integer ii
          real rt,x,step
          real  field, fmax
c ---------------------------------------------------
```

```
c
        open(unit=29,file='m'//list3//'.dat',status='UNKNOWN',
     $position='APPEND')
        fmax=0.e0
        do 225 mx=nx/2-20, nx/2+20
        field=a(mx)
        if (field.ge.fmax) fmax=field
225     continue
        print*, fmax
        write(29,16) real(rec)*step/1.e-4,fmax
        close(unit=29)
16      format(f10.5,f10.5)
c            fmax=rt
        alfabet='1234567890'
C----------------------BEGIN-----------------------C
c
        if(first_r.eq.0) then
           first_r=1
           goto 101
          end if
         if (sh6.lt.9) then
          sh6=sh6+1
          sheet6=alfabet(sh6:sh6)
         else
        sheet6='0'
        sh6=0
          if (sh5.lt.9)then
            sh5=sh5+1
            sheet5=alfabet(sh5:sh5)
               else
               print*, 'I can not save that many files'
c
C=======END IF SHEET3=========C
          end if
c
C======END IF SHEET4==========C
         end if
c / saving the INTENSITY distrubution as a grid file /
c
101     filename = 'i'//list3//sheet5//sheet6//'.dat'
        open(unit=31, file=filename, status='unknown')
        print*,'writing ', filename
          do 122 ii=nx/2, nx
         x=-IntX/2.+real(ii-1)*IntX/real(nx)
        write(31,*) x, a(ii)
122       continue
        close(unit=31)
```

```
!
       filename = 'm'//list3//sheet5//sheet6//'.dat'
        open(unit=32, file=filename, status='unknown')
        print*,'writing ', filename
          do ii=nx/2+1, nx
         x=-IntX/2.+real(ii-1)*IntX/real(nx)
        write(32,*) x, B1(ii)
        end do
        close(unit=32)
c
!!        open(unit=71, file='w'//list3//'.dat', status='UNKNOWN',
!!     $position='APPEND')
!!        write(71,10) a(nx/2-39:nx/2+40)
10     format(80f10.5)
!!        close(unit=71)
!
!!        open(unit=71, file='s'//list3//'.dat', status='UNKNOWN',
!!     $position='APPEND')
!!        write(71,10) B1(nx/2+1:nx/2+80)
!!        close(unit=71)
c
        return
        end
c  :-) ------------------------------------------------------ (-:
        subroutine store_init
c
        common/outr/sh5, sh6, first_r, sheet5,sheet6,list3
c
        integer*4 sh5, sh6, first_r
        character*1 sheet5, sheet6,list3
c
        sh5=0
        sh6=0
        first_r=0
        sheet5='0'
        sheet6='0'
        return
        end

c ---------------------------------------------------------------
c  :-) :-) :-) :-) :-) :-) :-) :-) :-) :-) :-) :-) :-) :-) :-) :-)
c ===============================================================
         subroutine getBigSignal(data)
         common/components/Npp
         common/discr/nx
         common/discr2/IntX
         integer Nx,Npp
```

```
        common/ArbUnits/ Theta0, Strech
        common/TotInt/rt
        common/widths/xw,xf
        real Theta0, Strech, rt
        complex data(nx,Npp)
        real xw, xf
        complex c
        real xste, IntX
        real x, ampl,fi
        integer i,jcomp     ! NC is the number of components in x and y
        integer itx         ! <--  counters for ThetaX and ThetaY
        real p
        real thetaX
        real InThX, dThX
        real  rt, rHat, RGN  ! Intensity normalization
        real sum ,sum1
        real pow,fi0, a0,a1,pi
! a0 is the radius of the supergaussian background beam
        real fx, ftx         ! dummy arguments for the functions below
        f(fx)=exp(-0.5*((fx/(70.*xw))**6))
!!          f(fx)=(2./(exp(fx/6.)+exp(-fx/6.)))**32
!!          f(fx)=2./(exp(fx/xw)+exp(-fx/xw))
        GN(ftx)=exp(-(ftx**2 )/Theta0**2)
!c ===================================================================
       Print*, 'Getting the signal ...'
!c
!c -------------------------------------------------------------------
!
        c=cmplx(0.,1.)
        pi=3.141593
        sum1=0.
        fi0=0.
        a0=(3.25e-1)*IntX
        a1=(4.5e-1)*IntX
        xste=IntX/real(nx-1)
        print*, 'xw =', xw
!!        print*, 'rt =  ', rt
!
        InThX=Strech*Theta0

       If(Npp.ne.1) then       ! incoherent case
!
        dThX=(2.*InThX)/real(Npp-1)
!
      sum=0.
        do 41 i=1, Npp
            p=-InThX+real(i-1)*dThX
```

```
            sum=sum+GN(p)
!!            print*, 'GN = ', GN(p), p
41      continue
!!        print*, ' sum = ', sum
        rHat = (rt/sum)
        print*, 'rhat = ...', rhat
!
        else       ! coherent case
           InThX=0.; dThX=0.;rhat=rt;
        end if

        jcomp=1                  ! Initialization of the component counter
        do 32 itx=1,Npp
!
         ThetaX = -InThX+dThX*real(itx-1)
!!         Print*, 'ThetaX, ThetaY ', ThetaX, ThetaY
         RGN=sqrt(rHat*GN(ThetaX))
!
         sum1=sum1+RGN**2       ! sum1 is being used for energy check only
!
        do 20 i=1,Nx
          x=-IntX/2.e0 +(real(i-1))*xste
!
              ampl=RGN*f(x)

!!!           Getting the phase of the dark beam (s)    (-:

                fi=ThetaX*x
!
              data(i,jcomp)=ampl*cexp(c*fi)
!
19      continue
20      continue
!
!!        call fillgrid(data(:,jcomp))
        jcomp=jcomp+1
32      continue
        print*,'sum1=', sum1
        return
        end
! ---------------------------------------------------------------
        subroutine spectrum(a,b)
        real a(nx)
        common /discr/nx
        integer nx,i
        complex b(nx)
!
```

```
        do i =1, nx
         b(nx)=a(nx)
        end do
!
        return
        end
c ---------------------------------------------------------------
c  :-) :-) :-) :-) :-) :-) :-) :-) :-) :-) :-) :-) :-) :-) :-) :-)
         subroutine InitParam
         parameter(Pi=3.141593)
         common/ArbUnits/ Theta0, Strech
         common/TotInt/rt
         common/steps/h,dz
         common/LogPar/ alpha2
         common/nonl/beta
         common/widths/xw,xf
         real Theta0, Strech, rt,dz      ! Theta0 is the width of Int. Distr.
         real  alpha2
         real xw,xf
         real x0, h, lng,Ld,LDi,ratio,iratio
   ! lng is the crystal lengthh in mikrometers
!
!     Strech determines the half interval
!     width for thetaX and thetaY. InThX = Stech*Theta0.
!     Theta0 is in degrees. All distance are in mikrometers.
!     rt is the ratio between the beam intensity and the background intensity
!
         real lambda, n0
         lambda=0.5145
         n0=2.35
         x0=10.
         xw=1.
         xf=0.
!
         Theta0=0.55    ! degrees
         Strech=2.7
         rt=10.
         beta=-37.
!              Transformation of Theta0 in radians and in a. u.
!              In fact the normalized value of Theta0 is the V parameter
!              that occurs in the logarithmic paper
!
          Theta0 =(4.*Pi*Pi*x0*Theta0*n0)/(lambda*360.)
           print*, 'Theta0 = ', theta0
          alpha2=Theta0**2+1.  ! The incoherence parameter in normalised units
          lng=1.e+4                       ! 1 cm in mikrons
          dz=lng/95000.
```

```
          Ld=(n0*2.*Pi/lambda)*(x0**2)    ! the coherent difraction length
                                  ! since the equation is normalized to it
          Ldi=Ld/sqrt(alpha2)             ! The incoherent diffraction length
          ratio=dz/Ld
          iratio=dz/Ldi    ! The fraction of the 'incoherent difraction length
!
          if (iratio.gt.0.025) then
            print*, 'your step is too big', h, iratio
          end if
            h=ratio
            print*, 'h, Ld, ratio,Ldi,iratio = '
            print*, h, Ld, ratio, Ldi, iratio
!
          print*, 'alpha2 = ', alpha2
         return
         end
!
! :-)  :-)  :-)  :-)  :-)  :-)  :-)  :-)  :-)  :-)  :-)  :-)  :-)  :-)
!-----------------------------------------------------------------------
           subroutine getPower(data, PW)
           common/components/Npp
           common/discr/nx
           integer nx,Npp
           complex data(nx,Npp)
           real PW(nx)
           integer comp,i
!
           PW(:)=0.
          do comp=1,Npp
             PW(:) = PW(:)+cabs(data(:,comp))**2
          end do
        return
        end
! :-)   :-)   :-)   :-)   :-)   :-)   :-)   :-)   :-)   :-)   :-)   :-)

! :-)  :-)  :-)  :-)  :-)  :-)  :-)  :-)  :-)  :-)  :-)  :-)  :-)  :-)
!-----------------------------------------------------------------------
           subroutine Power(data, PW)
           common/components/Npp
           common/discr/nx
           integer nx,Npp
           complex data(nx,Npp)
           real PW(nx)
           integer comp,i
!
           PW(:)=0.
          data=data/sqrt(real(nx))
```

```
          do comp=1,Npp
             PW(:) = PW(:)+cabs(data(:,comp))**2
          end do
        return
        end
! :-)   :-)   :-)   :-)  :-)   :-)   :-)   :-)   :-)   :-)   :-)   :-)   :-)
```

# Incoherent Solitons

by

Tamer Coskun

Presented to the Graduate and Research Committee
of Lehigh University
in Candidacy for the Degree of
Doctor of Philosophy

in
Electrical Engineering

Lehigh University

August 1999

Approved and recommended for acceptance as a dissertation in partial fulfillment of the requirements for the degree of Doctor of Philosophy.

Date

Dissertation Director

Accepted Date

Committee Members:

Demetrios N. Christodoulides

Alastair D. McAulay

Alistair K. MacPherson

Michelle S. Malcuit

Miltiadis K. Hatalis

# Acknowledgments

I would like to express my deep gratitude to Dr. Demetrios N. Christodoulides for his guidance and support during my graduate studies and my thesis research. He was always ready to spend countless hours in sharing his ideas and experience with me. Apart from being a perfect mentor, he has always been a kind, understanding, and supportive friend. I am also indebted to Dr. Mordechai Segev for his constructive discussions and advice. I would like to offer my appreciation to my committee members, Dr. Alastair D. McAulay, Dr. Alistair K. MacPherson, Dr. Michelle S. Malcuit, and Dr. Miltiadis K. Hatalis for carefully reviewing my thesis and their useful comments. I am especially grateful to my wife, Hacer for her unconditional love, devotion, and moral comfort. I could not have asked for more support and understanding during my study. Special thanks go to my daughter, Bukre Cenan and my son, Hasan Bera for being a source of joy and relief to me. I am absolutely beholden to my mother and father for their guidance throughout the years which allowed me to strive to move ahead to achieve my goals.

# Table of Contents

# List of Figures

# Abstract

This thesis investigates the dynamical and soliton-like behavior of spatially-partially incoherent light beams in non-instantaneous nonlinear materials. Self-trapping of incoherent beams and their coherence properties are studied in great detail. Two complimentary approaches are developed in order to explain the observed incoherent self-focusing behavior in biased photorefractive media; namely the coherent density approach and the self-consistent incoherent multimode method.

It is shown that under appropriate initial conditions, bright as well as dark-like incoherent solitons are possible in saturable nonlinear media. Our numerical simulations have demonstrated that the coherence properties of these beams are signi cantly affected by the self-trapping process. More speci cally, in the case of bright beams, we have found that the coherence length remains approximately constant around the center of the beam, whereas it increases at the margins. An exact (one/two dimensional) Gaussian solution was also obtained in the case where the nonlinearity is of the logarithmic type. These incoherent Gaussian solitons can

exist as long as their spatial width is appropriately related to the strength of the nonlinearity and the width of the angular power spectrum of the incoherent source. Moreover, two dimensional incoherent solitons can be elliptical or circular depending on whether the angular power spectrum of the incoherent source is symmetric or not.

Our analysis has demonstrated that dark incoherent solitons are possible only if a $\pi$-phase shift is initially imposed on the wave front, and that they are in fact gray. In this case, the coherence length has been found to be higher within the dark notch, with a depression at the center. These dark soliton entities involve radiation modes as well as bound states. Depending on the initial conditions, an even or an odd number of incoherent dark-like structures can be obtained in a self-defocusing environment. It was found that over a wide range of parameters, the Y-splitting is approximately the same irrespective of spatial coherence. It is important to note that the behavior of bright/dark incoherent solitons is fundamentally different from that of their coherent counterparts. For example, unlike a coherent gray soliton, an incoherent dark soliton does not exhibit a transverse velocity in spite of its grayness. Furthermore, it is shown that the evolution of incoherent dark solitons in non-instantaneous nonlinear media is associated with strong phase-memory effects which are otherwise absent in the linear regime.

# Chapter 1

# Introduction

Solitons represent ubiquitous entities in the general field of nonlinear science. Thus far, they have been successfully identified in several branches of physics, such as for example hydrodynamics, nonlinear optics, plasma and solid state physics, magma flow and high energy physics [1],[2]. By definition, solitons are stationary solutions to nonlinear dispersive partial differential equations which also retain their identity after a collision event. Losely speaking, the term can also be used in conjuction with self-trapped wave-packets which are described by non-integrable systems where the outcome of a collision is typically more involved.

Within the discipline of nonlinear optics, solitons are typically subdivided into two basic categories: spatial and spatio-temporal solitons [3]. In the case of spatio-temporal solitons, perhaps the best known example is the nonlinear Schroedinger

soliton which occurs in optical bers [4]. Fiber solitons, which may play a crucial role in tomorrow s high-speed ber optic networks, have been intensively investigated in the last two decades at both the experimental and theoretical level [5]. Other types of spatio-temporal solitons can also be mentioned. These include for example, self-induced-transparency solitons, three-wave mixing and Raman solitons, ampli er solitons [3] as well as Bragg or gap solitons [6].

An optical beam naturally tends to broaden during propagation in a homogenous medium. This broadening can occur in time, in space, or in both. In the temporal domain, the broadening is due to chromatic dispersion where each frequency component of the pulse (wave-packet) bears different phase velocities. On the other hand, in the spatial domain the broadening is due to diffraction which is similar to dispersion. A spatial beam can be viewed as a linear superposition of plane waves (akin to frequency components of a pulse) all having the same wavenumber, yet each propagating at a different angle, let say $\alpha$, with respect to the propagation axis. As for temporal pulses, each plane-wave component accumulates a different phase, since its propagation constant is proportional to $\cos(\alpha)$. This results in phase building differences between each spatial frequency and thus the beam diffracts. In general, narrower beams have broader plane-wave specta and diverge faster. Waveguiding is a commonly used method to eliminate diffraction. When the interference between total internal re ections from the boundaries of a waveguide is constructive, the

beam gets trapped inside the waveguide thus forming a guided mode .

An astonishing possibility to counteract diffraction effect manifests itself when the material is nonlinear, as rst suggested by Chiao, Garmire and Townes [7]. While diffraction causes the spatial beam to spread and decrease in amplitude, the nonlinear effects tend to make the beam steepen and become narrower. In the right situation, these opposing effects will complement each other, leaving the beam propagating without any distortion. As a matter of fact, the optical beam creates its own waveguide as it travels through the material. Thus a balance between diffraction and nonlinearity is reached and as a result the beam remains localized and preserves its shape forming a spatial soliton .

It is interesting to note, that the rst solitons to be investigated in the eld of nonlinear optics were in fact spatial solitons. Shortly after the discovery of the laser, Chiao, Garmire and Townes suggested the possibility of self-trapped optical beams or solitons in nonlinear Kerr media [7]. In this case, the self-trapping of such a needle of light in the bulk of a nonlinear medium is made possible by counteracting the linear process of diffraction through the lensing effect of self-focusing [8],[9]. Like their spatio-temporal counterparts, spatial solitons also show considerable promise in terms of practical applications. Several applications, ranging from all-optical switches to dynamic optical interconnects and routers may be envisioned,

operating at strategic locations in a high-speed optical network [10],[11]. Until recently, however, all efforts aimed to harness this potential were met with failure. The reason behind this difficulty is primarily twofold. First of all, the observation of Kerr spatial solitons always requires exceedingly high power levels [12]. This is because the nonlinear index change in this case is proportional to the light intensity. For example, a soliton of approximately 10 microns in diameter, will require more than 200 kWatts, if it is to be observed say in a highly transparent glass medium. This situation often becomes further complicated when other nonlinear processes are invited in (because of high power) such as stimulated Raman and Brillouin scattering as well as two-photon absorption which tend to spoil the soliton itself [12]. Moreover, because of these high power requirements, lasers can only be used under pulsed conditions. The second reason behind this difficulty is even more fundamental. More speci cally, Kerr solitons in two transverse dimensions are highly unstable since they will either catastrophically collapse or break up in multiple laments [13],[14]. Thus far, bright Kerr solitons were only observed in one-dimensional con gurations where slab waveguides have been used to compensate for the other dimension [10],[11]. This explains why two-dimensional spatial solitons have remained elusive for the last thirty years or so.

This picture totally changed when it was rst predicted that spatial solitons may

in fact be possible in biased photorefractive crystals [15],[16]. At the time, photorefractives have been traditionally regarded as the material of choice for real time holography, phase conjugation and optical data storage [17], [18]. Nevertheless, any notion of solitons in this material system was entirely unheard of. Shortly after, the rst successful observation of what are by now better known as quasi-steady-state photorefractive spatial solitons has been reported in strontium barium niobate (SBN) crystals [19],[20]. As their name implies, these solitons occur in transient, i.e. before the space charge eld settles down. Even more importantly, these soliton states were found to be stable or robust in both transverse dimensions and they were observed at extremely low power levels , i.e. microwatts. Stability of two dimensional self-trapping is due to the fact that the nonlinearity happens to be saturating which means that the induced index change can not exceed a maximum value. In turn, the run-away interaction that gives rise to catastrophic collapse in Kerr media can be fully arrested since the induced waveguide eventually becomes wider. As expected, the event revived considerable interest within the optics community in the hope that spatial solitons may now be within reach [21],[22]. Subsequently, the so-called steady state screening solitons have been independently predicted by Christodoulides et al and Segev et al [23],[24] and were experimentally observed in both one and two transverse dimensions in SBN [25],[26]. These latter entities

appear after the space charge has reached its steady-state. At the same time, photovoltaic spatial solitons were predicted [27] and observed in lithium niobate [28],[29]. In all cases, photorefractive solitons were found to be stable against spatial perturbations. Apart from fundamental differences associated with the mechanism behind their existence, what greatly distinguishes the class of photorefractive solitons from their Kerr counterparts, is the required power level. Unlike Kerr solitons which typically require hundreds of kWatts [10],[11],[12], photorefractive solitons can be observed using microwatt or even lower optical power levels [19],[20]. Evidently, there is a difference of approximately 11 orders of magnitude. Even for the newly discovered family of chi-2 solitons [30], which exhibit stable self-trapping in both transverse dimensions, one still has to use hundreds of kWatts. Another important distinction, arises from the fact that photorefractive solitons can write permanent waveguides in the bulk of a photorefractive crystal, which in turn can be used to guide other more intense beams at less photosensitive wavelengths. In this manner, a microwatt soliton in the blue can guide and control a 1 Watt beam at 1-1.55 micrometers, intended for telecommunication purposes [28]-[34].

Very recently, for the first time, incoherent light was found to self-trap itself in a biased photorefractive crystal [35],[36]. This very interesting twist of events, now suggests that nonlinear optics no longer needs to belong to the exclusive domain of powerful lasers. This is the first time we know of, that incoherent light determined

the outcome of a nonlinear optics experiment. This development is expected to have important scienti c and technological implications. Furthermore, this is the rst time in Physics that an incoherent wave-packet, that is a wave-packet whose phase varies randomly in space and time, has been self-trapped.

This dissertation is dedicated to theoretical investigation of a number of fundamental issues associated with this newly discovered class of incoherent solitons.

## 1.1 Spatial solitons in saturable media

Photorefractive solitons are generally classi ed into three generic categories each resulting from a different nonlinear mechanism which is essentially saturable. Saturation of nonlinearity indicates that the optically induced refractive index change can not exceed a maximum value. Saturating nonlinearities lead to more complicated systems as opposed to Kerr nonlinearities. However, as mentioned before, the presence of saturation solves the problem of instability associated with the Kerr nonlinearity in (2+1)D. In what follow we provide an overview of the photorefractive soliton types by giving special emphasis to the screening solitons.

### 1.1.1 Screening solitons

Screening solitons occur in biased photorefractive media after the space charge eld has reached steady state [23],[24]. Basically the principle behind screening solitons is rather simple. At relatively high bias eld strengths, the current in the photorefractive sample is dominated by drift whereas the rather weak diffusion component can be neglected. In this case, the photo excited carriers migrate in such a way that the conductivity of the photorefractive crystal becomes higher in the illuminated regions whereas is lower in the dark. As a result, the absolute value of the space charge eld is lower (screened out) in the illuminated regions [23],[24]. In turn, through the electrooptic or Pockels effect, the refractive index is modi ed in proportion to

the local space-charge eld. When the proportionality coefficient is fairly large and negative, this leads to a large index change in the dark regions, whereas the refractive index in the illuminated regions remains almost unaffected. Consequently, this leads to a graded-index waveguide which can then support a nonlinear mode or what is better known as a bright spatial screening soliton. Similarly, dark spatial solitons are possible in biased photorefractives provided the polarity of the bias eld is reversed. In this latter case, the refractive index is lower in the illuminated regions whereas is higher within the dark notch.

Screening solitons were independently predicted by Segev et al. and Christodoulides et al. [23],[24]. In these studies, bright, dark and gray one-dimensional spatial screening solitons were found to be possible in biased photorefractive crystals. Moreover it was shown that for a given physical system, these states depend only on two parameters, namely the strength of the applied bias eld $E_0$ as well as the so-called intensity ratio $r$ or $\rho$, i.e. the ratio of the optical peak intensity with respect to the dark irradiance of the crystal. The symbol $r$ represents the maximum intensity ratio of a bright soliton whereas $\rho$ stands for the maximum dark intensity ratio. Shortly after, the existence of bright screening solitons was experimentally con rmed in SBN crystals by Segev s group [25],[26]. These solitons were found to be stable in both one and two transverse dimensions. Concurrently, dark screening solitons and Y-splitting gray solitons were observed in a reverse biased SBN crystal

[32], [33],[34]. The evolution equations of bright solitons were also investigated [37] under arbitrary input conditions. In this study [37], various issues were considered including the stability of these states, the effects arising from loss, bias and the intensity ratio as well as the interaction forces among in-phase and out of phase coherent solitons. In another theoretical study, the effects of diffusion on these solitons were considered and it was predicted that self-bending should occur [38],[39]. This self-bending effect was later successfully veri ed [26]. The guiding properties of the circular waveguides permanently induced by such spatial solitons were also studied experimentally [40], along with the rst experiments on collisions between pairs of photorefractive solitons.

At the same time, screening solitons were also investigated by Iturbe-Castillo et al. in Bismuth Titanium Oxide (BTO) crystals [41]. In their studies, induced modulational instability [42] was observed as well as bright and dark solitons were studied in biased BTO crystals [43]. A theoretical model capable of describing the process of modulational instability in biased photorefractives was later developed by Carvalho et al. [44]. The effects arising from the presence of optical activity on solitons in BTO crystals were also theoretically investigated and it was found that in fact soliton behavior in this system can only be claimed at relatively short distances and at small intensity ratios [45],[46].

In addition to single screening solitons, one-dimensional vector-screening solitons have been predicted in crystals of appropriate symmetry [47]. Unlike their Kerr counterparts, these solitons can now be both self-coupled or cross-coupled depending on the properties of the electrooptic tensor [47]. Other studies have also addressed vector interactions among solitons [48] as well as the possibility of observing bright-dark vector soliton pairs [49]. In a recent study, incoherently coupled soliton pairs have also been proposed [50]. These pairs are possible provided that the two carrier beams share the same polarization and are mutually incoherent. They can appear in bright-bright, dark-dark as well as in dark-bright con gurations. The existence of such incoherent soliton pairs has been recently con rmed experimentally [51],[52],[53]. In these experiments, bright-bright and dark-bright pairs have been observed in accord with theory. In the same spirit, incoherent collisions among solitons have been investigated in both one and two transverse dimensions [54],[55],[56]. These latter experiments have opened up a new avenue in terms of controlling the interaction forces between solitons.

Another important development in this area includes the rst experimental demonstration of self-trapping in InP:Fe [57]. This material is compatible with existing semiconductor technologies and moreover it has the potential to respond much faster than any of the previously studied oxides (it responds approximately

1000 times faster at the same intensity). Evidently, this may have important applications in high-speed interconnects and in all-optical switching. Photorefractive solitons in semiconductors are possible in spite of the very small electrooptic coefficient in these materials. This is due to a large enhancement of the space-charge field in the region of the optical beam which may be up to 10 times the applied field. The enhancement results from a resonance which occurs when the dark generation rate of electrons is equal to the photo-generation rate of holes. This effect was observed by Chauvet et al.[57],[58]. An alternative way to achieve such desirable fast response times is also possible by employing photorefractive solitons of high intensity [59].

### 1.1.2 Quasi-steady-state solitons

Unlike steady-state screening solitons, quasi-steady-state solitons can only exist in transient, i.e. before the space charge field has reached equilibrium. Interestingly enough, quasi-steady-state solitons were the first to be predicted [15],[16] and observed in biased photorefractives [19],[20]. These solitons can only be observed during a time window which may be seconds or minutes depending on the material and the absolute beam intensity. The theory of quasi-steady-state solitons in biased photorefractives was first developed by Segev et al.[15],[16]. In this formalism, the self-trapping effect arises from the phase coupling among the spatial spectral components of an optical beam. This phase coupling mechanism is modelled using the

two-wave mixing response function [17],[18] under external bias conditions. The evolution equation describing these solitons is then obtained by truncating to first order the Taylor series expansion of the two-wave mixing response function. By doing so, the end result in turn suggests that in this case the light induced nonlinear index change now follows the spatial derivatives of the beam intensity distribution. Along these lines several results have been predicted. First, the solitons in this case (which can be either Gaussian or hyperbolic-secant like) are independent of the absolute beam intensity as long as the light intensity is well above the dark irradiance of the crystal [15],[16]. Second, these solitons are only possible when the bias field strength lies within a certain range of values. These properties were verified experimentally in strontium barium niobate [19],[20]. In this experiment, stable propagation of two dimensional solitons was observed which was also independent of the beam intensity. Subsequent experimental efforts conducted in the quasi-steady-state regime have also demonstrated one-dimensional solitons as well as planar dark and vortex solitons [19],[20],[60]. On the theoretical side, the stability of these class of solitons has been investigated [61] and the dynamical evolution of Gaussian beams in biased photorefractives has been solved exactly [62]. In [62], spatial compression and self-bending was found to be possible when the bias field exceeds the allowed range of values necessary to establish a Gaussian soliton. This behavior is in agreement with the experimental results reported thus far [19],[20].

In another recent study it has been also shown that quasi-steady-state solitons can be employed to write permanent waveguides intended for other beams at less photosensitive wavelengths. Even though these waveguides were established at microwatt levels, they were in fact able to guide other intense beams (in the bulk of the crystal) at power levels of approximately 1 Watt [31]. Note that no other method exists today that is capable of establishing waveguides in the bulk of a material. Alternative methods currently employed in Integrated Optics such as sputtering, liquid phase and molecular beam epitaxy, ion implantation, diffusion and ion exchange are extremely involved and expensive and can only provide waveguides at the surface of a substrate.

### 1.1.3 Photovoltaic solitons

Photovoltaic solitons are possible in photorefractive media with appreciable photovoltaic coefficients under steady-state conditions. These solitons were first predicted by Valley et al. [27] and observed by Taya et al. [28]. Unlike screening solitons or quasi-steady-state solitons, photovoltaic solitons do not require an external bias. Instead, in this case, the required nonlinear index change is set up by a strong photovoltaic current. So far, the theory of photovoltaic solitons has been developed in one transverse dimension [27] and by appropriately incorporating the photovoltaic nonlinearity into the wave equation. By doing so, explicit soliton solutions (dark

and bright) have been obtained that resemble those in Kerr saturable media [63]. From the mathematical point of view, the evolution of 1-D photovoltaic spatial solitons is governed by an equation very similar to that of photorefractive screening solitons where this time nonlinearity constant is proportional to the photovoltaic eld constant [27].

The rst experimental observation of photovoltaic solitons was carried out in lithium niobate by Taya et al [28]. This crystal exhibits a negative nonlinear index change and it is thus suited for dark solitons. In these experiments dark and gray solitons have been observed and the tensorial nature of the underlying photovoltaic effect also became evident. In a subsequent experiment, Y-junction waveguides have been formed by utilizing higher-order dark soliton splitting. These Y-junctions were then used to guide and split other more intense beams at higher wavelengths [29].

Recently, 2-D photovoltaic vortex solitons were successfully generated [64]. This is very surprising because the photovoltaic current in lithium niobate is inherently a polar current, i.e. the electrons are accelerated along the ferroelectric axis only. Nevertheless, the 2-D nature of the optical beam enforces a two-dimensional current and in turn a 2-D space-charge eld capable of supporting 2-D spatial solitons.

## 1.2 Incoherent solitons

In a recent experimental study, Mitchell et al. have reported for the rst time self-trapping of partially spatially incoherent light in a biased SBN crystal [35],[36]. As previously noted, this represents an important discovery not only in the area of photorefractives but in the entire eld of Optics in general. The experiment was carried out using laser light after a rotating diffuser. After the diffuser, the incoherent light beam (which can be considered to be quasi-thermal), was then launched in a biased SBN specimen. In the absence of any external bias, the input beam (30 micrometers in diameter) was found to expand to 102 microns after 6 millimeters of propagation. Instead, at a bias voltage of 550 Volts the incoherent beam remained invariant by counteracting diffraction effects. At even higher voltages, spatial compression was found to occur. These results clearly demonstrate that incoherent self-trapping effects were present and to some extent they suggest that spatial incoherent solitons may be possible. Of all the processes discussed in this section, this latter one used to be the least understood.

# Chapter 2

# Background

In a recent experiment [35], it has been demonstrated that incoherent light can self-trap itself in photorefractives. More speci cally, incoherent light was found to self-trap in a biased Strontium Barium Niobate (SBN:75) photorefractive crystal. This observation was made possible through the nonlinearity associated with photorefractive screening solitons. This nonlinearity has two properties which are critical for the self-trapping of incoherent light beams: Finite response time which can be much longer than the phase uctuation time across the incoherent beam; saturation which is essential to create a multimoded waveguide. Therefore, to further investigate the incoherent self-trapping process, it is important to understand the photorefractive nonlinearity and coherent screening solitons. In this chapter we will rst give a brief explanation of the photorefractive effect. We will later formulate

the theory of coherent photorefractive solitons and discuss the properties of partially spatially incoherent beams.

## 2.1 Photorefractive nonlinearity

The optical properties of photorefractive (PR) crystals have been a topic of considerable interest in the last three decades or so. The photorefractive effect was first discovered accidentally in Lithium Niobate ($LiNbO_3$) in 1966 by Ashkin et al. [65]. Since then, it has been observed in many electro-optic crystals such as Barium Titanate ($BaTiO_3$), Strontium Barium Niobate (SBN, $Sr_xBa_{1-x}Nb_2O_6$), Potassium Niobate ($KNbO_3$), Bismuth Silicon Oxide (BSO, $Bi_{12}\,\mathrm{Si}\,O_{20}$), Bismuth Titanium Oxide (BTO, $Bi_{12}TiO_{20}$), and several other materials such as polymers. Traditionally, photorefractive crystals have been employed in various applications including real-time holography, phase conjugation, and optical data storage [17],[18]. However, the prediction of optical solitons in photorefractive media [15], [16] has opened up a new exciting avenue for different applications.

In general, self-trapped optical beams or solitons are possible when the process of diffraction is exactly balanced by nonlinear self-focusing. In the case of biased photorefractives, the nonlinearity arises from the dominant drift conduction term. Currently the most widely accepted model describing the photorefractive effect is the one initially suggested by Vinetskii and Kukhtarev in 1975 [66],[67]. In this

model, a PR material involves both donor and acceptor centers. All donor impurities are assumed to be identical and have exactly the same energy level somewhere in the middle of the band gap. These neutral donor impurities $N_D$ can be ionized (resulting to electron donation) by absorbing photons of sufficient energy. In turn the ionized ones are capable of recapturing the donated photoelectrons. On the other hand, the acceptor impurities $N_A$ (whose density is typically much smaller than that of the donors) are assumed to be fully ionized at all times. Therefore, they only participate indirectly in the PR effect by providing charge neutrality when no optical illumination is present. In the absence of light, the ionized donor density $N_D^+$ is taken to be equal to the acceptor density $N_A$. Nonuniform illumination of the material with light of suitable wavelength ionizes the donors and generates free carriers (either electrons or holes, or both). The free electrons, generated in the bright regions of the incident optical beam, diffuse and drift away. As a result, a charge redistribution between illuminated and dark areas is induced. This space-charge density is associated, through Gauss s law, to a low frequency space-charge electric eld which, in turn, causes a refractive index pattern via the linear electro-optic Pockels effect. In other words, non-uniform illumination of the photorefractive medium results in a non-uniform change in the refractive index. The local change in the refractive index is given by $\triangle(1/n^2)_{ij} = r_{ijk}E_k$ where $E_k$ are space charge electric eld components and $r_{ij}$ are the linear electro-optic coefficients [17],[18].

Even though the electro-optic tensor involves a number of independent coefficients, this number decreases as the symmetry increases.

## 2.2 Steady-state photorefractive screening solitons

In this section, we develop the theory of steady-state photorefractive screening solitons. Under steady-state conditions, the evolution equations of one dimensional spatial optical beams in photorefractive media are obtained. As an example, we will consider screening solitons in a SBN photorefractive crystal where most of the experiments have been carried out.

### 2.2.1 Space-charge eld

To study the propagation of 1-D planar spatial beams in this material system, we consider a standard con guration where the optical beam propagates along the $z$ axis and it is allowed to diffract only along the $x$ coordinate. The optical $c$-axis of the SBN crystal is assumed to be oriented in the $x$ direction. Furthermore, an external electric eld is applied along the same coordinate. In this case, the perturbed extraordinary refractive index along the optical $c$ axis is given by $(n_e')^2 = n_e^2 - n_e^4 r_{33} E_{sc}$ where $r_{33}$ is the electro-optic coefficient involved, $n_e$ is the unperturbed extraordinary index of refraction, and $E_{sc}$ is the total electric eld. The induced space-charge eld $E_{sc}$

can be obtained from the Kuktarev-Vinetskii equations [66],[67],[68]. For a one dimensional con guration and under steady-state conditions these equations take the following form:

$$\gamma_R N_D^+ n = s_i \left(I + I_d\right)\left(N_D - N_D^+\right) \tag{2.1}$$

$$J = \text{constant} \tag{2.2}$$

$$J = e\mu\left(nE_{sc} + \frac{K_B T}{e}\frac{\partial n}{\partial x}\right) \tag{2.3}$$

$$\frac{\partial E_{sc}}{\partial x} = -\frac{e}{\epsilon_0 \epsilon_r}\left(N_A - N_D^+ + n\right) \tag{2.4}$$

The rst equation is the charge recombination equation and the second one is the continuity equation. The third one shows that the current density $J$ is the sum of the drift and diffusion terms. Moreover, $I = I(x, z)$ is the power density of the optical beam and is proportional to the square of the absolute magnitude optical eld envelope. $\gamma_R$ is the carrier recombination rate, $s_i$ is the photo-excitation cross section, $e$ is the electron charge, $\mu$ is the electron mobility, $n$ is the free electron density, and $K_B$ is Boltzmann constant; $T$ is the absolute temperature, $\epsilon_0\epsilon_r$ is the total permittivity, $N_D$ is the donor concentration, $N_A$ is the trap density, $N_D^+$ is the ionized donor density, $I_D$ is the dark irradiance of the crystal. Furthermore, let us assume that the optical intensity can remain constant at the tails far away from the beam, i.e. $I(x \to \pm\infty, z) = I_\infty$. It can then be shown that the space-charge eld is also constant at the tails, i.e., $E_{sc}(x \to \pm\infty, z) = E_0$. When the beam is well

con ned within the crystal s width $W$, the constant value $E_0$ is approximately equal to $V/W$ where $V$ is the external bias voltage. As usual, we assume that the donor concentration and the trap density is much bigger than the free electron density and that the ionized donor density is approximately the same as the trap density. Under these assumptions, the steady-state space charge eld can be obtained from the above Kuktarev-Vinetskii transport equations and given by [24],

$$\begin{aligned} E_{sc} &= E_0 \frac{(I_\infty + I_d)}{(I + I_d)} \left[ 1 + \frac{\epsilon_0 \epsilon_r}{eN_A} \frac{\partial E_{sc}}{\partial x} \right] - \frac{K_B T}{e} \frac{1}{(I + I_d)} \frac{\partial I}{\partial x} \\ &+ \frac{K_B T}{e} \frac{\epsilon_0 \epsilon_r}{eN_A} \left[ 1 + \frac{\epsilon_0 \epsilon_r}{eN_A} \frac{\partial E_{sc}}{\partial x} \right]^{-1} \frac{\partial^2 E_{sc}}{\partial x^2} . \end{aligned} \tag{2.5}$$

When the bias voltage $V$ is high, the space-charge eld $E_{sc}$ is dominated by drift and typically in photorefractive crystals $|(\epsilon_0 \epsilon_r / eN_A)\, \partial E_{sc}/\partial x| \ll 1$. In that case, the space-charge eld is approximately given by [23],[24]

$$E_{sc} \approx E_0 \frac{(I_\infty + I_d)}{(I + I_d)} . \tag{2.6}$$

### 2.2.2 Evolution equation

Starting from Maxwell s equations and by employing standard procedures, we nd that the envelope of the optical eld obeys the following differential equation [23],[24]:

$$i \frac{\partial \phi}{\partial z} + \frac{1}{2k} \frac{\partial^2 \phi}{\partial x^2} - \frac{k_0}{2} \left( n_e^3 r_{33} E_{sc} \right) \phi = 0 . \tag{2.7}$$

In this equation, $\phi$ is a slowly varying envelope. In turn, the optical eld

$$\vec{\varepsilon} = \hat{x} \phi (x, z) \exp (ikz)$$

is expressed in terms of this envelope. $k = (2\pi/\lambda_0)\, n_e$ and $\lambda_0$ is the free-space wavelength. Considering only the dominant drift process, the evolution equation for the envelope $\phi$ can be obtained by substituting Eq. 2.6 into Eq. 2.7. For simplicity, this equation can be further simpli ed by adopting normalized coordinates and quantities, i.e. $\xi = z/\left(kx_0^2\right)$, $s = x/x_0$, $\phi = \left(2\eta_0 I_d/n_e\right)^{1/2} U$ where $x_0$ is an arbitrary spatial scale and the beam intensity has been scaled with respect to dark irradiance. In that case, the normalized evolution equation is given by

$$i\frac{\partial U}{\partial \xi} + \frac{1}{2}\frac{\partial^2 U}{\partial s^2} - \beta\left(1+\rho\right)\frac{1}{1+\left|U\right|^2}U = 0 \tag{2.8}$$

where $\rho = I_\infty/I_d$ and the nonlinearity constant $\beta$ is proportional to effective electrooptic coefficient of the photorefractive crystal and the external bias eld, i.e. $\beta = \left(k_0 x_0\right)^2 n_e^4 r_{33} E_0/2$. Note that $\beta$ can be positive or negative depending on the polarity of the bias eld $E_0$. As it has been shown [24], bright, dark and gray one-dimensional spatial screening solitons can be possible in biased photorefractive crystals. Moreover it was shown that for a given physical system, these states depend only on two parameters, namely the strength of the applied bias eld $E_0$ as well as the so-called intensity ratio $r$ or $\rho$, i.e. the ratio of the optical peak intensity with respect to the dark irradiance of the crystal. The symbol $r$ represents the maximum intensity ratio of a bright soliton whereas $\rho$ stands for the maximum dark intensity ratio. Bright and dark soliton beam pro les are shown in Fig.2.1(a) and (b). The dependence of the normalized spatial intensity FWHM of these beams

respect to $r$ or $\rho$ in units of $x/\widehat{x}_0$ is given Fig. Fig.2.1(c) and (d). Here $\widehat{x}_0$ is a normalization parameter and given by $\widehat{x}_0 = 1/(k_0 n_e^2 \sqrt{r_{33} E_0/2})$. It is important to note that, bright soliton states require positive bias, $E_0 > 0$, whereas the dark and gray soliton states are possible only when the bias eld is negative or the photorefractive material is reverse biased, $E_0 < 0$.

Photorefractive solitons require very low powers, as low as 1 $\mu Watt$, because the nonlinear refractive index change depends on the $I/I_d$ ratio rather than the optical intensity $I$. In this way, even if the total power is very low, a very strong nonlinearity can be induced. Moreover, the nonlinearity can be adjusted by changing the external bias voltage thus introducing an extra free parameter to vary the size of the soliton beam. In addition, the nonlinear response of photorefractive materials is wavelength dependent. This means that, one can use a soliton induced waveguide to control powerful beams at wavelengths at which the material is less photosensitive. Moreover, the response time of the photorefractive material can change from nanoseconds to hours depending on the optical intensity. For example, the response time is in the order of seconds for a typical soliton formation in a SBN crystal. In fact, this property is one of the requirements for incoherent soliton formation.

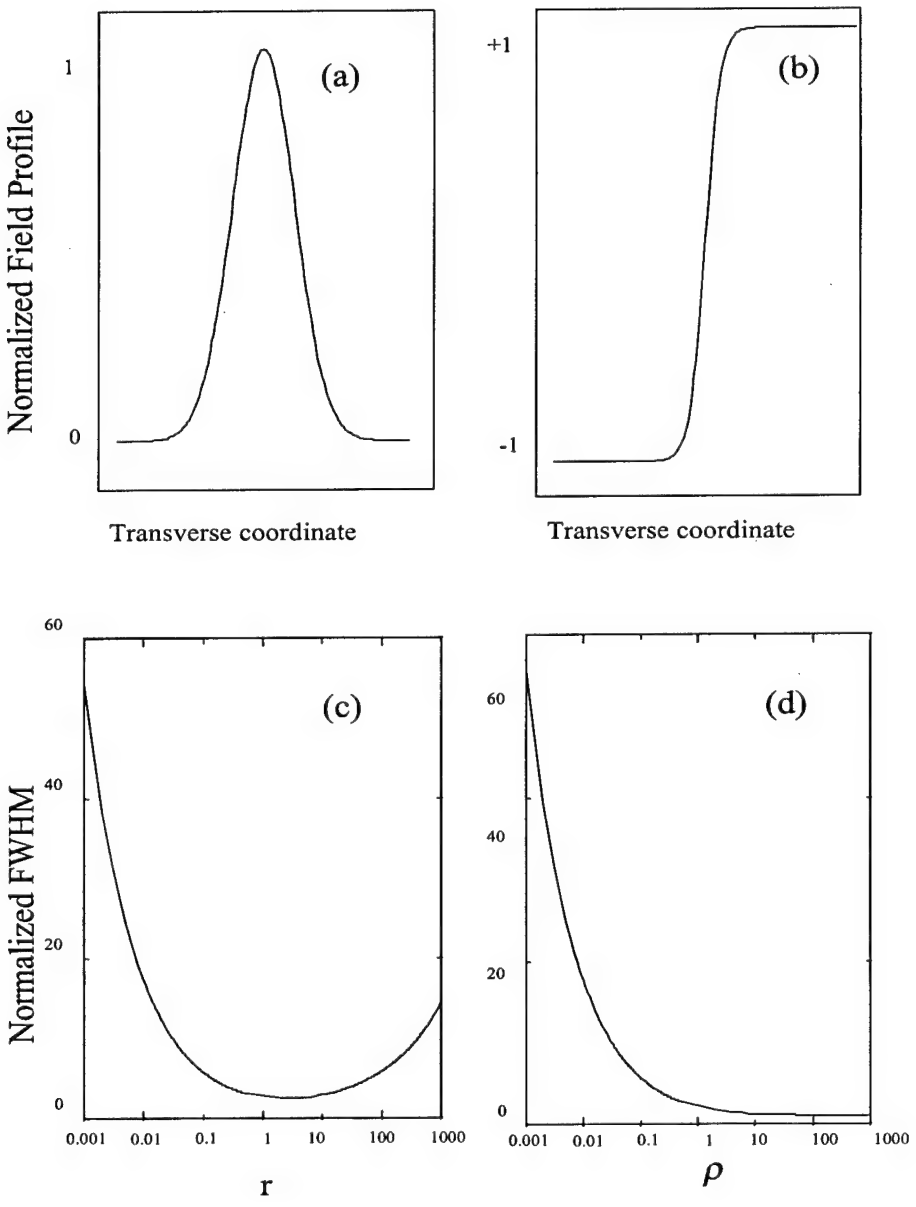


Figure 2.1: Field profiles of (a) bright and (b) dark screening spatial solitons. Normalized intensity full-width half-maximum versus intensity ratio for (c) bright and (b) dark screening solitons.

## 2.3 Spatially incoherent light and coherence length

For a coherent beam, the phases at all points of the beam varies in unison with time. On the other hand, the phases at different points across an incoherent beam vary in a statistical manner. This randomly changing phase distribution creates an intensity pattern known as speckle. Speckle size is an indication of the degree of coherence for a spatially partially incoherent beam. The diffraction characteristics of a beam are related to the speckle size or the degree of coherence: the smaller the speckles, the larger the diffraction. In other words, beams of higher coherence diffract less. When the beam is fully coherent, every point of the beam is well correlated with all other points. Therefore, the coherence length across a coherent beam is in nite. Each point of a fully incoherent beam , however, correlates only with itself and it is totally uncorrelated with other and thus the correlation length is zero. Between these two extreme cases, is the class of partially incoherent beams. Most of the sources in nature fall in this category. In this case, each point across the beam correlates with other points. This nite correlation distance is called coherence length.

The coherence of a source can be described by using a time averaged temporal

correlation between the electric field at different points across the beam. This property is given by a normalized spatial complex coherence function [69],[70] $\mu(x_1, x_2)$

$$\mu_{12}(x_1, x_2) = \frac{\langle E(x_1)E^*(x_2)\rangle}{\sqrt{I(x_1)I(x_2)}} \tag{2.9}$$

where $\langle . \rangle$ denotes the time average and $I$ is the optical beam intensity. In general, the complex coherence function can be an arbitrary function of both $x_1$ and $x_2$. Thus, it is often more convenient to describe the coherence properties of an optical beam through a coherence length $l_c$ which is defined as follows:

$$l_c(x) = \int_{-\infty}^{\infty} |\mu_{12}(x, \delta)|^2 \, d\delta \tag{2.10}$$

To understand the complex coherence function and its relation to optical intensity, consider two point sources, let say 1 and 2. The optical field, $E$, at an observation point will be superposition of the fields, $E_1$ and $E_2$, from these two points. In this case the total field at the observation point will be given by $E = E_1 + E_2$. Furthermore, if we assume that the field is stationary, i.e. the coherence function only depends on the separation between these two points $\tau = r_2 - r_1$ but not their placement, Eq.2.9 can be written as $\mu_{12}(\tau) = |\mu_{12}(\tau)| \exp[i\phi_{12}(\tau)]$. Here, $0 \leq |\mu_{12}(\tau)| \leq 1$ and $\phi_{12}(\tau) = \arg[\mu_{12}(\tau)]$ is a time averaged phase difference between two fields. Therefore the time averaged total intensity can be given as

$$\begin{aligned} I_T &= \frac{1}{2}\langle EE^*\rangle = I_1 + I_2 + 2(I_1 I_2)^{1/2} \operatorname{Re}[\mu_{12}(\tau)] \\ &= I_1 + I_2 + 2(I_1 I_2)^{1/2} |\mu_{12}(\tau)| \cos[\phi_{12}(\tau)] \end{aligned} \tag{2.11}$$

where $I_1$and $I_2$ are the intensities that would be produced at the observation point by two elds independently. Eq. 2.11 shows that, depending on the degree of coherence between two elds, different intensity patterns are formed. For example if the beams are completely coherent among each other, i.e.$|\mu_{12}(\tau)| = 1$, a fringe pattern with a maximum contrast will be observed. When the beames are completely uncorrelated, i.e. $|\mu_{12}(\tau)| = 0$, no fringe pattern will be observed. This latter case corresponds to complete incoherence. i.e. there is no de nite phase relationship between the waves arriving at the observation point from two different point sources. When these beams are partially correlated, $0 < |\mu_{12}(\tau)| < 1$, the contrast of the fringe pattern will change accordingly . This latter case corresponds to partially incoherent beams [69],[70].

The time averaged intensity of a partially spatially incoherent beam is different than its instantaneous intensity. If we observe the intensity of an incoherent light at any time, we will see a speckled intensity pattern as shown in Fig.2.2. What our eyes or a slow responding material see, in fact, will be an average of these randomly changing speckled patterns. If the averaging time is long enough, the resulting intensity will be smooth as shown in Fig.2.2. In this latter case, the third term (interference term) in Eq. 2.11 averages out to zero since the nonlinearity responds slower than the rate of random phase changes. Therefore, the total intensity that nonlinearity sees will be the summation of contributing intensities from each

individual point, i.e. $I_T = I_1 + I_2$.

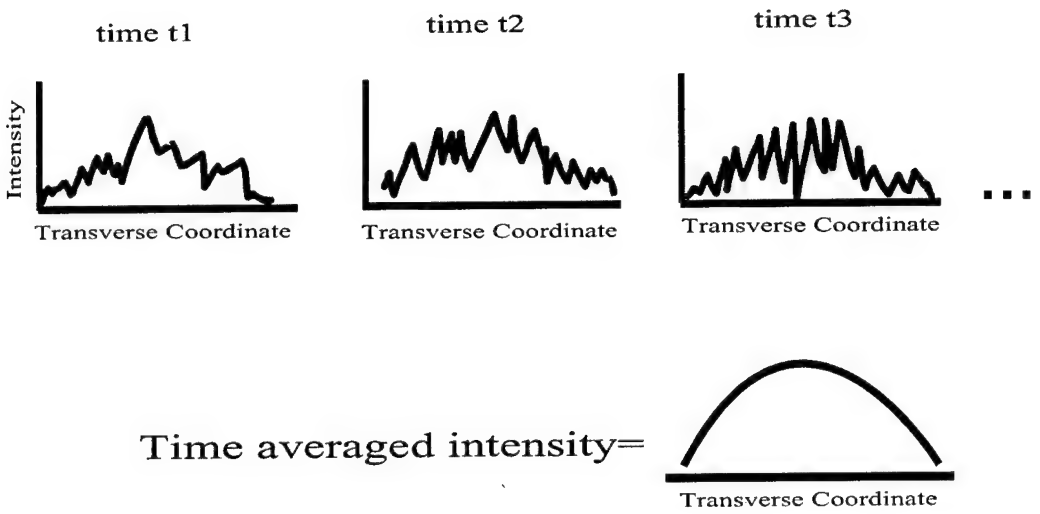


Figure 2.2: Illustration of the temporal avaraging of many instantaneous speckled patterns due to the noninstantaneous response of nonlinearity.

# Chapter 3

# Theory of incoherent beam propagation in nonlinear media

In this chapter, the coherent density approach, describing propagation and self-focusing of partially spatially-incoherent light beams in nonlinear media is developed. It is shown that this process is effectively governed by an in nite set of coupled nonlinear Schrödinger-like equations provided that they are initially appropriately weighted with respect to the incoherent angular power spectrum of the source. The particular case of spatially partially incoherent beam propagation in biased photorefractive media is considered in detail. Numerical simulations indicate that spatial compression as well as self-trapped states are possible under appropriate conditions. Our results are in good agreement with recent experimental observations.

## 3.1 Introduction

Optical self-focusing has been a subject of considerable interest in the last three decades or so. Over the years, this process has been systematically investigated in all states of matter with the aid of laser sources [12]. Thus far, several physical systems have been identi ed that can lead to optical self-trapping. These include for example, $\chi^{(3)}$ or Kerr-like media [10], [11], the $\chi^{(2)}$ family of materials [71],[72] as well as the class of photorefractives [19]-[25],[73]. Highly relevant to this topic is of course the very existence of optical spatial solitons [8],[9]. These latter entities can occur provided that diffraction effects are exactly balanced by optical self-trapping. At this point, it may be fair to say that both coherent self-focusing as well as the coherent excitation of solitons are by now in principle well understood. In a very recent study however, a successful observation of incoherent self-trapping has been reported for the rst time [35]. In this experiment, partially spatially incoherent light was found to self-trap in a biased strontium barium niobate (SBN) photorefractive crystal. Apart from its possible scienti c and technological implications, this observation [35] in turn poses a new fundamental challenge. More speci cally, a theory of incoherent self-focusing and possibly of incoherent solitons now needs to be developed. Unlike their coherent beam counterparts, for which the phase at all points varies in unison with time, the phases at different points across an incoherent beam vary in an uncorrelated manner [69],[70]. This introduces an

important new element in the nonlinear theory of self-focusing. Even though the properties of speckle-inhomogeneous fields have been considered in the past in connection with optical phase conjugation [74], the propagation behavior of partially incoherent (multimode) beams in nonlinear media has not yet been explored.

In this chapter, a theory of incoherent self-focusing in non-instantaneous nonlinear media, and in particular in biased photorefractive crystals is presented. We consider nonlinear media with response times much bigger than the characteristic phase fluctuation time across the optical beam which in turn will only experience the time-averaged intensity. In the case of stationary spatial source fluctuations, we show that this process can be effectively described by means of an infinite set of coupled nonlinear Schrödinger-like equations provided that they are appropriately weighted with respect to the source incoherent angular power spectrum. Our numerical computations demonstrate that spatial compression as well as self-trapped states are possible under appropriate conditions. In these cases, self-trapping can be intuitively understood as fusion of multi-particles. Pertinent examples are provided to further elucidate this behavior. A possible soliton solution to this system is also presented.

## 3.2 Coherent density approach

To start, let us consider for example a SBN crystal with its optical c-axis oriented in the x direction. Let us also assume that the optical beam propagates along the z axis and it is allowed to diffract only along the x direction. For simplicity, we limit our analysis to one transverse dimension ($x$) and we assume uniformity in $y$. Furthermore, an external bias electric eld is applied along x (i.e., the c-axis), in which case the perturbed extraordinary refractive index is given by [23],[24],[59] $(n_e')^2 = n_e^2 - n_e^4 r_{33} E_{sc}$, where $n_e$ is the unperturbed index of refraction, $r_{33}$ is the electrooptic coefficient involved, and $E_{sc}$ is the static space charge eld in this photorefractive crystal. Under strong bias conditions ($0.2 - 4\ kV/cm$) and for relatively broad bright-like beam con gurations ( $25\lambda_0/n_e$), the steady-state space charge eld is approximately given by [23], [24],[59] $E_{sc} = E_0 I_d \left[I_d + I(x,z)\right]^{-1}$ as shown in Chapter 2. Here $I = I(x,z)$ is the power density of the optical beam, $I_d$ is the so-called dark irradiance of the crystal and $E_0$ is the value of the space charge eld at $x \rightarrow \pm\infty$. If the spatial extent of the optical wave involved is much less than the $x-$width $W$ of the crystal, then for a constant bias voltage $V$, $E_0$ is approximately given by $\pm V/W$ [24].

Next, it is important to consider the diffraction behavior of this incoherent beam. Let us assume, as in the experiment reported [35], that the incoherent wavefront results from a quasi-thermal quasi-monochromatic source such as for example laser

light after passing through a rotating diffuser [35],[70],[75]. Let the $\hat{x}$ polarized electric field component of the optical wave be expressed in terms of a slowly varying envelope $\phi(x,z)$ i.e. $\vec{E}(x,z) = \hat{x}\phi(x,z)\exp(ikz)$ where $k = (2\pi/\lambda_0)n_e$. In the paraxial limit ($k_x/k \ll 1$) and in the linear regime, the envelope $\phi$ is known to evolve according to

$$\phi(x,z) = \frac{1}{2\pi}\int_{-\infty}^{\infty} dk_x \hat{\Phi}(k_x)\exp\left\{i[k_x x - (k_x^2/2k)z]\right\} \tag{3.1}$$

where $\hat{\Phi}(k_x)$ is the Fourier transform of the field right at the input, i.e. at $z = 0$. Let the optical field at the origin also be written as $\phi(x, z = 0) = f(x)\phi_0(x)$ where $f(x)$ is a spatial modulation function and $\phi_0(x)$ is the field before modulation which implicitly contains all the spatial statistical properties of the source. If the source fluctuations obey a stationary random process [76], then the spatial statistical autocorrelation function of $\phi_0(x)$ is given by $\left\langle \phi_0(x)\phi_0^*(x')\right\rangle = R(x-x')$. In turn, the autocorrelation function of the source spectrum can be obtained, i.e. $\left\langle \hat{\Phi}_0(k_x)\hat{\Phi}_0^*(k_x')\right\rangle = 2\pi\delta(k_x - k_x')G(k_x')$ where $\hat{\Phi}_0(k_x)$ and $G(k_x)$ are the Fourier transforms of $\phi_0(x)$ and $R(x)$ respectively and $\delta(x)$ is a delta function. Physically the real function [76] $G(k_x)$ represents the incoherent angular power spectrum of the source. Using the frequency convolution theorem and the fact that $\hat{\Phi}(k_x)$ is the Fourier spectrum of the product $f(x)\phi_0(x)$, one can readily derive the following result:

$$\left\langle \hat{\Phi}(k_x)\hat{\Phi}^*(k_x')\right\rangle = (1/2\pi)\int_{-\infty}^{\infty} d\eta G(\eta)F(k_x-\eta)F^*(k_x'-\eta) \tag{3.2}$$

where $F(k_x)$ is the Fourier transform of the spatial modulation function $f(x)$. Keeping in mind that the intensity of this wave is given by $I(x,z) = \left\langle |\phi|^2 \right\rangle$ and by employing Eq.3.1 and 3.2 we nally obtain

$$I(x,z) = \int_{-\infty}^{\infty} d\theta G_N(\theta) \left| \frac{1}{2\pi} \int_{-\infty}^{\infty} dk_x F(k_x) \exp[ik_x(x-\theta z)] \exp[-ik_x^2(z/2k)] \right|^2 \quad (3.3)$$

where $G_N(\theta)$ in Eq.3.3 has been normalized for convenience, and $\theta = k_x/k$ represents an angle (in radians) with respect to the $z$ axis. At this point it may be useful to make few remarks. First, the quantity in the brackets of Eq.3.3 represents in fact the intensity pro le resulting from an otherwise coherent beam when its initial eld pro le is $f(x)$. Furthermore, this coherent component propagates at an angle $\theta$ with respect to the $z$-axis by obeying the paraxial equation of diffraction: $i\,(U_z + \theta U_x) + (1/2k)U_{xx} = 0$ where $U_z = \partial U/\partial z$ etc. In essence, Eq.3.3 leads to the following important conclusion: the diffraction behavior of an incoherent beam can be effectively described by the sum of the intensity contributions from all its coherent components provided that their eld pro les at the origin have been appropriately scaled with respect to the incoherent angular power spectrum $G_N(\theta)$, i.e. $U(x, z = 0) = G^{1/2}(\theta) f(x)$. As one may anticipate, in the limit $G_N(\theta) \to \delta(\theta)$, the result of Eq.3.3 reduces to that of the coherent case. Note, that similar arguments have been previously employed in connection with incoherent imaging [77], theory of speckle-inhomogeneous elds [74], and incoherent wave propagation in dispersive media [78].

Up to this point our treatment is quite general. On the other hand, when an incoherent optical beam propagates in a slowly-responding nonlinear medium, one should also expect that each of these coherent components or quasi-particles will be in uenced by the nonlinearity involved. In turn, an intensity-dependent nonlinearity will follow the incoherent (intensity) superposition of all these components. In the particular case of a biased photorefaractive crystal, the nonlinear index change $\triangle n = (n_e^3/2)\, r_{33} E_{sc}$ can then be readily incorporated into the underlying equations of motion by following the procedure of [23], [24],[59]. By doing so and by discretizing the diffraction integral of Eq.3.3 (i.e. $\theta \rightarrow j\triangle\theta$), then under steady-state conditions we are nally led to the following in nite set of coupled nonlinear Schrödinger-like equations:

$$i\left\{\frac{\partial U_j}{\partial z} + (j\triangle\theta)\frac{\partial U_j}{\partial x}\right\} + \frac{1}{2k}\frac{\partial^2 U_j}{\partial x^2} - \frac{k_0}{2} n_e^3 r_{33} E_0 \frac{U_j}{1+I(x,z)} = 0 \qquad (3.4)$$

where $I(x,z)$ is the intensity pro le of the incoherent beam which is given by

$$I(x,z) = \sum_{j=-\infty}^{\infty} |U_j(x,z)|^2 \qquad (3.5)$$

and the discrete index $j = 0, \pm 1, \pm 2, \ldots$ . Effectively, Eqs.3.4 and 3.5 describe the process of incoherent self-focusing in biased photorefractives in the limit $\triangle\theta \rightarrow 0$. Moreover, in these equations each coherent fragment has been scaled with respect to $I_d$, and at the origin we have assumed that $U_j(x,0) \propto G_N^{1/2}(j\triangle\theta) f(x)$.

## 3.3 Incoherent bright photorefractive solitons

As an example let us consider a biased SBN:75 crystal. Here, the parameters used will be very similar to those reported in [35]. In particular, let $r_{33} = 1022$ $pm/V$, $\lambda_0 = 488$ $nm$, $n_e = 2.3$, $W = 6$ $mm$ and let the length of propagation be 6 $mm$. Let us also assume that the input intensity pro le as well as the incoherent angular power spectrum are Gaussian, i.e. $f(x) = \exp\left(-x^2/2x_0^2\right)$ and $G_N(\theta) = \left(\pi^{1/2}\theta_0\right)^{-1} \exp\left(-\theta^2/\theta_0^2\right)$. In our numerical computations we use 201 components ($-100 \leq j \leq 100$) equidistantly spanning the range $\pm 2.5$ $\theta_0$. From our previous discussion, the eld of each coherent component at the origin is set to be $U_j(x,0) = \hat{r}^{1/2} f(x) \exp\left[-\left(j\triangle\theta\right)^2/2\theta_0^2\right]$ where $\hat{r}$ is an appropriate constant which is related to the maximum intensity ratio $r_T$ (with respect to $I_d$) of the input incoherent beam. More speci cally $r_T = \hat{r} \sum_j \exp\left[-\left(j\triangle\theta/\theta_0\right)^2\right]$. Equations 3.4 and 3.5 are solved by means of standard split-step Fourier methods. The accuracy of our results was then checked against the conservation laws of Eqs. 3.4 and 3.5 and by increasing the number of coherent components. As a rst example let us consider an incoherent Gaussian beam with $x_0 = 18$ $\mu m$, in which case its input intensity FWHM is 30 $\mu m$. Moreover let the width of the source angular power spectrum be $\theta_0 = 9.56$ *milliradians* or $0.548^o$. In this case, the beam linearly diffracts to a FWHM of 102 $\mu m$ after 6 $mm$ of propagation as shown in Figure 3.1. Note that if this beam was spatially coherent, it would have diffracted to 35.4 $\mu m$ after $6mm$, as has been

observed in [35]. Once the crystal is appropriately biased, self-trapping effects start to emerge. Fig.3.2(a) depicts the intensity evolution of this beam ($x_0 = 18\ \mu m$, $\theta_0 = 0.548^o$) when the applied voltage is 400 $V$ and $r_T = 3$. After 6 $mm$, the beam has developed a rectangular-like pro le with a FWHM of $\sim 34.7\ \mu m$ as shown in Fig.3.2(b). Evidently self-focusing played an important role in this example even though it was not enough to balance diffraction effects. Figure 3.3 on the other hand shows what would happen if the bias is increased to 550 $V$. In this case, the incoherent beam propagates almost undistorted and it behaves like a quasi-soliton. In other words, all the coherent components or quasi-particles have appropriately fused together thus producing a stationary beam. Figs.3.4 and 3.5 show intensity evolution of two coherent fragments of this self-trapped beam at $\theta \approx 0.27^o$ and $\theta \approx 0.54^o$ respectively. At an even higher voltage, $V = 1000\ V$, the beam starts to exhibit considerable spatial compression. Figure 3.6 shows that cycles of compression and expansion are now possible during propagation. At the output, i.e. $z = 6$ $mm$, its intensity FWHM is $\sim 18\ \mu m$. Note that behavior of this sort (including the rectangular-like beam features of Figs.3.2 and 3.6) is consistent with previous experimental observations (In Reference [35] only the self-trapped case was reported. Nevertheless, rectangular-like beam behavior at low bias and beam compression at high bias voltages has been observed as well). Moreover, had this beam (30 $\mu m$ FWHM) been fully coherent, it would have disintegrated as a result of speckle noise

instabilities. Next, let us consider what will happen at higher intensity ratios $r_T$. Figure 3.7 shows the propagation of an incoherent Gaussian beam when $V = 550$ $V$, $\theta_0 = 0.548^o$ and $r_T = 40$. At $z = 6$ $mm$, the beam now expands from 30 $\mu m$ FWHM to 87 $\mu m$. As in the coherent limit [23],[24],[59], this expansion is attributed to the saturation of the photorefractive nonlinearity when $r_T \gg 1$. In our simulations the angular width $\theta_0$ was also found to play an important role. Fig.3.8 depicts the propagation of such an incoherent Gaussian beam (30 $\mu m$ FWHM at the input) when $V = 550$ $V$, $r_T = 3$ and $\theta_0 = 0.8^o$. As the gure shows, the beam expands in a rectangular-like fashion to a FWHM of 51.3 $\mu m$ after 6 $mm$ of propagation. Clearly, for $\theta_0 = 0.8^o$ a higher bias voltage is required to overcome diffraction effects and indeed at $\sim 950$ $V$ self-trapping is reestablished.

## 3.4 Solitary wave solution

We would also like to point out that the in nite system of coupled nonlinear partial differential equations of Eq.3.4 does in fact admit solitary wave solutions. To obtain such a solution we write $U_j(x,z) = u_j(x,z)\exp\left\{i\left[(j\triangle\theta)^2(kz/2) - j\triangle\theta kx\right]\right\}$ and $u_j = r_j^{1/2}Q(x)\exp(i\mu z)$, where $Q(x)$ is a normalized function, i.e. $0 \leq Q(x) \leq 1$. Direct substitution of these latter forms in Eq.3.4 leads to the following ordinary

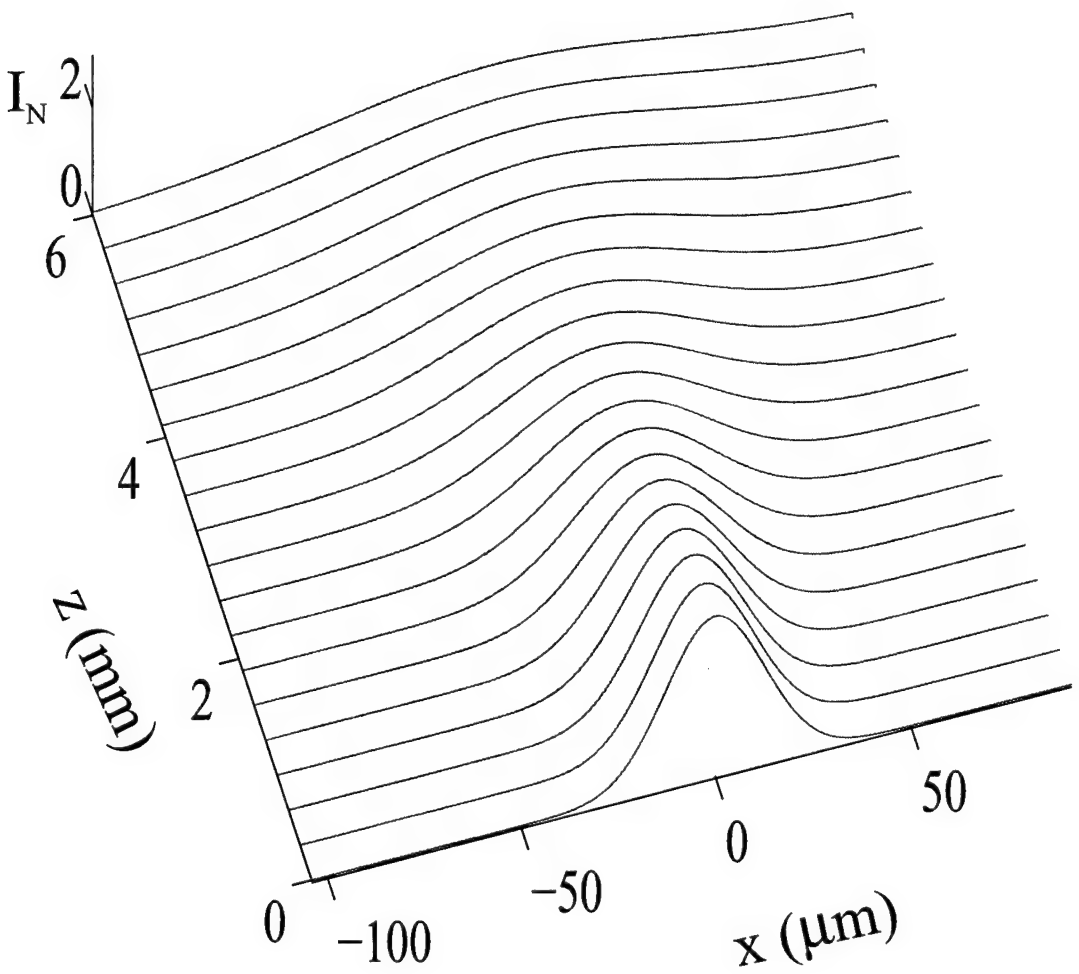


Figure 3.1: Diffraction of an incoherent Gaussian beam when its initial FWHM is *30 μm, $\theta_0$=0.548°, $r_T$=3.0.*

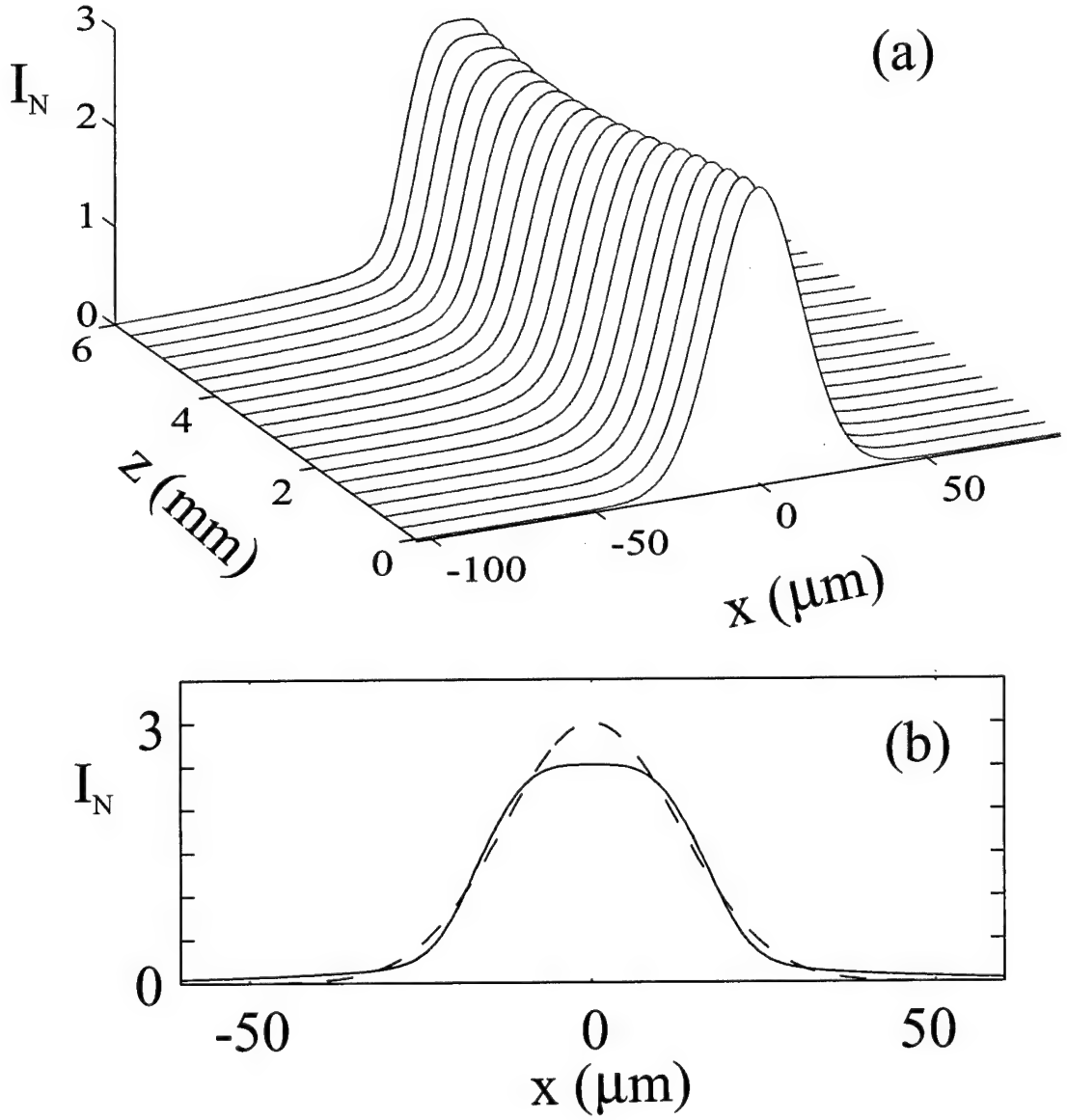


Figure 3.2: (a) Evolution of the normalized intensity profile resulting from an incoherent Gaussian beam when its initial FWHM is *30 μm*, $\theta_0=0.548^o$, $r_T=3.0$ and when the applied voltage is *400 V*; (b) The input (dashed curve) and output at $z=6$ *mm* (solid curve) intensities.

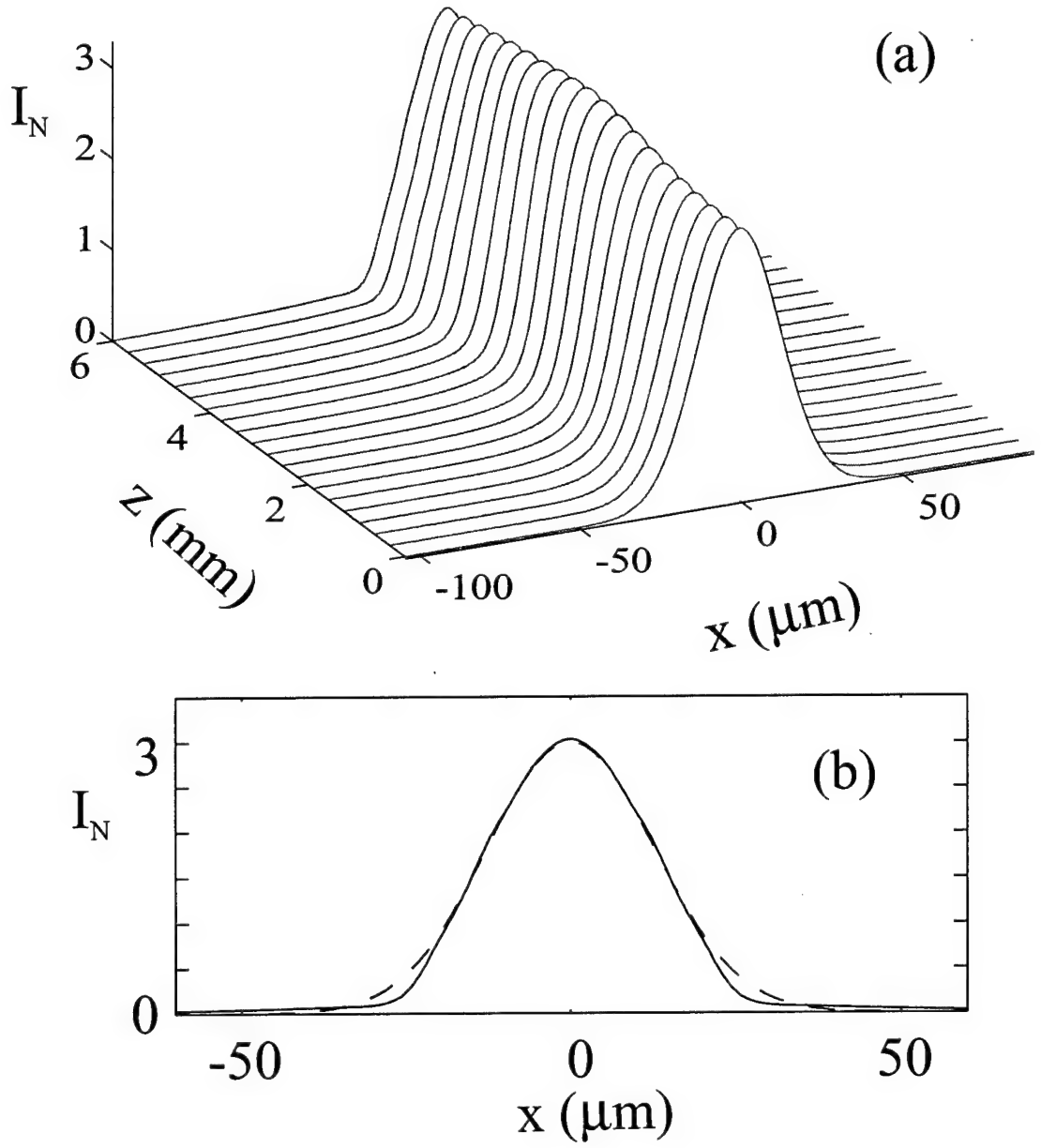


Figure 3.3: (a) Evolution of the normalized intensity profile resulting from an incoherent Gaussian beam when its initial FWHM is *30 μm*, $\theta_0=0.548^o$, $r_T=3.0$ and when the applied voltage is *550 V*; (b) The input (dashed curve) and output at *z=6 mm* (solid curve) intensities.

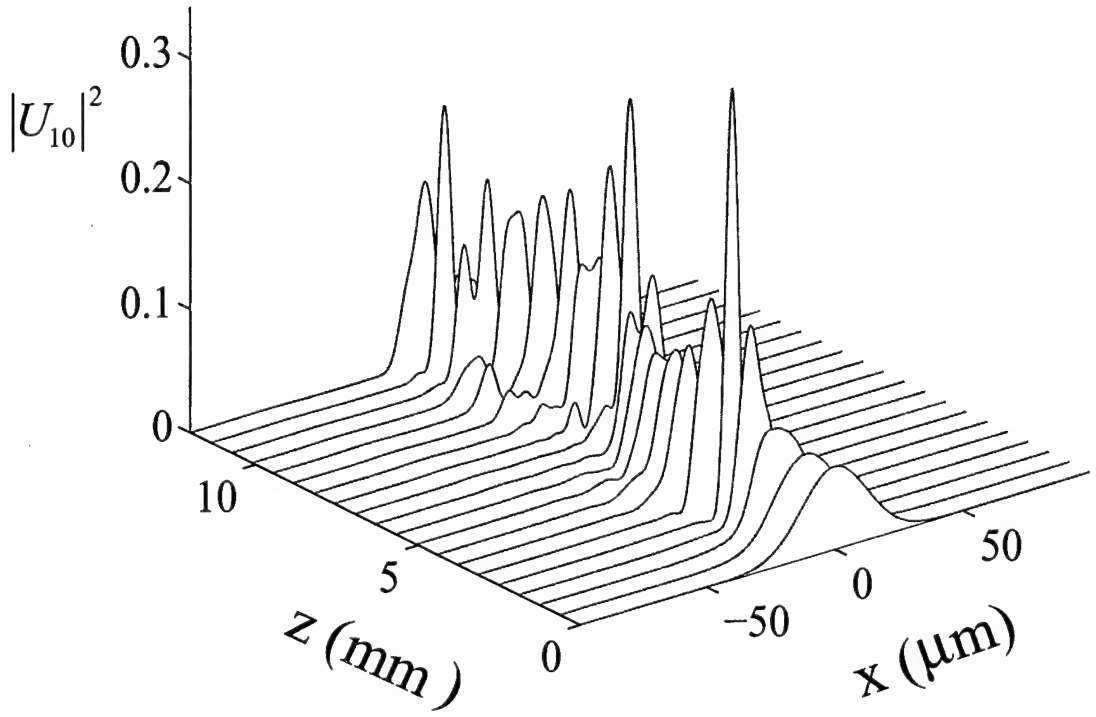


Figure 3.4: Intensity evolution of *10th* component $|U_{10}(x, \theta_0 \sim 0.27^o)|^2$ of the quasi-soliton shown in Fig.3.3.

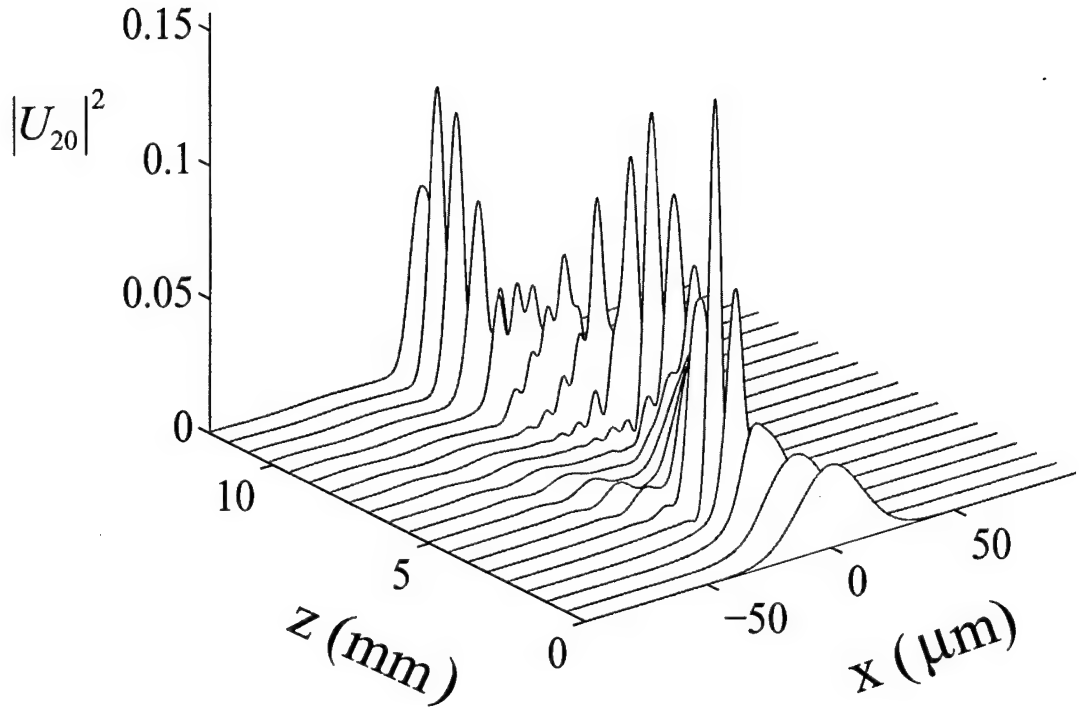


Figure 3.5: Intensity evolution of *20th* component $|U_{20}(x, \theta_0 \sim 0.54^o)|^2$ of the quasi-soliton shown in Fig.3.3.

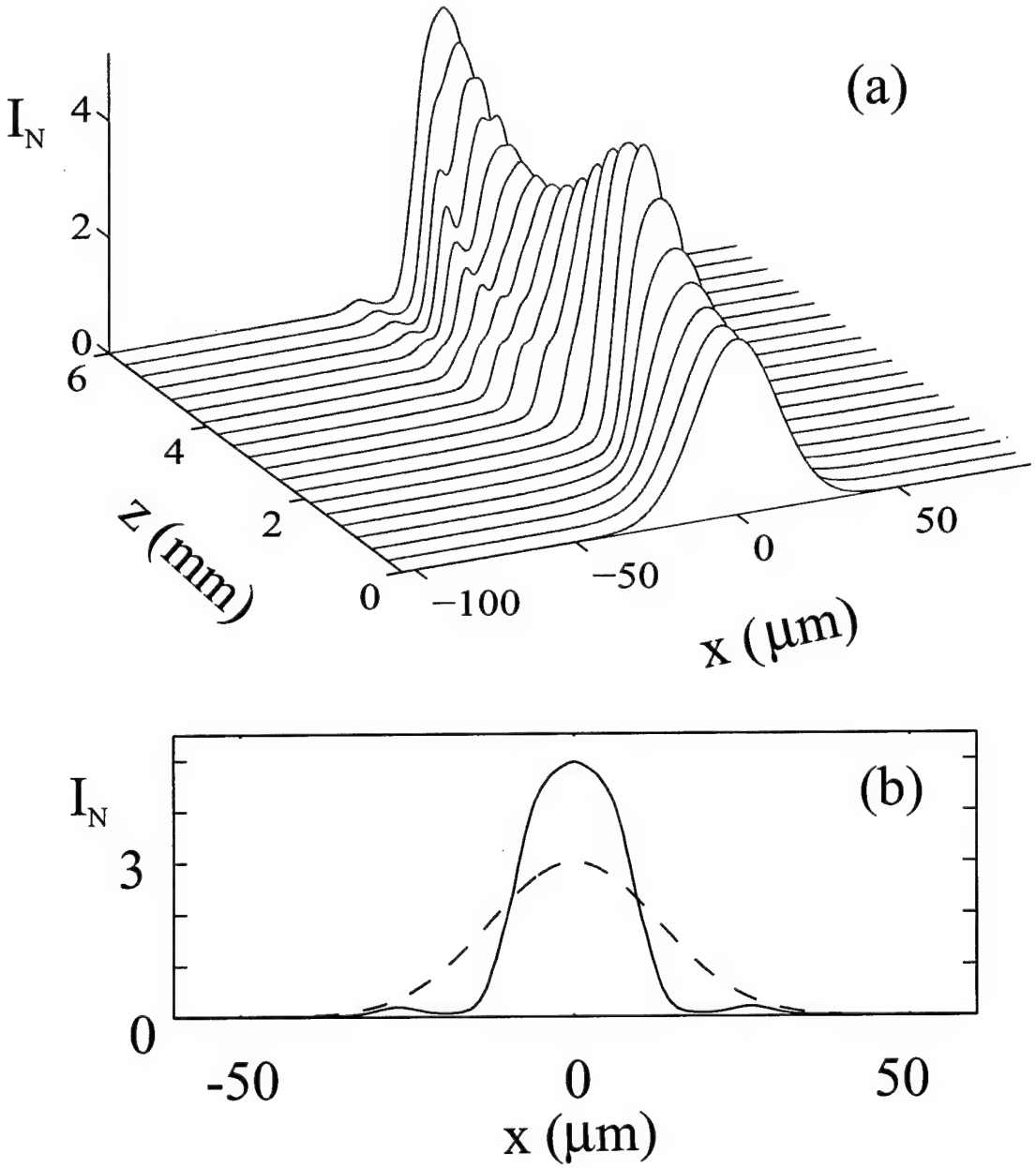


Figure 3.6: (a) Evolution of the normalized intensity profile resulting from an incoherent Gaussian beam when its initial FWHM is *30 μm*, $\theta_0=0.548^o$, $r_T=3.0$ and when the applied voltage is *1000 V*; (b) The input (dashed curve) and output at $z=6$ *mm* (solid curve) intensities.

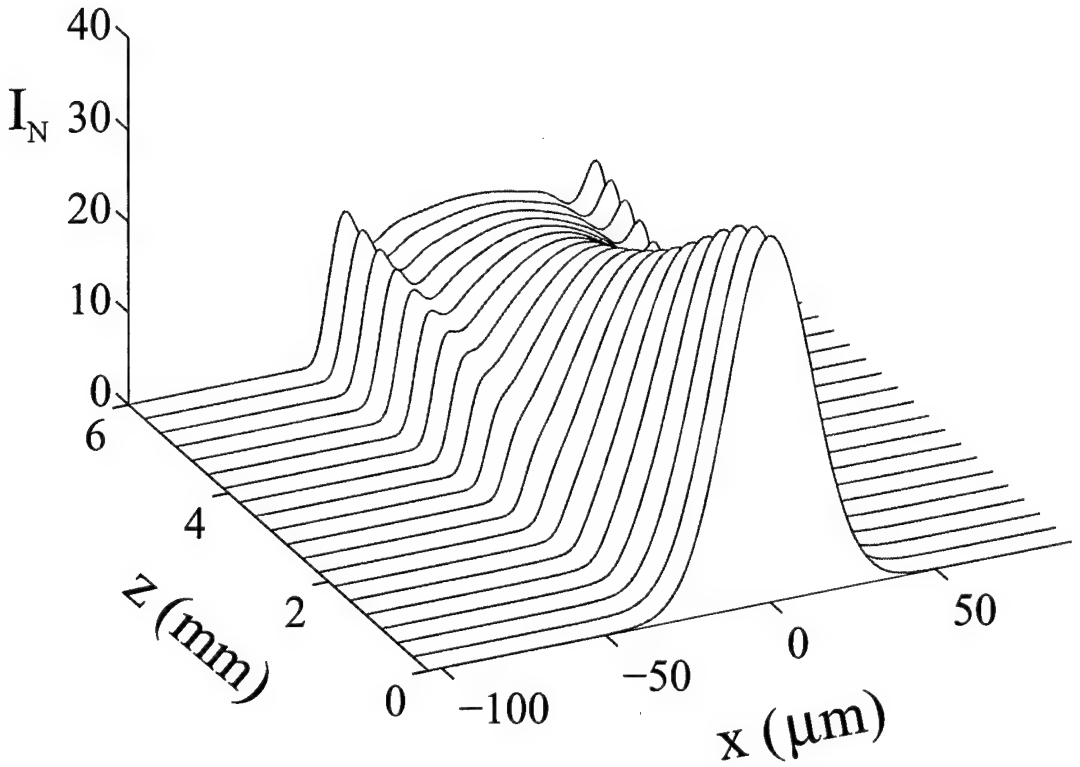


Figure 3.7: Propagation of an incoherent Gaussian beam in a biased SBN:75 crystal when the applied voltage is *550 V*, its initial FWHM is *30 μm*, $\theta_0=0.548^o$, $r_T=40$.

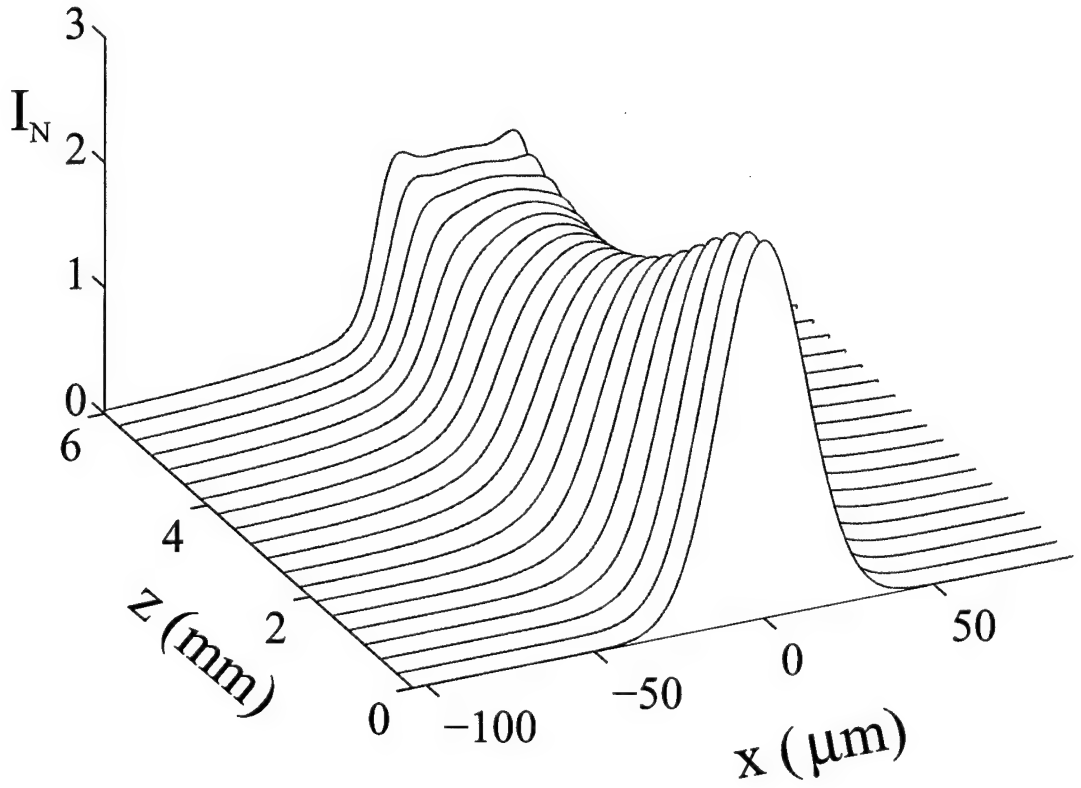


Figure 3.8: Propagation of an incoherent Gaussian beam in a biased SBN:75 crystal when the applied voltage is *550 V*, its initial FWHM is *30 μm*, $\theta_0=0.8^o$, $r_T=3.0$.

differential equation

$$\frac{d^2Q}{dx^2} - 2\mu kQ - \left(k^2 n_e^2 r_{33} E_0\right) \frac{Q}{1 + r_T Q^2} = 0 \tag{3.6}$$

which is known to allow bright solitons [23],[24],[59] when $E_0 > 0$ and

$$\mu = -\left(k n_e^2 r_{33} E_0 / 2 r_T\right) \ln(1 + r_T) \ .$$

In Eq.3.6, $r_T$ is the total intensity ratio, i.e. $r_T = \sum_j r_j$. We would like to emphasize however that physically this solitary wave solution has a limited range of applicability. More speci cally the employed $U_j - u_j$ transformation implies in reality that all the coherent components propagate in parallel along $z$. Thus a solitary solution of this sort may only be applicable when $\theta_0$ is quite small in which case all quasi-particles may tend to propagate almost in parallel after fusion. In fact, the above mentioned solution represents a generalization of the so-called incoherent coupled photorefractive soliton pairs previously discussed in the literature [50],[34].

## 3.5 Conclusions

In conclusion, a theory of incoherent self-trapping in biased photorefractives has been developed. It has been shown that this process can be effectively described by an in nite set of coupled nonlinear Schrödinger-like equations provided they have been initially weighted with respect to incoherent angular power spectrum of the

source. Relevant examples have been provided. Our numerical computations were in close agreement with recent experimental data. We wish to emphasize that our theoretical approach applies not only to photorefractive media but also to any other nonlinear material whose temporal response time is much bigger than the phase uctuation time of an optical beam.

# Chapter 4

# Incoherent spatial solitons in saturable nonlinear media of the logarithmic type

By using the coherent density approach, it is shown that partially incoherent spatial solitons are possible in saturable nonlinear media. This is demonstrated by means of an exact Gaussian solution in the case where the saturable nonlinearity is of the logarithmic type. The conditions necessary to establish these soliton states as well as their associated characteristics are discussed in detail. Pertinent examples are provided to further elucidate their behavior.

## 4.1 Introduction

In the last chapter, a theory was developed in order to explain the observed incoherent self-focusing behavior in biased photorefractive media [79]. More speci cally, it was found that this process can be effectively described by an in nite set of nonlinear Schrödinger-like equations provided that they are initially appropriately weighted with respect to the incoherent angular power spectrum of the source. The numerical simulations resulting from this theoretical approach [79] were found to be in good agreement with the experimental observations of Ref. [35]. It is also important to note that these experimental [35] and theoretical [79] investigations have demonstrated that a stationary incoherent beam or a quasi-soliton could exist under appropriate conditions. Nevertheless, there is no solid evidence (in terms of an analytical solution) as to whether such incoherent solitons exist or not.

In this chapter, we show that partially incoherent spatial solitons are indeed possible in saturable nonlinear media. This is demonstrated by means of an exact Gaussian soliton solution in the case where the saturable nonlinearity is the logarithmic type. The conditions necessary to establish these incoherent soliton states as well as their associated characteristics are discussed in detail. Our analysis indicates, that, for a given strength of the logarithmic nonlinearity, these solitons exist only within a certain range of incoherent angular spectral widths. Relevant computer simulations are provided to further elucidate their behavior.

## 4.2 Theoretical formulation

Let us consider a saturable nonlinear medium, the refractive index of which varies logarithmically with intensity $I$, i.e. ,

$$n^2(I) = n_0^2 + n_2 \ln(I/I_t) \tag{4.1}$$

where $n_0$ is the linear refractive index of this material, $n_2$ is a positive dimensionless coefficient associated with the strength of the nonlinearity and $I_t$ is a threshold intensity. Note that a logarithmic nonlinearity of this sort has been recently employed by Snyder and Mitchell in their study of mighty morphing spatial solitons and bullets [80]. To avoid any unphysical singularities, we may assume that the $\ln(I/I_t)$ nonlinearity results from the more realistic $\ln(1 + I/I_t)$ model in the limit $I \gg I_t$. Let us also assume that the light beam propagates along the $z$ axis and diffracts only in the $x$ direction, i.e., for simplicity we are dealing with a planar incoherent beam. Moreover, we will make the important assumption that the nonlinear material involved responds much slower than the characteristic phase uctuation time across the optical beam as in the case of photorefractives. As a result, the material will experience only the time averaged intensity. Under these conditions and by following the procedure given in the last chapter, one may then show that the normalized intensity $I_N = I/I_t$ of this incoherent light beam obeys the following set

of equations:

$$i\left\{\frac{\partial f}{\partial z}+\theta\frac{\partial f}{\partial x}\right\}+\frac{1}{2k}\frac{\partial^2 f}{\partial x^2}+\frac{k_0 n_2}{2n_0}\ln\left(I_N\left(x,z\right)\right)f=0 \tag{4.2}$$

where

$$I_N\left(x,z\right)=\int_{-\infty}^{\infty}\left|f\left(x,z,\theta\right)\right|^2 d\theta \tag{4.3}$$

and at $z=0$,

$$f\left(z=0,x,\theta\right)=r^{1/2}G_N^{1/2}\left(\theta\right)\phi_0\left(x\right) \quad . \tag{4.4}$$

In the above equations, $f$ represents the so-called coherent density, $\theta$ is an angle in radians with respect to the $z$ axis, $k=k_0 n_0$ and $k_0=2\pi/\lambda_0$ . $G_N\left(\theta\right)$ is the normalized angular power spectrum of the incoherent source, $\phi_0\left(x\right)$ is the input spatial modulation function and $r$ is an intensity ratio, that is $r=\max\left(I_N\right)$ . Note that, in the last chapter, the process was described in terms of the so-called coherent components which are in fact a discrete version of the coherent density employed here. Let us now assume that the input intensity pro le as well as the incoherent angular power spectrum are Gaussian, i.e., $\phi_0\left(x\right)=\exp\left(-x^2/2x_0^2\right)$ and $G_N\left(\theta\right)=\left(\pi^{1/2}\theta_0\right)^{-1}\exp\left(-\theta^2/\theta_0^2\right)$. In this case, the input intensity pro le can be obtained from Eqs.4.3 and 4.4 and it is given by

$$I_N\left(x,z=0\right)=r\exp\left(-x^2/x_0^2\right) \quad . \tag{4.5}$$

For convenience, we will also employ the following dimensionless coordinates and variables; $\xi=z/kx_0^2$, $s=x/x_0$, $\alpha=kx_0\theta$ and $\beta=\left(n_2/2\right)\left(k_0x_0\right)^2$.

At this point let us also assume for a moment that the intensity of the incoherent beam remains invariant or stationary during propagation. If we let $f = F\exp(i\beta\xi\ln r)$, we then obtain from Eqs.4.2 and 4.5

$$i\left\{\frac{\partial F}{\partial \xi}+\alpha\frac{\partial F}{\partial s}\right\}+\frac{1}{2}\frac{\partial^2 F}{\partial s^2}-\beta s^2 F=0 \tag{4.6}$$

where at $\xi = 0$, $F = \hat{r}^{1/2}\exp\left(-\theta^2/2\theta_0^2\right)\exp\left(-s^2/2\right)$ and $\hat{r} = r\pi^{-1/2}\theta_0^{-1}$. Equation 4.6 can now be solved using a Gaussian wavepacket solution[81], i.e.

$$F = A(\xi)\exp\left[-\frac{\eta^2}{2w^2(\xi)}\right]\exp\left\{i\left[g(\xi)+\eta p(\xi)+\eta^2 q(\xi)\right]\right\} \tag{4.7}$$

where $\eta = s - v(\xi)$. $w(\xi)$ represents the variable spot-size of the coherent density and $v(\xi)$ is the displacement of this wavepacket along the $x$ axis. Equation 4.7 satis es Eq. 4.6 provided that the following relations hold true: $A^2 w = A_0^2 w_0$, $\dot{v} = \alpha + p$, $q = \dot{w}/2w$, $\dot{p} = -2\beta v$, $\dot{g} = (1/2)(p^2 - w^{-2} - 2\beta v^2)$ and $\dot{q} = -(1/2)(4q^2 + 2\beta - w^{-4})$ where $\dot{v} = dv/d\xi$ etc. The initial conditions (at $\xi = 0$) associated with these equations are given by: $A_0 = \hat{r}^{1/2}\exp\left(-\theta^2/2\theta_0^2\right)$, $w_0 = 1$, $p_0 = v_0 = 0$ and $\dot{w} = 0$. In that case, it can be readily shown that

$$v(\xi) = \alpha(2\beta)^{-1/2}\sin\left[(2\beta)^{1/2}\xi\right] \tag{4.8}$$

and

$$w^2(\xi) = \frac{2\beta+1}{4\beta}+\frac{(2\beta-1)}{4\beta}\cos\left[(8\beta)^{1/2}\xi\right] \quad . \tag{4.9}$$

The rest of the variables $A$, $p$, $g$, and $q$ can then be deduced by directly employing the results of Eqs. 4.8 and 4.9.

In turn, from Eqs. 4.7, 4.8 and 4.9, the normalized intensity $I_N$ can be obtained and it is given by

$$I_N = \frac{r}{Q^{1/2}} \exp\left[-\frac{s^2}{Q}\right] \tag{4.10}$$

where

$$Q = w^2(\xi) + \frac{k^2 x_0^2 \theta_0^2}{2\beta} \sin^2\left[(2\beta)^{1/2}\xi\right] \quad . \tag{4.11}$$

Seeking a soliton solution, we must require that the intensity $I_N$ remains stationary during propagation. From Eqs. 4.5 and 4.10 it is evident that this is possible only if $Q = 1$ for all values of $z$ or $\xi$. Combining the results of Eqs. 4.9 and 4.11 we then readily obtain the condition necessary to establish a partially incoherent spatial soliton, which is $2\beta - 1 = k^2 x_0^2 \theta_0^2$, or

$$x_0 = \frac{1}{k_0\sqrt{n_2 - n_0^2\theta_0^2}} \quad . \tag{4.12}$$

Therefore, given the strength of the logarithmic saturable nonlinearity $n_2$ and the width of the incoherent angular power spectrum of the source $\theta_0$, Eq. 4.12 uniquely determines the spatial width of the partially incoherent spatial soliton state that can propagate in this material. In this case, the partially incoherent soliton beam maintains an invariant Gaussian intensity pro le, i.e. $I_N = r\exp(-x^2/x_0^2)$, even though the associated coherent density function $f$ evolves considerably as a function of $\xi$ or $z$. In the special case where $\theta_0 \to 0$ or $G_N(\theta) = \delta(\theta)$, our result correctly reduces to the coherent spatial soliton limit ($x_0 = k_0^{-1} n_2^{-1/2}$) previously obtained by

Snyder and Mitchell [80]. On the other hand, Eq. 4.12 shows that as $\theta_0$ increases, the soliton width $x_0$ increases. Nevertheless, it is clear from Eq. 4.12, that there is an upper limit for the incoherent angular spectrum width $\theta_0$ above which a soliton beam is not allowed. This upper value $\theta_{0\,\max}$ is equal to $n_2^{1/2}/n_0$.

## 4.3 Results and discussion

We will now illustrate our results by means of relevant examples. Let us consider a logarithmically saturable nonlinear medium with $n_0 = 2$ and $n_2 = 10^{-4}$. Moreover let the optical wavelength $\lambda_0$ be 0.5 $\mu m$. For this set of parameters, the maximum source angular spectrum width $\theta_0$ that can be self-trapped is $\theta_{0\,\max} = 5\ mrad$. Let us also assume that the angular power spectrum width $\theta_0$ of the incoherent source is $\theta_0 = 4.5\ mrad$. In this case $x_0 \simeq 18\ \mu m$ and thus the intensity FWHM of this partially-incoherent spatial soliton is $\sim 30\ \mu m$. Figure 4.1 shows the stationary propagation of this soliton as obtained by numerically solving Eqs. 4.2 and 4.3. In all our computations we have used the better behaved $\ln(1 + I/I_t)$ nonlinearity with an intensity ratio of one thousand ($r = 10^3$). Note that had this same incoherent beam been launched in a linear material ($n_0 = 2$, $n_2 = 0$) it would have diffracted to a FWHM of $\sim 90\ \mu m$ after a distance of 1 $cm$. Fig.4.2 on the other hand, depicts the coherent density associated with this soliton beam when $\theta = 3\ mrad$.

Evidently, the density periodically expands and contracts during propagation

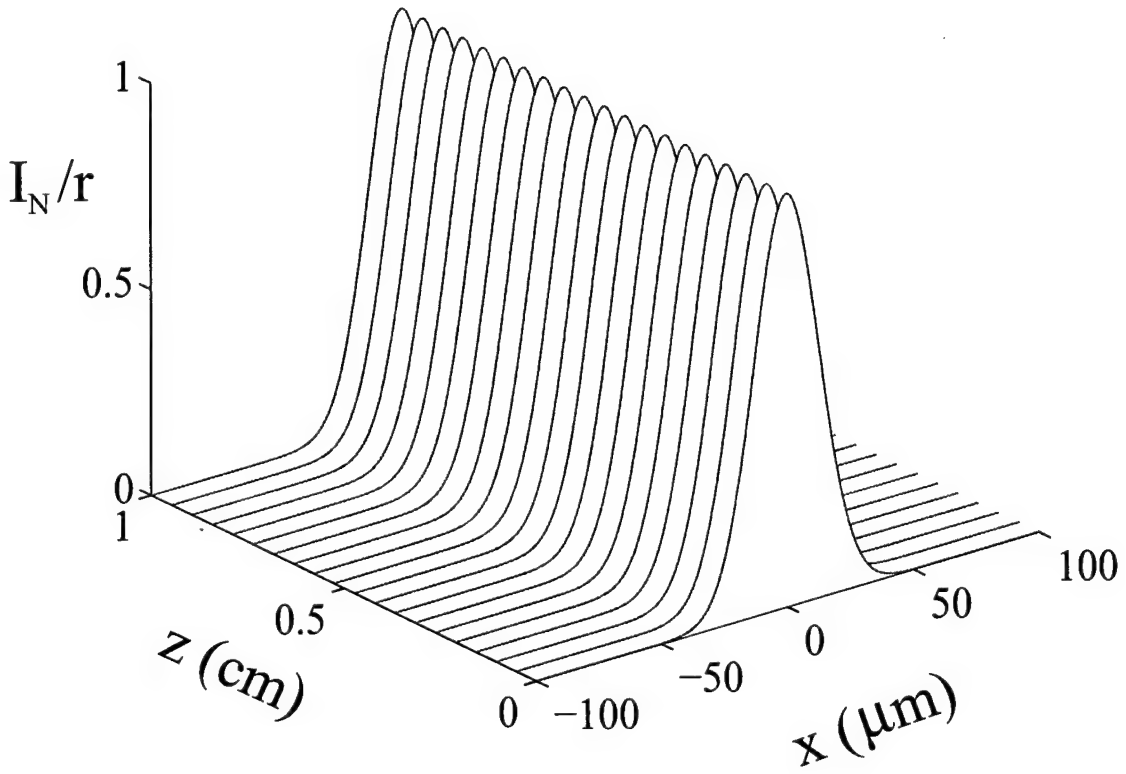


Figure 4.1: Stationary propagation of a partially-incoherent spatial soliton when $x_0=18\ \mu m$, $\theta_0=4.5\ mrad$ and $n_2=10^{-4}$.

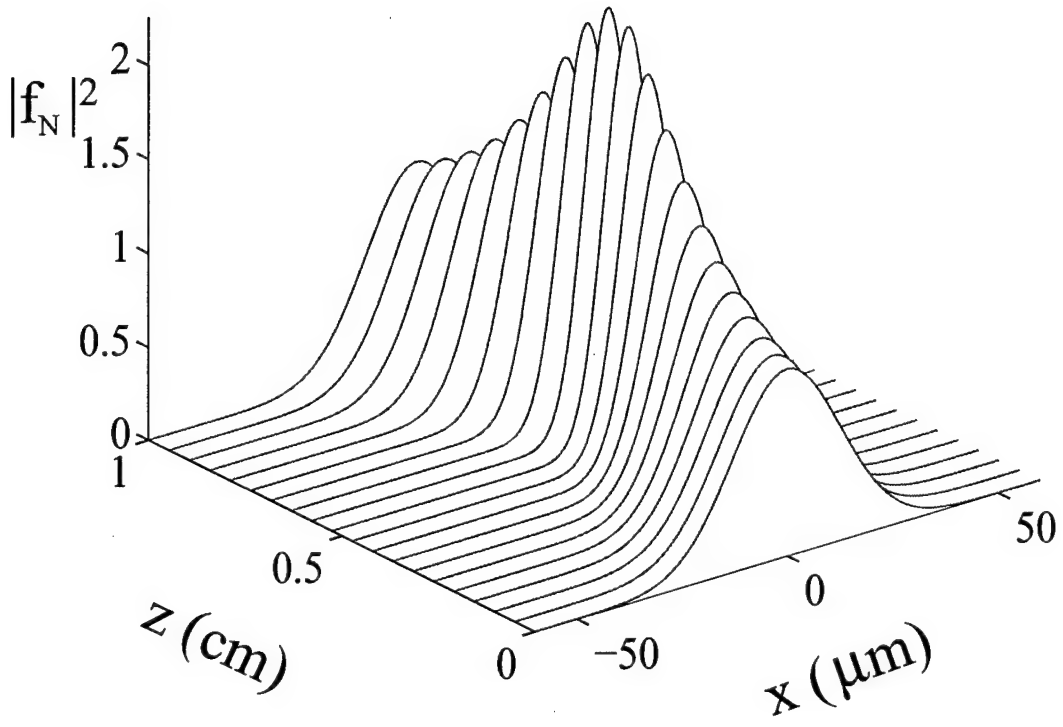


Figure 4.2: Evolution of the normalized coherent density function *f* associated with the incoherent soliton shown in Fig.4.1.

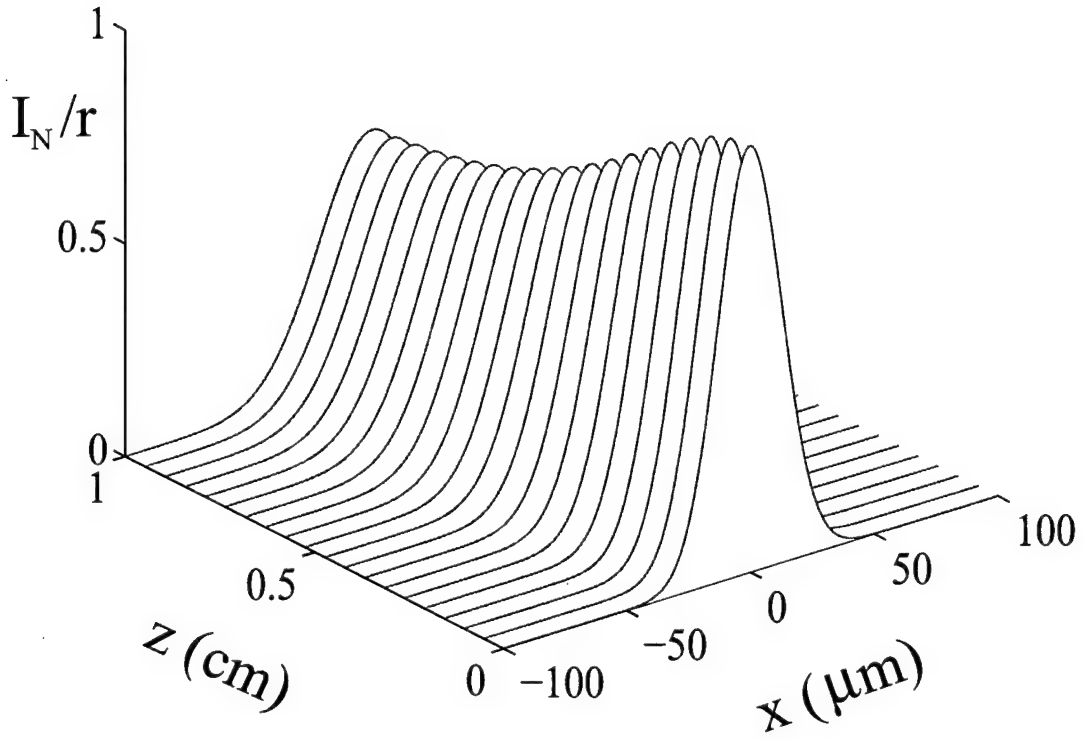


Figure 4.3: Propagation of a partially incoherent Gaussian beam in logarithmically saturable nonlinear medium when $x_0$=18 μm, $\theta_0$=6.0 mrad.

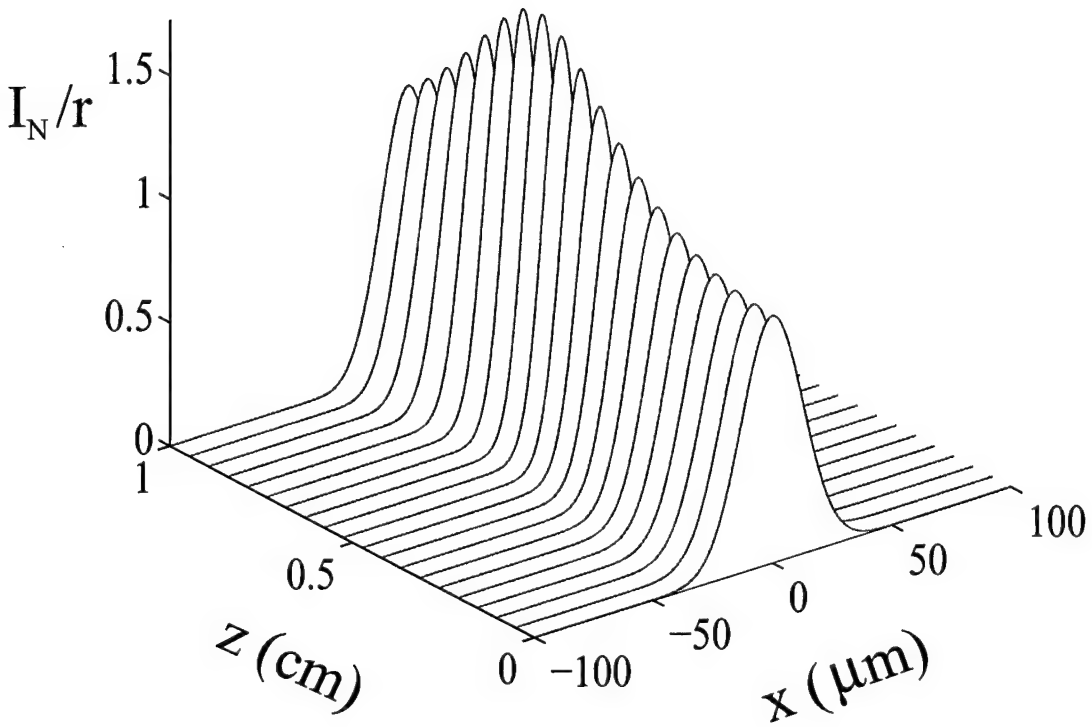


Figure 4.4: Propagation of a partially incoherent Gaussian beam in logarithmically saturable nonlinear medium when $x_0$=18 μm, $\theta_0$=4.0 mrad.

and oscillates around the center of the beam. In spite of this, the overall intensity pro le $I_N$ of the incoherent light beam remains stationary as long as Eq. 4.12 is satis ed. Figure 4.3 shows what would happen to this Gaussian incoherent beam if $\theta_0 = 6\ mrad$ ($\theta_0$ is above the upper bound $\theta_{0\max} = 5\ mrad$) provided that again $x_0 = 18\ \mu m$. In this case, the beam rst expands and then compresses and at $z = 1\ cm$ its intensity FWHM is $\sim 52\ \mu m$. If $\theta_0$ is, on the other hand, lower than the that prescribed by Eq. 4.12, say $\theta_0 = 4\ mrad$ and for $x_0 = 18\ \mu m$, then the beam exhibits cyclic compressions and expansions as shown in Fig.4.4. Even though our analysis does not directly apply to biased photorefractive crystals (where the saturable nonlinearity is different), it provides valuable insight into the considerable more complex incoherent dynamics in this material system. In fact, the scenario depicted in Figs.4.1, 4.3 and 4.4 is quite reminiscent of the incoherent wave dynamics previously encountered in biased photorefractives in the previous chapter [35],[79].

## 4.4 Conclusions

In conclusion we have shown that partially incoherent spatial solitons are possible in saturable nonlinear media. An exact Gaussian solution was obtained in the case where the nonlinearity is of the logarithmic type. These incoherent Gaussian solitons can exist as long as their spatial width is appropriately interrelated with the strength of the nonlinearity and the width of the incoherent angular power spectrum of the

source. The behavior of these beams above and below this limit was also investigated using computer simulations.

# Chapter 5

# Multimode Incoherent Spatial Solitons in Non-Instantaneous Kerr Media

In this chapter, by using the self-consistent multimode approach, we show that incoherent solitons are possible in non-instantaneous Kerr-like nonlinear media. The coherence characteristics of multimode incoherent spatial solitons in this material system are investigated. Other properties of these incoherent solitons are also discussed as a function of their modal composition.

## 5.1 Introduction

In Chapter 3, the coherent density approach, describing propagation and self-focusing of partially spatially-incoherent light beams in nonlinear media is developed. In the last chapter, this approach was found to lead to closed form solutions for logarithmic type of nonlinearities [82]. It has been also shown [83], that a self-consistent multimode method can also be used to investigate incoherent soliton formation in nonlinear materials. This latter model seeks, in a self-consistent fashion, multimode soliton solutions whose total intensity can be obtained via intensity superposition of all the modes guided within the nonlinearly induced waveguide. This method is capable of identifying incoherent spatial soliton states, their range of existence and coherence properties [83]. Another approach for describing broad incoherent bright solitons was also suggested by Snyder and Mitchell [84]. This ray model is to some extend related to the Vlasov transport description previously suggested by Hasegawa in the theory of random-phase solitons in plasmas [85], [86], [87].

It is worth noting that incoherent solitons, as viewed from the perspective of the self-consistent modal theory, are in fact related to the so-called incoherently coupled solitons in photorefractives [32]-[34],[50] or to the vector solitons in Kerr media [88]. Within the context of incoherently coupled solitons [32]-[34],[50], Vysloukh et al [89],[90] has shown that multi-component coupled soliton modes can be incoherently

superimposed in weakly saturating photorefractive crystals. We would like to emphasize however that there is a subtle difference between self-trapping an incoherent beam and creating a multi-component soliton. This difference is due to the statistically varying modal weights of the incoherent beam. Consider first a situation where self-trapping occurs from an incoherent light source. During self-trapping, the beam continuously excites several modes of the jointly induced waveguide, established by the time averaged intensity of the speckled beam itself. If the time averaged intensity is decomposed into the modes of the induced waveguide, each mode will have a certain coupling amount or weight. On the other hand, when multiple laser beams are incoherently superimposed (engineering the beam profiles), the relative modal weights are time independent and only the relative phase between each pair of modes changes with time. As far as the crystal could tell, the two situations are exactly the same. The difference lies in the time dependence of the mode occupancies.

In this chapter we demonstrate that incoherent spatial solitons are possible in non-instantaneous Kerr-like media. Closed form solutions are obtained using the self-consistent multimode approach [83]. It is shown that the intensity profile of these incoherent soliton states is of the $\mathrm{sech}^2\,(x/x_0)$ type. Moreover, our analysis indicates that, in this case, the peak intensity and spatial width of these incoherent spatial solitons are related to the number of allowed modes. The coherence properties of these soliton states are investigated in detail. Relevant examples are provided.

## 5.2 Self-consistent multimode approach

We consider a spatially partially-incoherent optical beam which propagates in a nonlinear self-focusing Kerr-like medium along the $z$-axis. For simplicity we assume that this beam is planar, that is, it diffracts only along $x$ the direction. The refractive index of this Kerr-like material varies linearly with optical intensity $I$ i.e. let $n^2 = n_0^2 + n_2 I$, where $n_0$ is the linear part of the refractive index and $n_2$ is the nonlinear Kerr coefficient. We also make the important assumption that the nonlinearity responds much slower that the characteristic phase uctuation time across the incoherent beam, so as to avoid speckle-induced lamentation instabilities [91]. In this regime, the material will experience only the time averaged beam intensity. For example, such noninstantaneous Kerr nonlinearities can be encountered in biased photorefractives in the low-intensity regime, (i.e., when the so-called dark irradiance is much larger than the intensity of the optical beam [23],[24]) or in materials with thermal nonlinearities [92],[93]. Furthermore, let the total electric eld $E$ of this spatially incoherent beam be written in terms of a slowly varying envelope $U$, that is, let $E = U \exp(ikz)$, where the wavevector $k$ is given by $k = k_0 n_0 = (2\pi/\lambda_0) n_0$ and $\lambda_0$ is the free-space wavelength. In this case, it can be readily shown that the envelope $U$ evolves according to:

$$i\frac{\partial U}{\partial z} + \frac{1}{2k}\frac{\partial^2 U}{\partial x^2} + \frac{k_0^2 n_2 I}{2k} U = 0 \tag{5.1}$$

Let us now assume that the incoherent spatial soliton in this Kerr-like medium has a $\mathrm{sech}^2(x/x_0)$ intensity pro le, that is

$$I = I_0 \sec \mathrm{h}^2 (x/x_0) \tag{5.2}$$

where represents the peak intensity of the optical incoherent multimode beam and $x_0$ is associated with its spatial extent. In this case, Eq. 5.1 takes the form

$$i\frac{\partial U}{\partial \xi} + \frac{1}{2}\frac{\partial^2 U}{\partial \eta^2} + \frac{\alpha^2}{2} \sec \mathrm{h}^2 (\eta)\, U = 0 \tag{5.3}$$

In this equation we have used normalized coordinates and quantities, i.e., $\eta = x/x_0$, $\xi = z/kx_0^2$, and $\alpha^2 = k_0^2 x_0^2 n_2 I_0$. The incoherent spatial soliton solutions of this equation can then be obtained by expressing the optical envelope through a superposition of all the modes involved, that is, $U \propto \sum_m c_n^m u_n^m (\eta) \exp i\beta_m (\xi)$, where $c_n^m$ are the mode-occupancy coefficients that vary randomly with time, $u_n^m (\eta)$ is the pro le of the $m$th-order mode, and $\beta_m$ its phase constant. The discrete index $n$ stands for the total number of modes allowed in the system. By substituting this form of $U$ into Eq. 5.3, we obtain, for each mode, the following ordinary differential equation:

$$\frac{\partial^2 u_n^m}{\partial \eta^2} + \left[\alpha^2 \sec \mathrm{h}^2 (\eta) - 2\beta_m\right] u_n^m = 0 \quad . \tag{5.4}$$

The mode pro les $u_n^m(\eta)$ and their phase constants $\beta_m$ can then be found by solving Eq. 5.4. In order to nd the mode occupancy coefficients, the self-consistency of this solution must be satis ed, i.e., the total intensity of this incoherent beam is given

by Eq. 5.2. The self-consistency method relies on the basic concept that a soliton itself is a mode of the self-induced (via the nonlinearity) waveguide. This was first suggested by Askar yan [94] and later developed into a self-consistency methodology by Snyder at al [95]-[98] as means to analyze coherent solitons.

## 5.3 Results and Discussion

To find the modal structure of these multimode incoherent spatial solitons, we first adopt the transformation $t = \tanh(\eta)$, in which case Eq.5.4 takes the form:

$$\left(1-t^2\right)\frac{d^2u_n^m}{dt^2} - 2t\frac{du_n^m}{dt} + \left[\alpha^2 - \frac{2\beta_m}{(1-t^2)}\right]u_n^m = 0 \quad . \tag{5.5}$$

It can now be easily shown that, when $\alpha^2 = n(n+1)$, where $n = 1, 2, ...,$ (an integer determined by the amount of nonlinearity) and $m = 1, 2, ..., n$, the allowed modes can be expressed in terms of associated Legendre functions [99], i. e.,

$$u_n^m(\eta) = P_n^m(\tanh(\eta)) \quad , \tag{5.6}$$

and $\beta_m = m^2/2$, where $P_n^m(x)$ are associated Legendre functions of the first kind. In general, $P_n^m(x) = (1-x^2)^{m/2} d^m P_n(x)/dx^2$ where $P_n(x)$ denote Legendre polynomials. The value of the integer $n$ (associated with $\alpha^2$ or the degree of nonlinearity) represents the number of allowed modes in the self-induced waveguide and $m$ the mode index for this case. Note that the lowest order mode occurs

when $m = n$ whereas the highest at $m = 1$. For a given value of $n$, the statistically varying optical field of the incoherent spatial soliton is given by $U(\eta, \xi) \propto \sum_{m=1}^{n} c_n^m P_n^m (\tanh(\eta)) \exp(im^2\xi/2)$. Note that the self-consistency condition also requires that the mode-occupancy coefficients also depend on the number of modes $n$. The time averaged intensity of this beam can then be evaluated from

$$\left\langle |U|^2 \right\rangle \propto I = \sum_{m=1}^{n} \left\langle |c_n^m|^2 \right\rangle [P_n^m (\tanh(\eta))]^2 \quad , \tag{5.7}$$

where we made use of the fact that under incoherent excitation the time-average of cross-interference terms among modes is zero, $\left\langle c^i (c^j)^* \right\rangle \propto \delta_{ij}$. Finally, Eq. 5.7 can be used to obtain the mode-occupancy coefficients $c_n^m$ that self-consistently lead to the incoherent spatial soliton $I = I_0 \operatorname{sech}^2(\eta)$ assumed in the very beginning of this analysis. It proves convenient to normalize the eigenmodes in the following fashion: $\widetilde{u}_n^m(\eta) = \left[\frac{\langle |c_n^m|^2 \rangle}{I_0}\right]^{1/2} u_n^m(\eta)$ or equivalently $I_0 \sum_{m=1}^{n} [\widetilde{u}_n^m(\eta)]^2 = I_0 \operatorname{sech}^2(\eta)$. The functional form of the normalized eigenfunctions $\widetilde{u}_n^m(\eta)$ is given in Appendix A. Figure 5.1 depicts the normalized mode profiles, $\widetilde{u}_n^m(\eta)$ for a three-component ($n = 3$) multimode incoherent soliton whereas Fig. 5.2 for a four component structure ($n = 4$).

Having found closed form solutions for these spatial incoherent solitons, the question naturally arises as to what factors contribute to their spatial FWHM (full-width half-maximum). To answer this question one has to consider the expression $\alpha^2 = n(n+1)$. More specifically, since $\alpha^2 = k_0^2 x_0^2 n_2 I_0$, then given the number of

guided modes $n$, and the peak intensity $I_0$, the spatial width $x_0$ can be determined. In turn one quickly nds the following result: $x_0 = [n(n+1)/k_0^2 n_2 I_0]^{1/2}$. Using Eq. 5.2 and provided that $n$ is known, the intensity FWHM of these soliton states $w_n$, can be calculated from $w_n = 1.76x_0$, and thus

$$w_n = \frac{1.76}{k_0}\left[\frac{n(n+1)}{n_2 I_0}\right]^{1/2} \quad . \tag{5.8}$$

Note that when $n = 1$ ( single-mode soliton), this latter expression is in full agreement with the results previously obtained for coherent Kerr spatial solitons [100]. Equation 5.8 can also be written in terms of a normalized FWHM $(w_n/\lambda_0)$ as function of the maximum induced nonlinear index change $(\Delta n = n_2 I_0)$, i.e., $w_n/\lambda_0 = (1.76/2\pi)[n(n+1)/\Delta n]^{1/2}$. Figure 5.3 shows the dependence of the normalized intensity FWHM of these incoherent optical solitons on $\Delta n$ for different values of $n$. This gure clearly shows that for a given nonlinear index change, the intensity FWHM tends to increase with the number of modes involved. This should have been anticipated since the incoherency increases with $n$. It is also important to note that in Fig.5.3, the existence curves are discrete as opposed to continuum range found in Ref. [83]. This is due to the speci c $\mathrm{sech}^2(x/x_0)$ intensity shape assumed at the beginning of our analysis.

We now investigate the coherence properties of these spatial solitons. This is done by evaluating the complex coherence factor $\mu_{12}$ of these soliton states [69], which is given by $\mu_{12}(\eta, \eta+\delta) = \langle U(\eta,\xi)\, U^*(\eta+\delta,\xi)\rangle / \left[\left\langle |U(\eta)|^2\right\rangle \left\langle |U(\eta+\delta)|^2\right\rangle\right]^{1/2}$, where

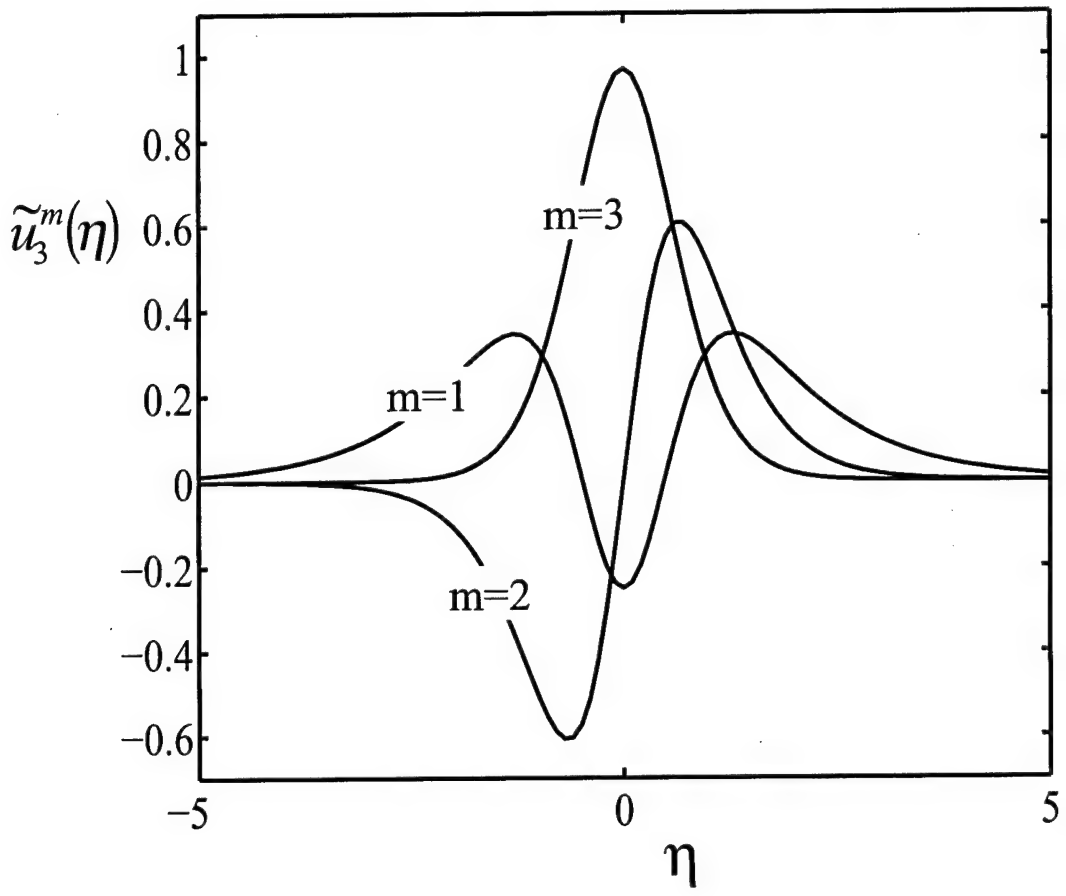


Figure 5.1: Normalized mode-profiles as a function of $\eta$ for $n=3$.

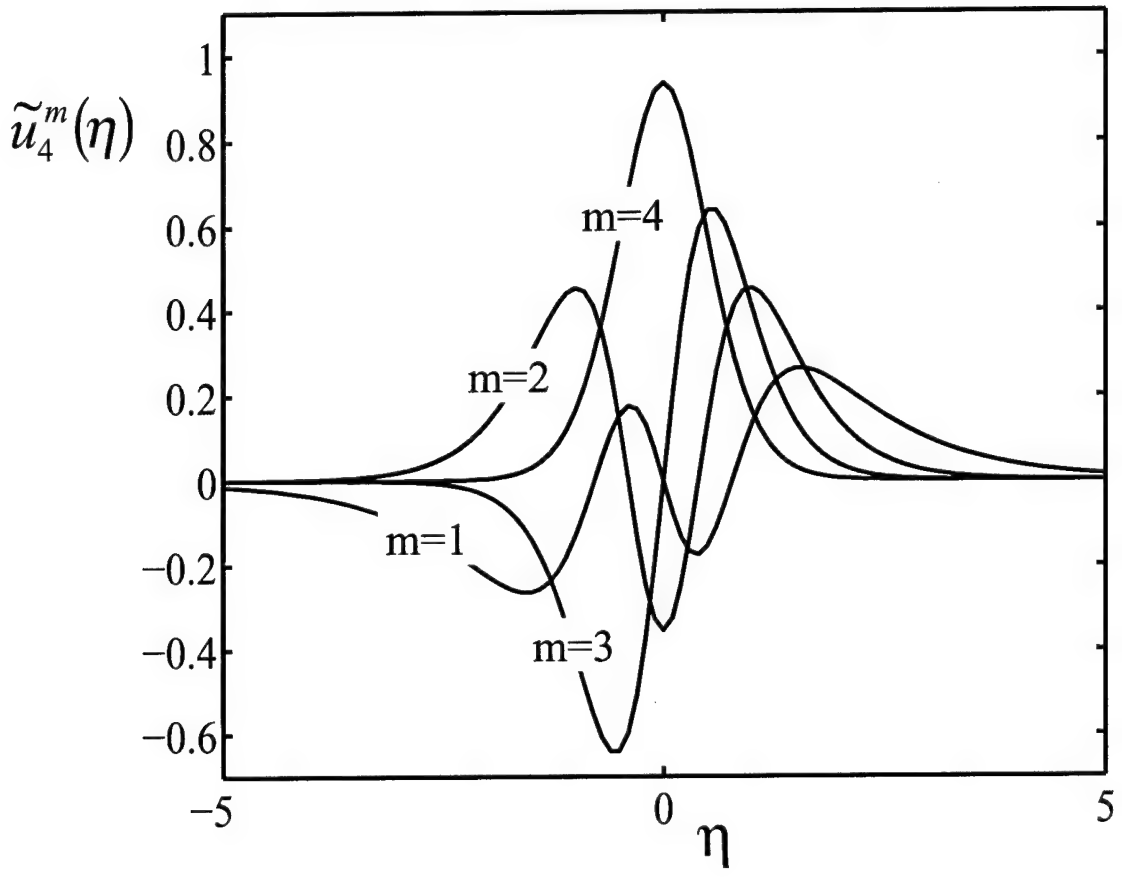


Figure 5.2: Normalized mode-profiles as a function of $\eta$ for *n=4*.

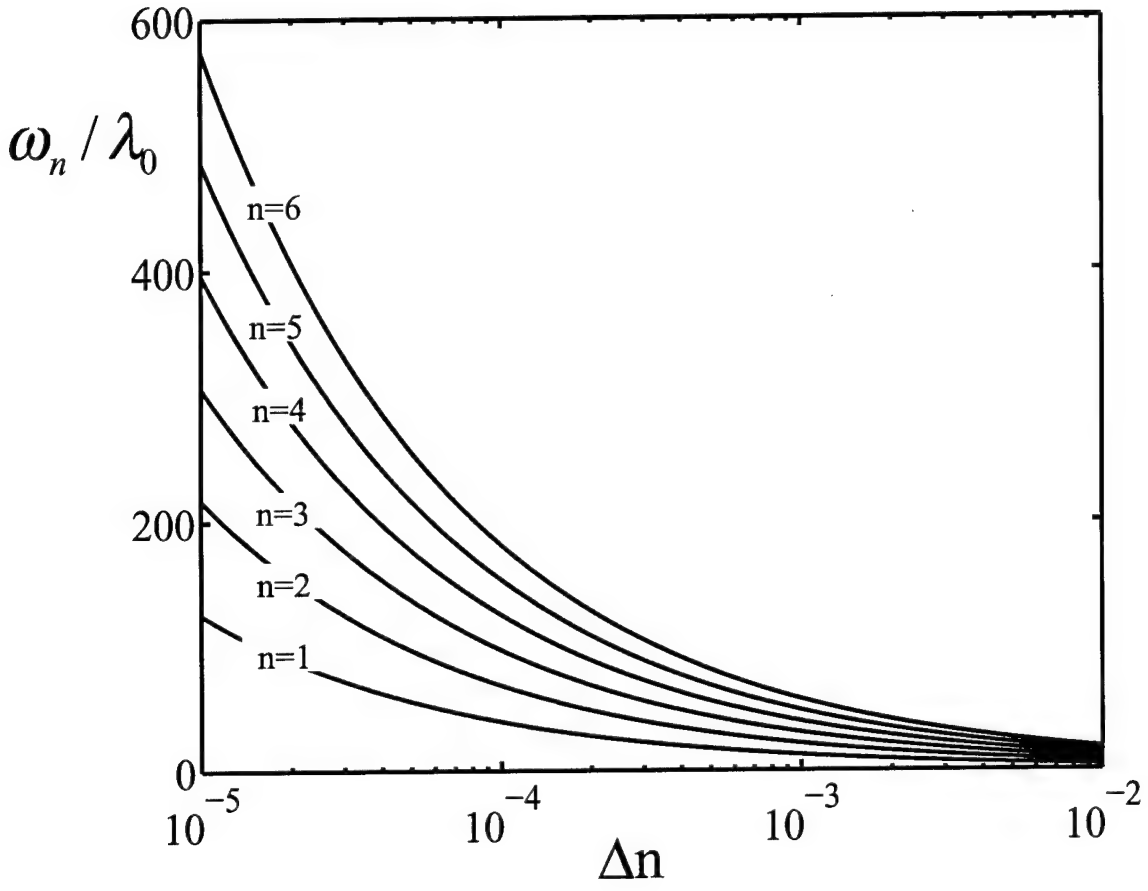


Figure 5.3: Normalized intensity FWHM of Kerr-like incoherent spatial solitons versus nonlinear index change $\Delta n$, for $n=1, 2, \ldots, 6$.

$\delta$ represents the normalized distance between two points. From Eq. 5.2, and by using the modal expansion of the optical envelope $U$, then for a given $n$, we obtain

$$\mu_{12}(\eta, \eta+\delta) = \frac{\sum_{m=1}^{n} \tilde{u}_n^m(\eta)\, \tilde{u}_n^m(\eta+\delta)}{\operatorname{sec h}(\eta)\operatorname{sec h}(\eta+\delta)} \quad , \tag{5.9}$$

where again we made use of the fact that the time-average of cross-interference terms is zero under incoherent excitation. The complex coherence factors $\mu_{12}(\eta, \eta+\delta)$ up to $n = 5$ have been tabulated in Appendix B. When $n = 1$, which corresponds to a coherent optical soliton, $\mu_{12}(\eta, \eta+\delta) = 1$ as should have been anticipated. This in turn implies an in nite correlation length. As the number of modes $n$ increases, the coherence properties of these incoherent soliton states become more complicated. Figure 5.4 provides a two-dimensional plot of $\mu_{12}$ as a function of normalized position $\eta$ and point separation $\delta$ when $n = 2$. As expected, $\mu_{12} = 1$ when $\delta = 0$ and this true for every value of $n$. Note that any cut ($\eta$ =constant) of these two dimensional plots provides the correlation (magnitude and phase) between the two points located at $\eta$ and $\eta + \delta$. Moreover, as it is well known [69], the magnitude of the complex coherence factor is always $|\mu_{12}| \leq 1$. In general, two points are mutually coherent if $\mu_{12} = 1$ and mutually incoherent (poor correlation) if $\mu_{12} \approx 0$. Figure 5.5 depicts a cross-section of the complex coherence $\mu_{12}$ as obtained right at the center ($\eta = 0$) of an incoherent soliton when $n = 2$. In this case, $\mu_{12}(0, \delta) = \operatorname{sech}(\delta)$, which implies that correlation between the center and any other point of this soliton decreases with $\delta$. This latter expression also demonstrates that the tails of this beam ($\delta \to \pm\infty$)

and the center are totally uncorrelated. Fig.5.6 on the other hand shows how a point at the tails (at $\eta = -3$) correlates with the rest of the beam when again $n = 2$. For example, when $\delta \approx 3$, in which case the second point is close to the beam center, $\mu_{12} \approx 0$ (poor correlation), in agreement with Fig.5.5. As $\delta \rightarrow -\infty$, (i.e. both points are on the left tail of the beam) there is maximum correlation ($\mu_{12} \simeq 1$). This high degree of coherence is due to the following fact: at the tails there is essentially only one mode, (the highest-order mode, $m = 1$) which is coherent in itself. For $\delta \rightarrow +\infty$, $\mu_{12} \simeq -1$ and this $\pi$ phase-shift is due to the anti-symmetric character of this highest-order mode. Fig.5.7, provides the same information at the intermediate point $\eta = -0.4$, when $n = 2$. Note that all these cross-sections are very different in character from those found in the case of logarithmically saturable nonlinear media (see Chapter 6). In Log systems, the statistical process is everywhere stationary, i.e. $\mu_{12}$ depends only on $\delta$ and it is Gaussian in nature. As shown here for the Kerr case, the coherence curves depend also on the position $\eta$ and do not always go to zero as $\delta \rightarrow \pm\infty$. This feature was also encountered in saturable Kerr media of the type $I/(1+I)$ (as will be seen in Chapter 7). This important difference is due to the nite number of modes associated with the Kerr incoherent solitons. In particular, the induced waveguides in Kerr and Kerr-saturable media exhibit cutoffs ( nite number of modes) whereas the logarithmic one does not. Figure 5.8 depicts the coherence function for $n = 3$ . Similar cuts are also provided in Figs. 5.9,

5.10, and 5.11. Fig.5.9 shows how the center correlates with rest of the beam for $n = 3$. Interestingly enough, in this case, there is a weak correlation between the center ($\eta = 0$) and the tails ($\delta \to \pm\infty$). This is because the highest-order mode ($m = 1$), which survives at the tails, happens to be even and it is thus nite at the center. Fig.5.10 gives the correlation between a point at the tails ($\eta = -3$) and the rest of the beam. Note the high degree of coherence ($\mu_{12} \approx 1$) between the two tails. Unlike the case shown in Fig.5.6, the correlation is in phase since again in this case the highest-order mode is even. Finally Fig.5.11 gives the coherence factor at $\eta = \text{sech}^{-1}\left(2/\sqrt{5}\right) \approx \pm 0.4812$ when $n = 3$. Using the coherence factor given in Appendix B, it can be readily shown that these particular points are completely uncorrelated with the tails of this incoherent soliton. Figures 5.12 and 5.13 depict the coherence factors for $n = 4$ and 5, respectively. It is interesting to observe the similarity between the $\mu_{12}$ surfaces when $n$ is odd or even. Clearly, as the order of the soliton increases, the coherence surfaces become more involved.

## 5.4 Conclusions

In conclusion, we have shown that multimode incoherent spatial solitons are possible in non-instantaneous Kerr-like media. Closed form solutions were obtained using the self-consistency approach provided that their intensity pro le is of the $\text{sech}^2(x/x_0)$ type. The coherence properties of these incoherent soliton states were

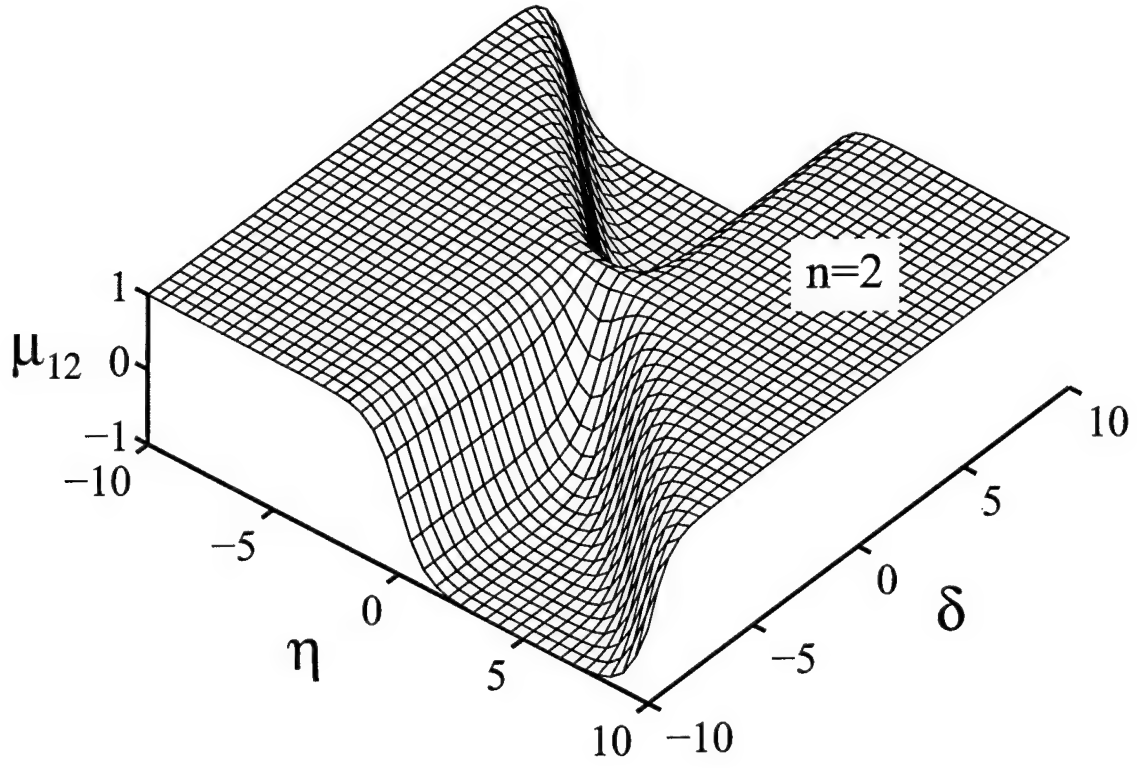


Figure 5.4: Spatial coherence function as a function of $\eta$ and $\delta$ when $n=2$.

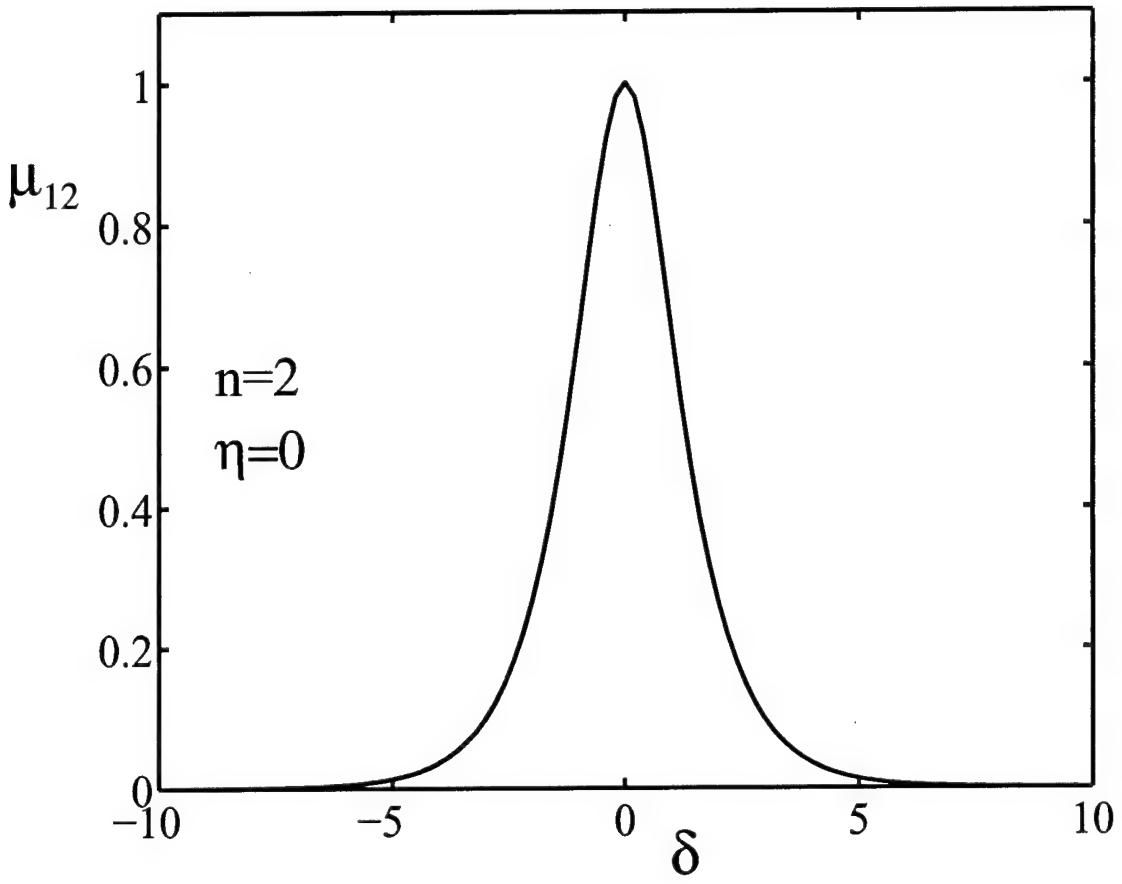


Figure 5.5: Cross-section of the coherence function when $n=2$ and $\eta=0$.

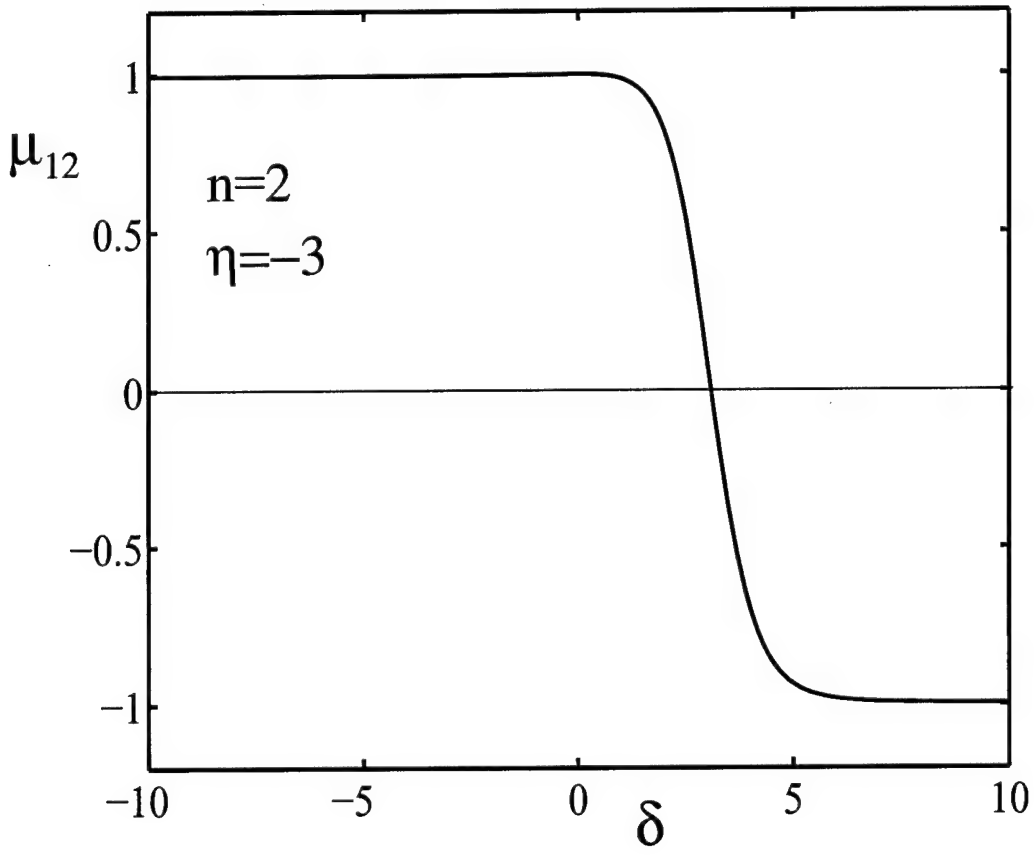


Figure 5.6: Cross-section of the coherence function when $n=2$ and $\eta=-3$.

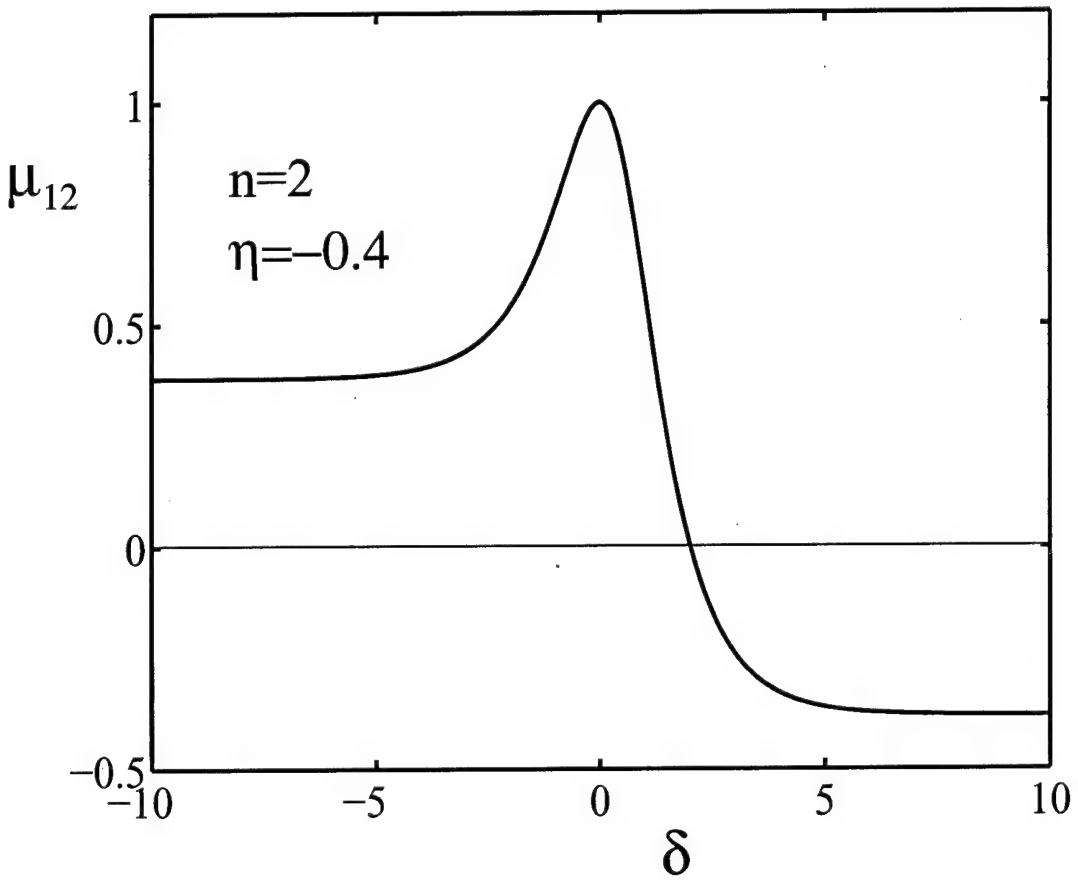


Figure 5.7: Cross-section of the coherence function when $n=2$ and $\eta=-0.4$.

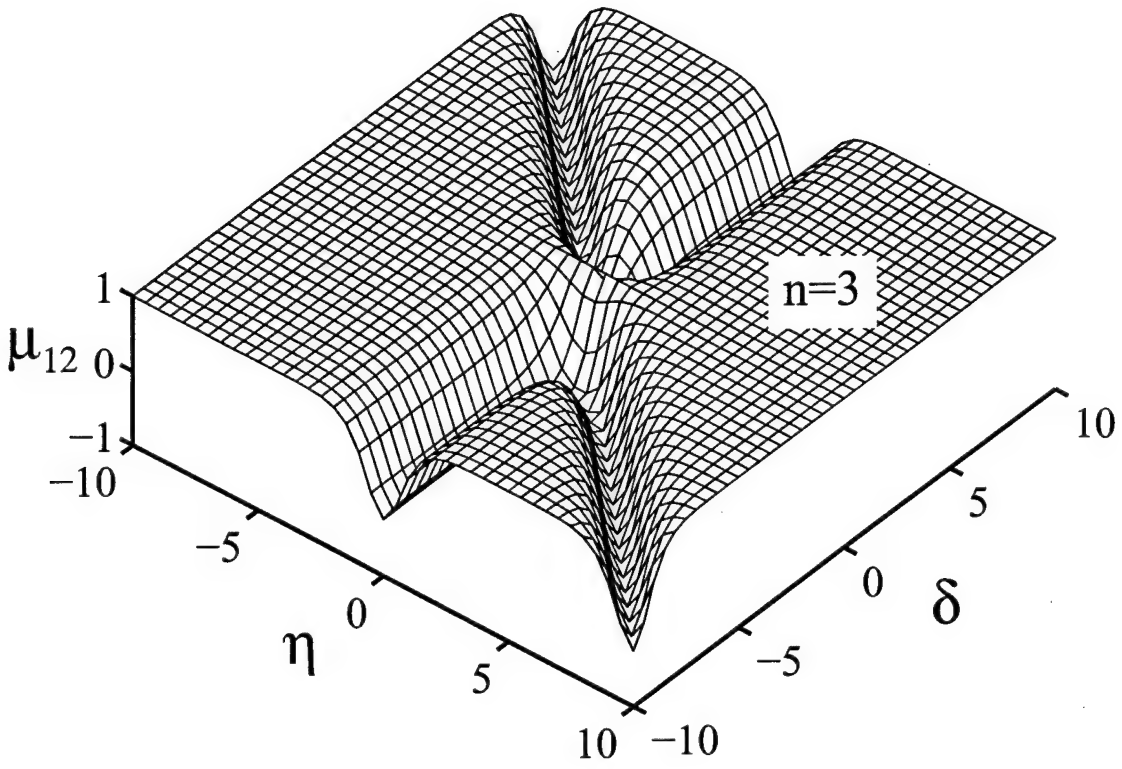


Figure 5.8: Spatial coherence function as a function of $\eta$ and $\delta$ when $n=3$.

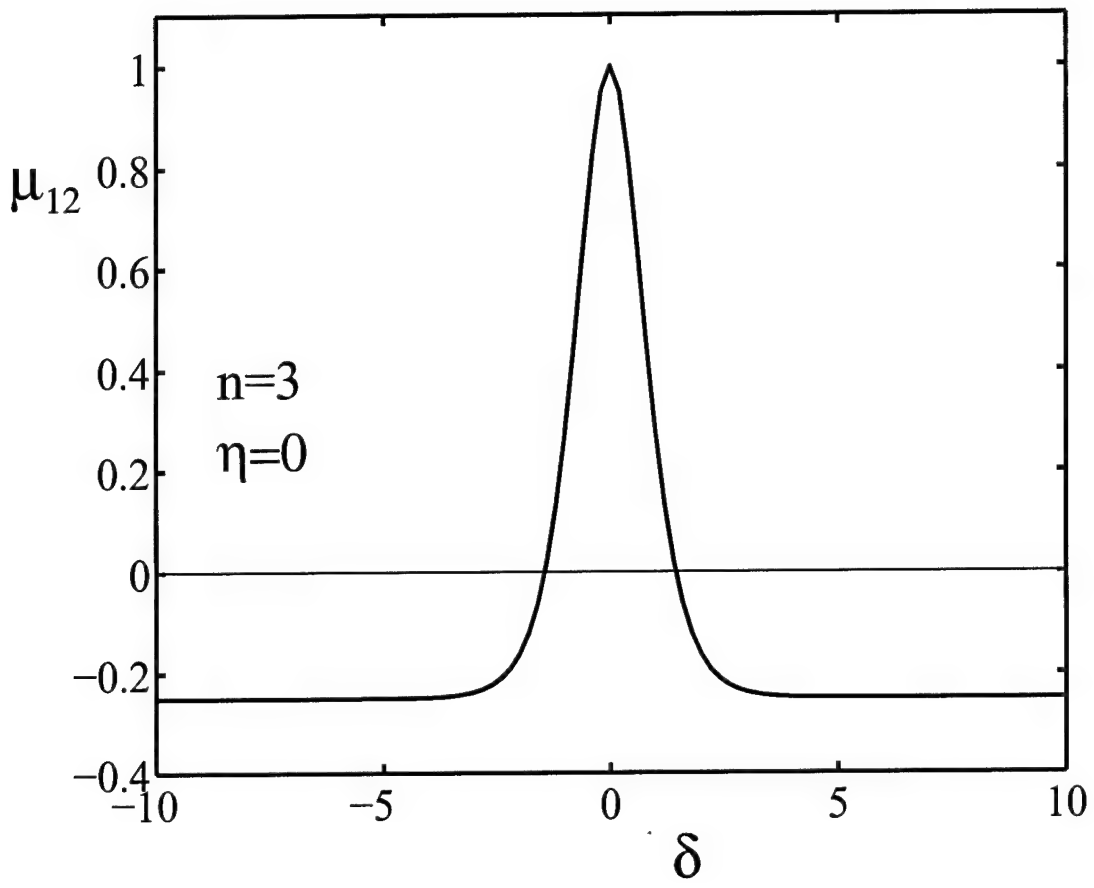


Figure 5.9: Cross-section of the coherence function when $n=3$ and $\eta=0$.

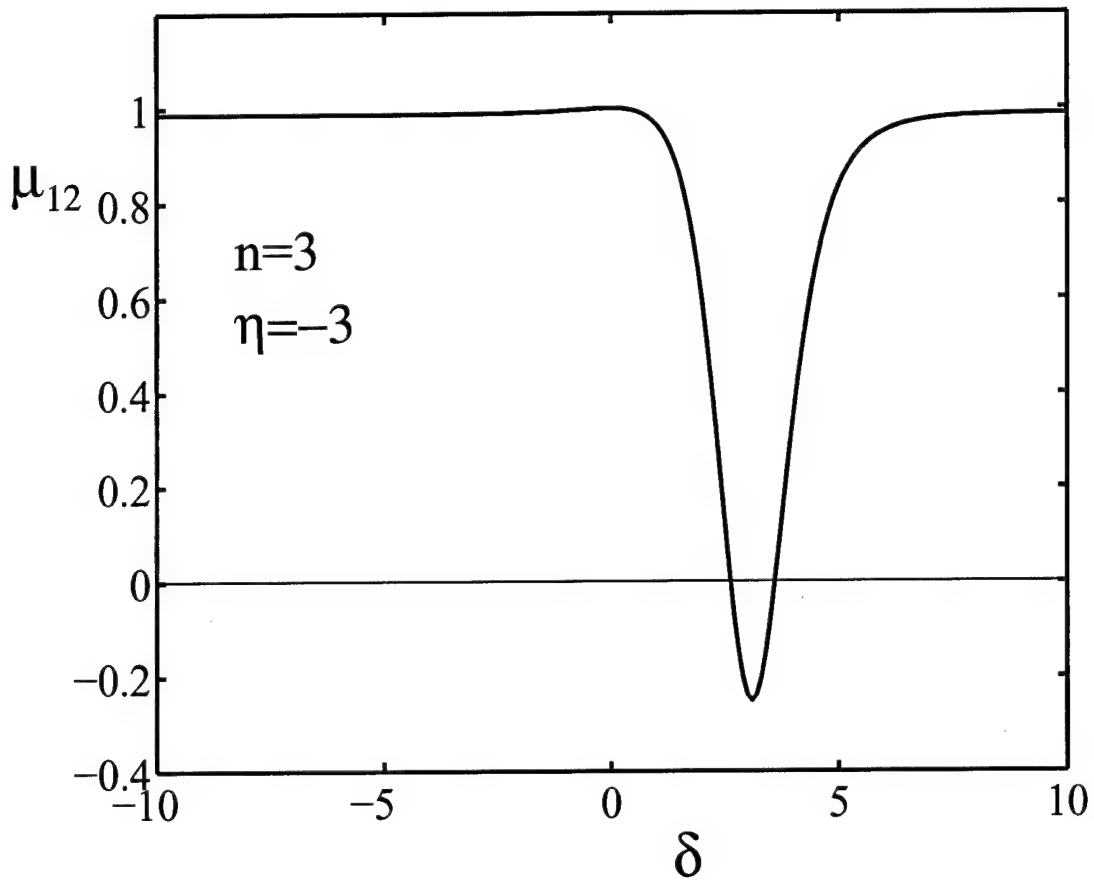


Figure 5.10: Cross-section of the coherence function when $n=3$ and $\eta=-3$.

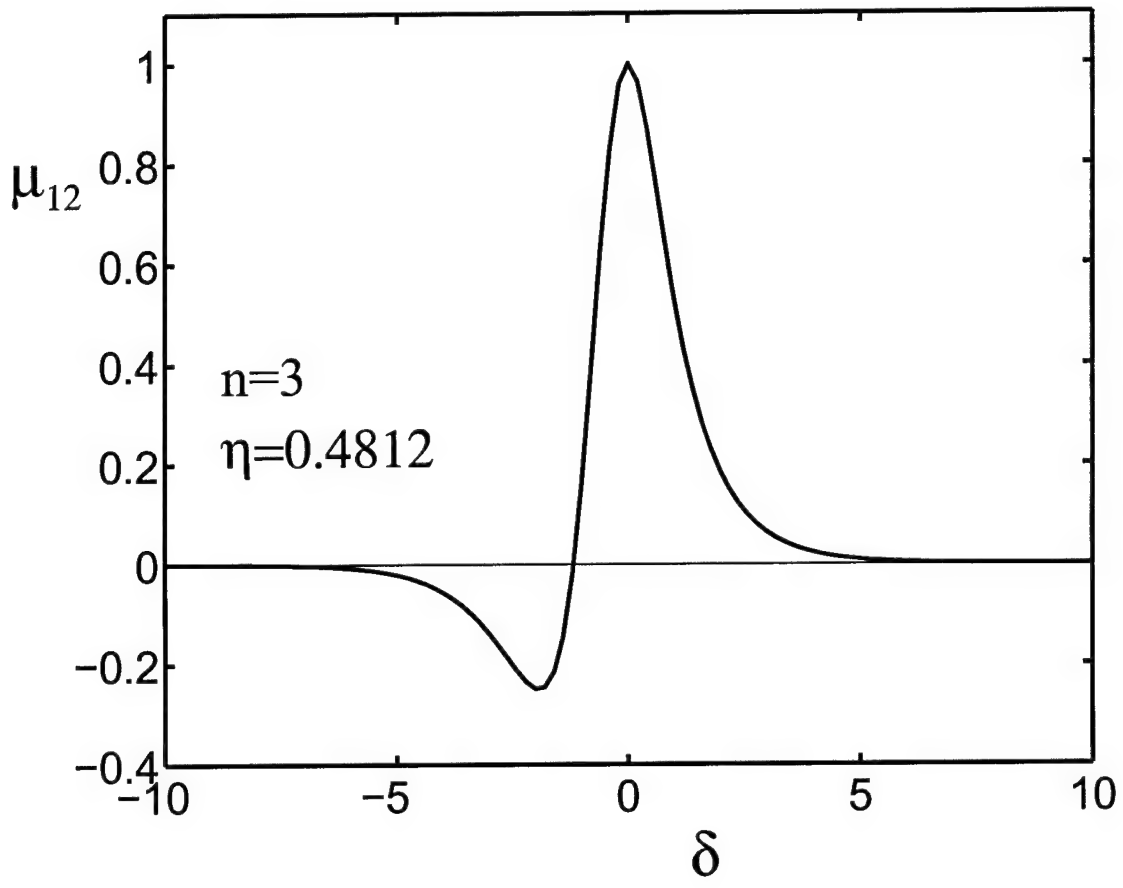


Figure 5.11: Cross-section of the coherence function when $n=3$ and $\eta=0.4812$.

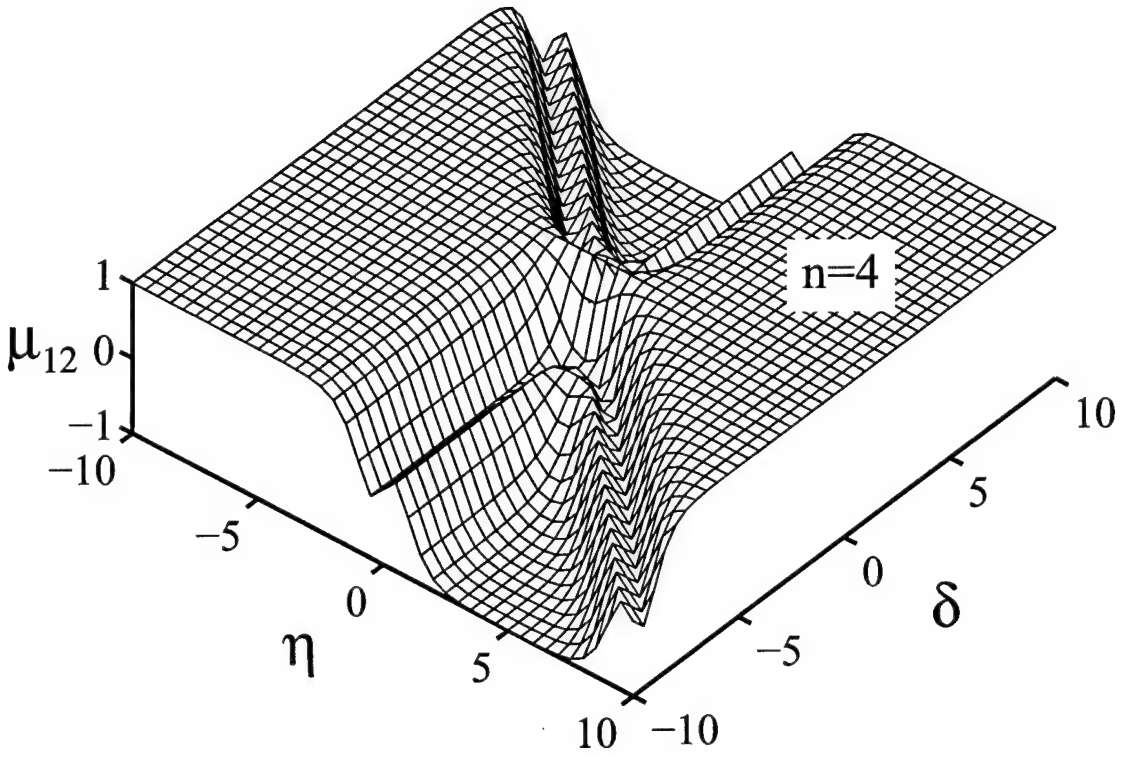


Figure 5.12: Spatial coherence function as a function of $\eta$ and $\delta$ when $n=4$.

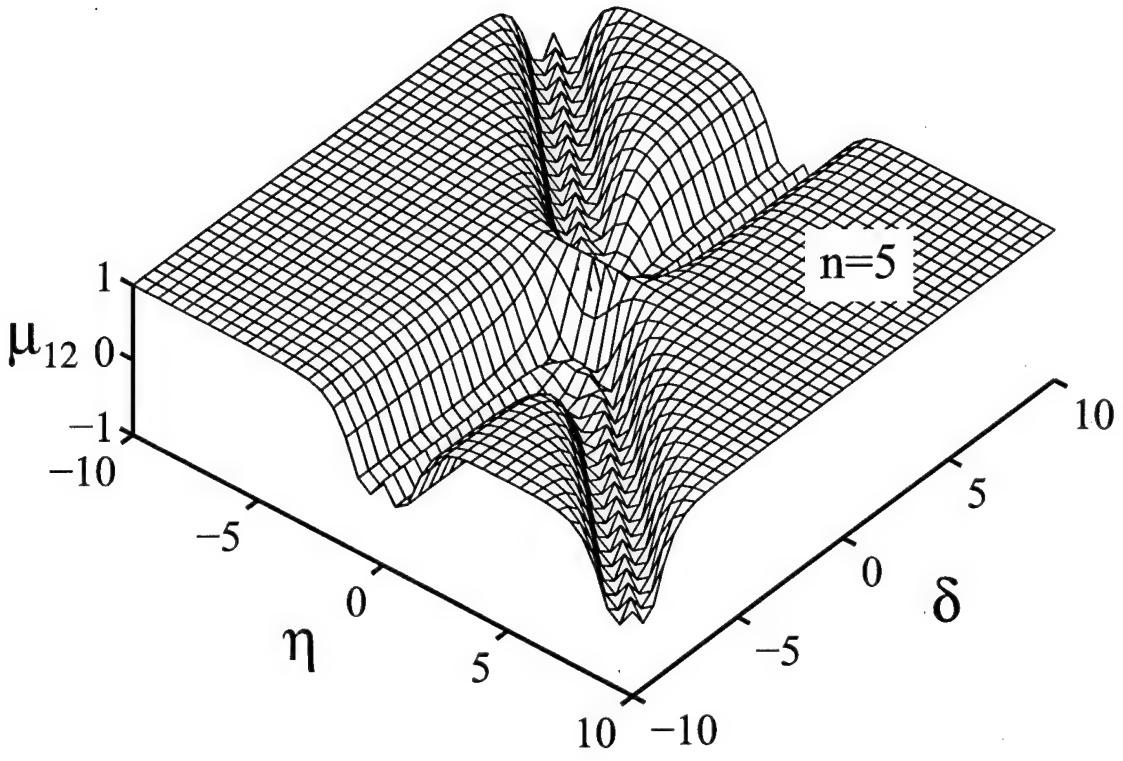


Figure 5.13: Spatial coherence function as a function of $\eta$ and $\delta$ when $n$=5.

also investigated in detail and explained by means of their modal composition.

# Chapter 6

# Multimode incoherent solitons in saturable nonlinear systems

In this chapter, we show that multimode incoherent spatial solitons are possible in log-type saturable nonlinear systems. The mode-occupancy function associated with these soliton states is found to obey a Poisson distribution. Our analysis indicates that two approaches, i.e. the dynamic coherent density description as well as the static self-consistent multimode method lead to exactly the same results. Closed form solutions are obtained for (1+1) D as well as for (2+1) D circular and elliptical incoherent solitons.

## 6.1 Introduction

Using coherent density approach it has been shown that (1+1) D incoherent spatial solitons are in fact possible in saturable nonlinear media of the logarithmic type. It is important to note however, that in general, the coherent density model is by nature better suited to describe dynamic evolution and thus it does not readily lend itself toward identifying stationary solutions such as incoherent spatial solitons. With the exception of the saturable logarithmic model (perhaps the only exactly soluble model in the coherent density description), the question naturally arises as to whether incoherent spatial solitons also exist (or not) in other saturable nonlinear systems (such as in biased photorefractives). In order to address this problem, we developed an alternative theory which is essentially a self-consistent incoherent multimode approach [83]. In brief, in this procedure, an incoherent spatial soliton is sought, which intensity-wise is a superposition of all the modes self-consistently guided in its nonlinearly induced waveguide. By doing so, (1+1) D photorefractive incoherent spatial solitons, the conditions necessary for their existence as well as their coherence characteristics were obtained[83]. Furthermore, in the last chapter, by using this approach, we showed that multimode incoherent spatial solitons are possible in non-instantaneous Kerr-like media. At a rst sight, the two theories [79],[83] may seem to have very little in common. Thus it is important to ask whether the two approaches are mutually-consistent or lead to the same results.

Moreover, it is interesting to know whether (2+1) D incoherent spatial solitons are also possible in saturable nonlinear media.

In this chapter we show that multimode incoherent spatial solitons are possible in logarithmically saturable nonlinear media. The mode-occupancy function of these soliton states is found to obey a Poisson distribution. Our analysis demonstrates, that in this case, the two theories, i.e. the dynamic coherent density description and the static self-consistent multimode method lead to identical results. Two-dimensional circular and elliptical incoherent spatial solitons along with their characteristics are also obtained in closed form. Even though the saturable logarithmic nonlinearity differs from the photorefractive, it provides nevertheless a platform (perhaps the only platform) upon which the equivalence of the two previously mentioned approaches can be established in closed form. Finally, as recently argued by Snyder and Mitchell [101] and by Shen [102], simpli cations of this sort in terms of accessible nonlinearities, can provide valuable insight and still maintain the characteristic features of the underlying physical process.

## 6.2 Incoherent multimode bright solitons

We begin our analysis by considering a saturable nonlinear medium of the logarithmic type, similar to that previously considered by Snyder and Mitchell in their

study of mighty morphing spatial solitons and bullets [80], i.e.

$$n^2(I) = n_0^2 + n_2 \ln(I/I_t) \tag{6.1}$$

where $n_0$ is the linear refractive index of the material, $n_2$ is a positive dimensionless coefficient associated with the strength of the nonlinearity and $I_t$ is a threshold intensity. To avoid any logarithmic singularities we assume that the $\ln(I/I_t)$ nonlinearity results from the more realistic $\ln(1 + I/I_t)$ model in the limit $I \gg I_t$ . Let the optical beam propagate in the $z$ direction. We also make the important assumption that the nonlinearity responds much slower than the characteristic phase uctuation time across the incoherent beam so as to avoid speckle-induced lamentation instabilities [91]. Thus, in this regime the material will experience only the time averaged beam intensity as in the case of photorefractives. Furthermore let the electric component of the optical eld be written in terms of a slowly varying envelope $U$, i.e., $E = U\exp(ikz)$ where $k = k_0 n_0$ and $k_0 = 2\pi/\lambda_0$. In that case, it can be readily shown that the envelope $U$ in this nonlinearly induced waveguide evolves according to

$$i\frac{\partial U}{\partial \xi} + \frac{1}{2}\left(\frac{\partial^2 U}{\partial s^2} + \frac{\partial^2 U}{\partial \eta^2}\right) + \frac{\alpha^2}{2}\ln(I_N)\,U = 0 \tag{6.2}$$

where $I_N = I/I_t$ is a normalized intensity and in Eq. 6.2 we have used normalized coordinates and quantities, that is, $s = x/w_0$, $\eta = y/w_0$, $\xi = z/kw_0^2$, $\alpha^2 = n_2(k_0 w_0)^2$ where $w_0$ is an arbitrary spatial scale or spot size.

## 6.3 One dimensional incoherent solitons

We rst employ the self-consistent incoherent multimode description in the case when the incoherent beam is one-dimensional or planar. For the time being, let us assume that an incoherent spatial soliton of a Gaussian intensity pro le exists, i.e. $I_N = r\exp(-s^2)$ where $r$ is an intensity ratio with respect to $I_t$. From these last assumptions, Eq. 6.2 takes the form

$$i\frac{\partial U}{\partial \xi} + \frac{1}{2}\frac{\partial^2 U}{\partial s^2} + \frac{\alpha^2}{2}\left[\ln(r) - s^2\right]U = 0 \quad . \tag{6.3}$$

The allowed modes in this parabolic waveguide can then be easily obtained in terms of Gauss-Hermite functions [103] and thus the optical eld can be expressed through superposition, i.e., $U = \sum_{m=0}^{\infty} c_m u_m$ where

$$u_m = H_m\left(\alpha^{1/2}s\right)\exp\left(-\alpha s^2/2\right)\exp\left(i\beta_m\xi\right) \tag{6.4}$$

and $c_m$ are the mode-occupancy coefficients that vary randomly in time. In Eq. 6.4, $H_m(x)$ are Hermite polynomials, $\beta_m = (1/2)\left[\alpha^2\ln(r) - (2m+1)\alpha\right]$ and $m = 0, 1, 2, \ldots$ . The time-average intensity of this beam can then be obtained from

$$I_N = \left\langle |U|^2 \right\rangle = \sum_{m=0}^{\infty} \left\langle |c_m|^2 \right\rangle |u_m|^2 \tag{6.5}$$

where we made use of the fact that the time average of the cross-interference terms is zero ($\left\langle c_i c_j^* \right\rangle \propto \delta_{ij}$) under incoherent excitation [83],[104]. Yet, at this point, we still do not know the mode-occupancy function $\left\langle |c_m|^2 \right\rangle$ that self-consistently leads

to the incoherent Gaussian soliton $I_N = r\exp(-s^2)$ assumed in the very beginning of this analysis. Let the mode-occupancy, as in the case of quantum mechanical coherent or Glauber states [69],[103], be described by a Poisson distribution [105], that is

$$\left\langle |c_m|^2 \right\rangle = \hat{r}\exp\left(-p/2\right)\frac{(p/2)^m}{m!} \tag{6.6}$$

where $p$ is the Poisson parameter and $\hat{r}$ is a constant to be determined. From Eqs. 6.4-6.6 and with the aid of Mehler s formula [106],

$$\sum_{m=0}^{\infty}\frac{(p/2)^m}{m!}H_m(x)\,H_m(y) = \frac{1}{\sqrt{1-p^2}}\exp\left[\frac{2pxy - p^2\left(x^2+y^2\right)}{1-p^2}\right] \tag{6.7}$$

one can then obtain the following result

$$I_N = \frac{\hat{r}\exp\left(-p/2\right)}{\sqrt{1-p^2}}\exp\left[-\alpha s^2\left(\frac{1-p}{1+p}\right)\right] \quad . \tag{6.8}$$

Thus the assumed Poisson distribution self-consistently leads to the incoherent spatial soliton $I_N = r\exp(-s^2)$ provided that $\hat{r} = r\sqrt{1-p^2}\exp(p/2)$ and

$$p = \frac{\alpha - 1}{\alpha + 1} \quad . \tag{6.9}$$

From Eq.6.7 it is evident that in this case, the positive Poisson parameter $p$ must be below unity ($p < 1$) for this incoherent soliton to exist. Or alternatively, from Eq.6.9, $\alpha > 1$ which implies that at a given wavelength $\lambda_0$, the quantity $n_2^{1/2}w_0$ has a cut off, below which no incoherent spatial solitons are allowed.

To establish the equivalence between this result, Eqs.6.8 and 6.9, with that previously obtained using the coherent density approach in Chapter 4 one must

resort to diffraction data. More speci cally, during linear diffraction ($n_2 = 0$), the intensity of each Gauss-Hermite mode evolves according to [103] (see Appendix C)

$$|u_m(s,\xi)|^2 = \frac{1}{\sqrt{1+\alpha^2\xi^2}} \exp\left(-\frac{\alpha s^2}{1+\alpha^2\xi^2}\right) H_m^2\left[\frac{\alpha^{1/2}s}{\sqrt{1+\alpha^2\xi^2}}\right] . \tag{6.10}$$

By keeping in mind that the mode-occupancy function $\left\langle |c_m|^2 \right\rangle$ satis es the Poisson distribution of Eq.6.6 and by employing again Eqs.6.7 and 6.9, we nd that upon diffraction the normalized intensity pro le $I_D$ (see Appendix D) is given by

$$I_D = \frac{r}{\sqrt{1+\alpha^2\xi^2}} \exp\left(-\frac{s^2}{1+\alpha^2\xi^2}\right) . \tag{6.11}$$

Equation 6.11 clearly shows that during diffraction this incoherent beam remains Gaussian. Given the fact that the initial modulation function [79] is Gaussian, i.e. $\phi_0(s) = \exp(-s^2/2)$ and that the diffraction behavior of this statistically stationary beam obeys a convolution integral, Eq.3.3 of Chapter 3, it then becomes immediately apparent that the angular power spectrum $G_N(\theta)$ of the incoherent source must also be Gaussian. In this regard, let $G_N(\theta) = (\pi^{1/2}\theta_0)^{-1} \exp(-\theta^2/\theta_0^2)$ where $\theta_0$ is the width of the incoherent angular power spectrum. Thus, had we treated the diffraction regime within the coherent density approach [71] (see Appendix E), we would have arrived at the following result

$$I_D = \frac{r}{\sqrt{1+(1+V^2)\,\xi^2}} \exp\left(-\frac{s^2}{1+(1+V^2)\,\xi^2}\right) \tag{6.12}$$

where $V \equiv kw_0\theta_0$. Since diffraction-wise, the results of Eqs. 6.11 and 6.12 are the

same, we conclude that $\alpha^2 = 1 + V^2$ or that

$$w_0 = \frac{1}{k_0\sqrt{n_2 - n_0^2\theta_0^2}} \quad . \tag{6.13}$$

The result of Eq.6.13 is exactly what has been previously obtained in Chapter 4, Eq.4.12, using the coherent density approach. At a more fundamental level, our analysis demonstrates that the two theories, i.e. the dynamic coherent density description as well as the self-consistent multimode method lead in this case to exactly the same results. In the coherent limit $\theta_0 \rightarrow 0$ or $\alpha \rightarrow 1$, the soliton spot size reduces to $w_0 = (k_0 n_2^{1/2})^{-1}$ as previously found by Snyder and Mitchell [80]. In this same limit, Eq. 6.9 suggests that the Poisson parameter $p \rightarrow 0$ and thus the beam itself is single-moded or fully coherent. Moreover, the width $\theta_0$ of the angular power spectrum of the incoherent source and the Poisson parameter $p$ are now related through the following expression $p = \left[(1+V^2)^{1/2} - 1\right] / \left[(1+V^2)^{1/2} + 1\right]$. Of course these incoherent spatial soliton states exist as long as $p < 1$ or $\alpha > 1$ or equivalently $\theta_0 < n_2^{1/2}/n_0$.

## 6.4 Two dimensional incoherent solitons

In the same vein, one may show that two-dimensional incoherent spatial solitons also exist in this nonlinear system. To do so, let us assume in general an elliptic

Gaussian incoherent beam,

$$I_N = r \exp\left[-(s^2 + \sigma^2\eta^2)\right] \tag{6.14}$$

where the parameter $\sigma$ is associated with its degree of ellipticity. Substituting Eq. 6.14 in Eq. 6.2 we get

$$i\frac{\partial U}{\partial \xi} + \frac{1}{2}\left(\frac{\partial^2 U}{\partial s^2} + \frac{\partial^2 U}{\partial \eta^2}\right) + \frac{\alpha^2}{2}\left[\ln(r) - s^2 - \sigma^2\eta^2\right] U = 0\,. \tag{6.15}$$

The optical field $U$ in this elliptic paraboloid potential can be obtained as a superposition of the allowed Gauss-Hermite modes, i.e. $U = \sum_{m=0}^{\infty}\sum_{n=0}^{\infty} c_{m,n}u_{m,n}$ where

$$u_{m,n} = H_m\left(\alpha^{1/2}s\right) H_n\left(\alpha^{1/2}\sigma^{1/2}\eta\right) \exp\left[-(\alpha/2)\left(s^2 + \sigma\eta^2\right)\right] \exp\left(i\beta_{m,n}\xi\right) \tag{6.16}$$

where $\beta_{m,n} = (\alpha/2)\left[\alpha\ln(r) - (2m+1) - \sigma(2n+1)\right]$. The overall intensity of this beam can then be found from

$$I_N = \sum_{m=0}^{\infty}\sum_{n=0}^{\infty}\left\langle |c_{m,n}|^2\right\rangle |u_{m,n}|^2 \tag{6.17}$$

where we have assumed again that under incoherent excitation $\langle c_{ij}c_{kl}^*\rangle \propto \delta_{ik}\delta_{jl}$. If we now allow the mode-occupancy $\left\langle |c_{m,n}|^2\right\rangle$ to obey a double Poisson distribution

$$\left\langle |c_{m,n}|^2\right\rangle = \hat{r}\exp\left[-\frac{1}{2}(p+q)\right]\frac{(p/2)^m(q/2)^n}{m!n!} \tag{6.18}$$

then the two dimensional incoherent spatial soliton $I_N = r\exp\left[-(s^2 + \sigma^2\eta^2)\right]$ can be self-consistently recovered using Eqs. 6.7, 6.17, and 6.18 provided that the two Poisson parameters $p$, $q$ satisfy

$$p = \frac{\alpha - 1}{\alpha + 1} \tag{6.19}$$

$$q = \frac{\alpha - \sigma}{\alpha + \sigma} \tag{6.20}$$

and moreover $\hat{r} = r\left[\left(1-p^2\right)\left(1-q^2\right)\right]^{1/2} \exp\left[\left(p+q\right)/2\right]$. These incoherent solitons can be elliptical ($\sigma \neq 1$) or circular ($\sigma = 1$) depending on whether the angular power spectrum of the incoherent source (exciting this structure) is symmetric or not. Moreover, these states exist as long as $0 < (p,q) < 1$ or $\alpha > \max(1,\sigma)$. The possibility of generating (2+1) D elliptical solitons in isotropic nonlinear media seems to be unique to incoherent multi-mode solitons, since it has been shown that their coherent counterparts change their widths periodically during propagation [80].

## 6.5 Coherence properties

Having found the modal composition of these solitons, their coherence properties [69] can then be described by following procedures similar to those employed in Refs. [104] and [107]. Using Eqs.6.7, and 6.16-6.20, one can show that the complex coherence factor $\mu_{12}$ of these solitons is given by

$$\mu_{12}\left(s,\eta;s+\delta,\eta+\varepsilon\right) = \exp\left\{-\left[\frac{p\delta^2}{\left(1-p\right)^2} + \frac{q\sigma^2\varepsilon^2}{\left(1-q\right)^2}\right]\right\} \quad . \tag{6.21}$$

This latter result demonstrates that the coherence function $\mu_{12}$ is independent of position $(s,\eta)$ within the soliton beam and instead it depends only on the deviation distances $\delta$ and $\varepsilon$. For a circular incoherent soliton ($p = q$, $\sigma = 1$), the actual correlation length $l_c$ (the distance where $\mu_{12}$ falls to its $e^{-1}$ value) can be obtained

from Eq.6.21 and it is given by $l_c = w_0(1-p)p^{-1/2}$. Evidently, $l_c \to \infty$ when $p = 0$ (single mode case) whereas $l_c \to 0$ when $p \to 1$. These results are in agreement with our previous discussion. In fact, for one dimensional solitons, the complex coherence factor $\mu_{12}$ is identical to the statistical autocorrelation function of the source $R(x_1 - x_2)$, $R(x_1 - x_2)$ can be obtained from $G_N(\theta)$ via an inverse Fourier transform [79], which is given by $R(x_1 - x_2) = \exp\left(-\delta^2 V^2/4\right)$ where $x_1 - x_2 = w_0\delta$. This is true since, from Eqs. 6.13 and 6.19, $p(1-p)^{-2} = V^2/4$. In other words, the correlation length of a logarithmic incoherent soliton remains invariant during propagation and it is equal to that of the exciting incoherent source. Moreover, as in the fully coherent case [80], the dynamics of these two-dimensional solitons (during compression or expansion, i.e. when $p$ and $q$ deviate from the prescribed values of Eqs.6.19 and 6.20) can also be described in closed form. We would like to emphasize that by its very nature the logarithmic nonlinearity leads to an in nite set of modes which are in turn related through a Poisson distribution. Of course this is also true for the $\ln(1 + I_N)$ nonlinearity provided that the maximum intensity at the center of the beam is much greater than $I_t$. In particular, computer simulations show that intensity-wise the $\ln(I_N)$ model nicely approximates the $\ln(1 + I_N)$ nonlinearity as long as the intensity ratio, $\max(I_N) > 100$. However for relatively low intensity ratios the mode occupancy (in the $\ln(1 + I_N)$ model) is not exactly Poissonian and the correlation length (even though at in the middle) tends to increase at the low

intensity boundaries of the beam. This is in full agreement with the results we have previously obtained [83] for incoherent photorefractive spatial solitons where $\triangle n\,(1+I_N)^{-1}$. Finally at very high intensity ratios, the correlation length becomes again constant across the Gaussian beam as suggested by Eq. 6.21.

## 6.6 Results and discussion

As an example, let us consider a logarithmically saturable nonlinear medium with a $\ln(1+I_N)$ nonlinearity, $n_0 = 2$ and $n_2 = 10^{-4}$. The free space optical wavelength is taken to be $\lambda_0 = 0.5\ \mu m$ and the width of the angular power spectrum of the source is $\theta_0 = 0.258^o$. Fig.6.1(a) shows stationary propagation of a 1-D incoherent soliton when $r = 10^3$ and $x_0 \simeq 18\ \mu m$ (intensity FWHM is $\sim 30\ \mu m$) as obtained numerically from the coherent density method. Fig.6.1(b) on the other hand, illustrates the intensity pro le of the rst four modes involved in this Gaussian soliton as obtained from beam propagation methods. Evidently, these individual modes remain invariant as a function of distance. As expected, the sum of the individual modes provides the intensity pro le of Fig.6.1(a). These results are in excellent agreement with our theoretical analysis.

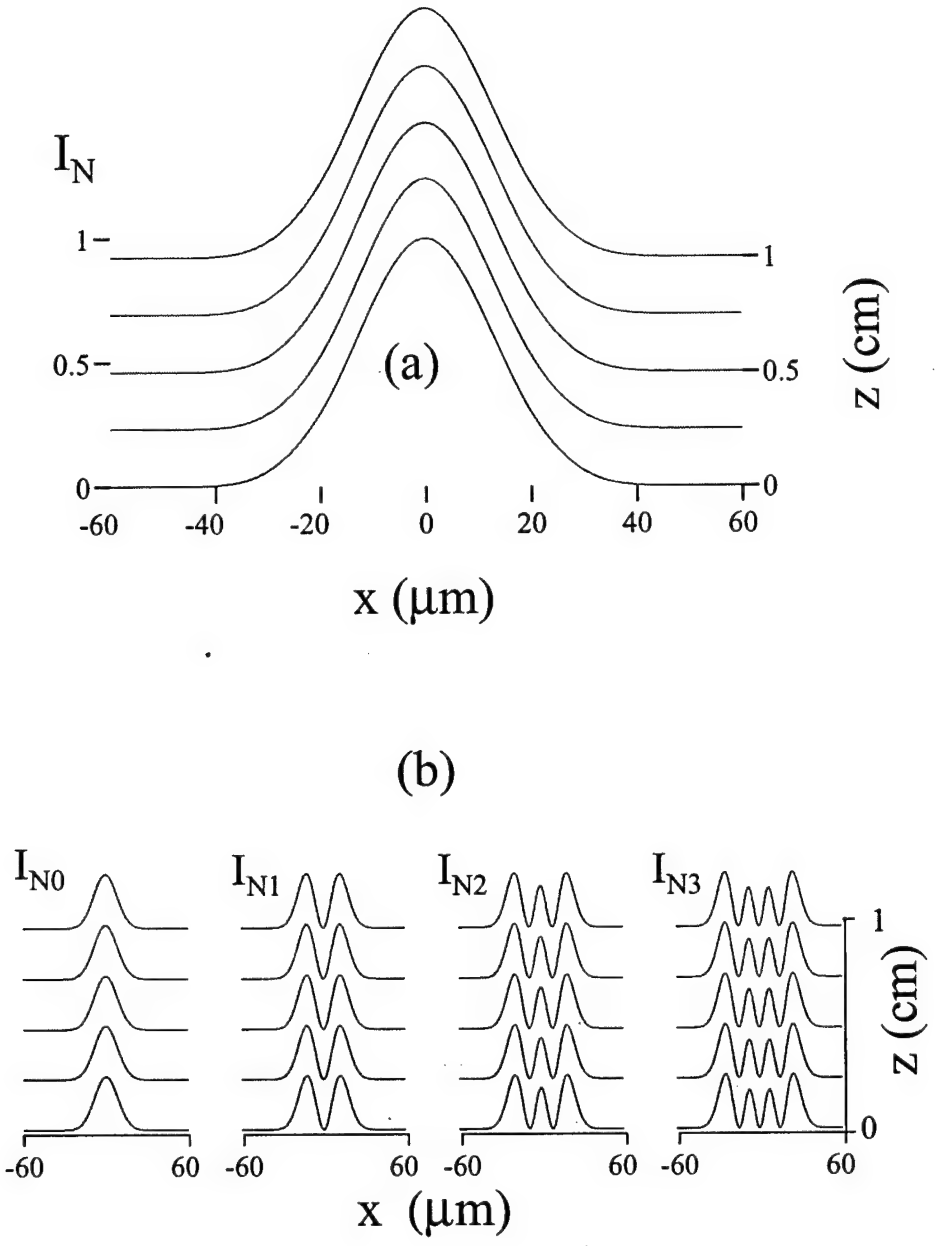


Figure 6.1: (a) Stationary propagation of an incoherent Gaussian soliton in a $\ln(1+I_N)$ nonlinear medium up to a distance of 1 *cm*. (b) Evolution of the intensity profiles of the first four modes associated with this soliton.

## 6.7 Conclusions

In conclusion we have shown that incoherent spatial solitons are possible in logarithmically saturable nonlinear media. These solitons can exist as long as their mode-occupancy function obeys a Poisson distribution. We have found that two approaches, that is the dynamic coherent density description as well as the self-consistent multimode method lead in this case to exactly the same results. Two dimensional (circular and elliptical) multimode spatial solitons have also been obtained in closed form.

# Chapter 7

# Dynamics of incoherent self-trapped beams

In this chapter, using the coherent density approach, we study the propagation dynamics of incoherent bright and dark beams in biased photorefractive crystals. We show that under appropriate initial conditions, bright as well as dark-like incoherent quasi-solitons can be established in this material system. Our numerical simulations demonstrate that the coherence properties of these beams can be signi cantly affected by the self-trapping process.

## 7.1 Introduction

In Chapter 3, a theory based on the so-called coherent density approach has been developed and good agreement was found between the experimentally observed behavior and the theoretical results of this model [79]. In Chapter 4, using the coherent density approach, an exact analytical solution has been obtained for (1+1) D incoherent spatial solitons in saturable nonlinear media of the logarithmic type [82]. We have also developed an alternative method which is capable of identifying static incoherent spatial soliton states [83]. This latter model, seeks in a self-consistent fashion multimode soliton solutions whose total intensity can be obtained via intensity superposition of all the modes guided in the nonlinearly induced waveguide. In this manner, we have found (1+1) D photorefractive incoherent spatial solitons, the conditions necessary for their existence as well as their spatial coherence characteristics [83]. In Chapter 5, by using this latter approach, we have shown that incoherent solitons are possible in non-instantaneous Ker-like nonlinear media. In Chapter 6, on the other hand, it is demonstrated that the log type incoherent solitons can also be described by using self-consistent multimode method [114]. These studies have shown that incoherent spatial bright solitons are indeed feasible in any non-instantaneous nonlinear media. Yet at this point, there are still several other issues that merit further investigation. For example, it is not at all clear whether incoherent dark solitons are also possible. Moreover, it is of interest to know how the

coherence properties or uctuation statistics of these beams are in uenced during propagation by the photorefractive nonlinearity.

In this chapter, we study the dynamics of incoherent bright and dark beams in biased photorefractives, which represent an example of a non-instantaneous saturable nonlinear material system. We employ the dynamic coherent density approach and numerically solve the underlying nonlinear Schrödinger-like integro-differential equation. We predict that under odd initial beam conditions, a dark-like incoherent spatial soliton will emerge and after a certain distance it takes the form of a gray structure. As in the case of coherent solitons, incoherent gray soliton pairs (doublets) and triplets are also possible under even and odd initial beam conditions respectively. In all cases (dark and bright), we show that the photorefractive nonlinearity signi cantly alters the coherence properties of these beams. For bright beams, we nd that the correlation length across the beam nally evolves according to the predictions of Ref. [83]. Moreover, we emphasize that, our results are of a general nature, i.e. they can be used to describe incoherent beam dynamics in any non-instantaneous nonlinear medium.

## 7.2 Evolution dynamics of incoherent beams in biased photorefractive media

### 7.2.1 Evolution equation

In a standard biased Strontium Barium Niobate (SBN) photorefractive crystal arrangement [23],[24], the normalized intensity $I_N = I/I_d$ of an incoherent beam obeys the following nonlinear integro-differential equation (see Chapters 3 and 4):

$$i\left(\frac{\partial f}{\partial z} + \theta\frac{\partial f}{\partial x}\right) + \frac{1}{2k}\frac{\partial^2 f}{\partial x^2} - \frac{k_0}{2}n_e^3 r_{33}E_0\left(1+\rho\right)\frac{f}{1+I_N\left(x,z\right)} = 0 \qquad (7.1)$$

where

$$I_N\left(x,z\right) = \int_{-\infty}^{+\infty} \left|f\left(x,z,\theta\right)\right|^2 d\theta \qquad (7.2)$$

and at $z = 0$

$$f\left(z=0,x,\theta\right) = \left(r,\rho\right)^{1/2} G_N^{1/2}\left(\theta\right)\phi_0\left(x\right) \qquad . \qquad (7.3)$$

In the above equations, $f$ represents the so-called coherent density, $\theta$ is an angle (in radians) with respect to the $z$ axis, $k = k_0 n_e$, and $k_0 = 2\pi/\lambda_0$. $I_d$ is the dark irradiance, $n_e$ the extraordinary refractive index and $r_{33}$ the electrooptic coefficient involved. $E_0 = \pm V/W$ where $V$ is the applied bias and $W$ the $x$-width of the crystal. $G_N(\theta)$ is the normalized angular power spectrum of the incoherent source and $\phi_0(x)$ is the input complex spatial modulation function. Moreover, $r$ is the maximum intensity of a bright incoherent beam whereas $\rho$ is the normalized intensity of a

dark beam at $x \rightarrow \pm\infty$. Equation 7.3 restates the fact that the coherent density has been initially weighted with respect to the source angular power spectrum.

### 7.2.2 Coherence length

The coherence properties of these evolving partially incoherent beams can be obtained through a modi ed version of the Van Cittert-Zernike theorem [74], particularly suited for the coherent density approach. The complex coherence factor $\mu_{12}$ is obtained from

$$\mu_{12}(x_1, x_2) = \frac{1}{\sqrt{I_N(x_1, z)\, I_N(x_2, z)}} \times \int_{-\infty}^{+\infty} f(x_1, z, \theta)\, f^*(x_2, z, \theta) \exp\left[ik\theta(x_1 - x_2)\right] d\theta \quad . \tag{7.4}$$

In general, the complex coherence factor can be an arbitrary function of both $x_1$ and $x_2$. Thus, it is often more convenient to describe the coherence properties of an optical beam through the so-called correlation length $l_c$ which is de ned as follows

$$l_c(x) = \int_{-\infty}^{+\infty} \left|\mu_{12}\left(x, x'\right)\right|^2 dx' \quad . \tag{7.5}$$

## 7.3 Dynamics of incoherent bright and dark beams and their coherence properties

As an example let us consider a biased SBN:75 crystal with $n_e = 2.3$, $r_{33} = 1022$ $pm/V$, $\lambda_0 = 488$ $nm$, $W = 6$ $mm$, similar to that used in Ref. [35]. Let us also assume that at the input, the source fluctuations obey a stationary random process (i.e. $\mu_{12}$ depends only on $x_1 - x_2$) and that the normalized angular power spectrum of the incoherent source is Gaussian, i.e. $G_N(\theta) = (\pi^{1/2}\theta_0)^{-1}\exp(-\theta^2/\theta_0^2)$ where $\theta_0$ is associated with its angular width [79]. Equations 7.1 and 7.2 are numerically solved by appropriately discretezing them in $\theta$ and by using beam propagation methods. In turn, the correlation length is obtained from Eqs. 7.4 and 7.5.

### 7.3.1 Incoherent bright beams

Let us first consider an incoherent Gaussian bright beam whose spatial modulation function is given by $\phi_0(x) = \exp[-x^2/(2x_0^2)]$ in which case $I_N = r\exp(-x^2/x_0^2)$ where $x_0$ is related to the intensity FWHM. At the input, the intensity FWHM of this beam is 30 $\mu m$, and its maximum normalized intensity is $r = 3$. The width of the angular power spectrum is taken here to be $\theta_0 = 0.55^o$. Since we have assumed stationary source fluctuations, it can then be readily shown that at $z = 0$, $\mu_{12}(\delta) = \exp\left[-\delta^2/\delta_0^2\right]$ where $\delta = x_1 - x_2$ and $\delta_0 = 2/(k\theta_0)$. Thus, the incoherent beam at $z =$

0 exhibits a constant coherence length $l_c = \sqrt{2\pi}/(k\theta_0)$ which is independent of the spatial modulation function $\phi_0(x)$ or $I_N(x, z = 0)$. For the above given parameters, the coherence length of the source is approximately 8.8 $\mu m$. It can be shown, that during linear diffraction the FWHM of this bright beam increases to 165 $\mu m$ after 1 $cm$. The coherence length $l_c(x, z)$ of this Gaussian beam also increases with $z$ while remaining constant across $x$. Note that, this latter feature is particular to Gaussian-Schell sources. If the input complex envelope $\phi_0(x)$ is not Gaussian, the correlation length $l_c$ is no longer constant across the beam during diffraction. On the other hand, by activating the photorefractive nonlinearity, by applying a bias voltage, the coherence properties change dramatically. For example, by setting the applied bias to 550 $V$, this incoherent bright beam propagates almost undistorted and behaves like a quasi-soliton as shown in Fig.7.1. This incoherent quasi-soliton tends to slightly oscillate in an effort to adjust to its new statistical-phase environment. In this case, the coherence length remains approximately constant around the center of the beam whereas it increases at the margins as depicted in Fig.7.2 within a spatial window of $\pm 40$ $\mu m$. This behavior is in good agreement with the static predictions of Ref. [83]. The existence of this bright quasi soliton can be understood on the basis of the multimode approach [83]. The increase of the coherence length at the margins of the beam can be explained from the fact, that away from the center, only the higher order modes contribute to the coherence. Our numerical simulations also show that

further increase of the bias voltage sets the beam into cycles of compression and expansion. In this latter case, the coherence length decreases at the center of the beam during compression and it increases when the beam expands.

### 7.3.2 Incoherent dark beams

As a second example, we consider the dynamics and coherence properties of an incoherent dark-like beam under odd and even initial conditions. In particular, let the spatial modulation function at the input be $\phi_0(x) = \tanh(x/x_0)$ under odd initial conditions, and $\phi_0(x) = [1-(1-\epsilon^2)\,\mathrm{sec}\,h^2(x/x_0)]^{1/2}$ under even. Here $x_0$ is associated with the intensity FWHM of this beam and $\epsilon^2 < 1$. In this example, the intensity FWHM of these dark beams is taken to be 10 $\mu m$ and their normalized background intensity is $\rho = 3$. Let again, $\theta_0$ be $0.55^o$ with a source coherence length $l_c \simeq 8.8$ $\mu m$. It is important to note, that, during linear diffraction the coherence length of an incoherent dark beam becomes a function of $x$ which implies that eld uctuations are no longer stationary. Moreover, unlike their coherent counterparts, incoherent dark beams tend to quickly disappear during diffraction, without leaving any trace of their previous existence. For example, after 1 $cm$ of propagation, an odd dark beam whose initial FWHM is 10 $\mu m$ will diffract to 138 $\mu m$, and its grayness will be $\sim$ 90%, and the dark notch almost disappears. Our numerical simulations show that photorefractive nonlinearity plays again an important role.

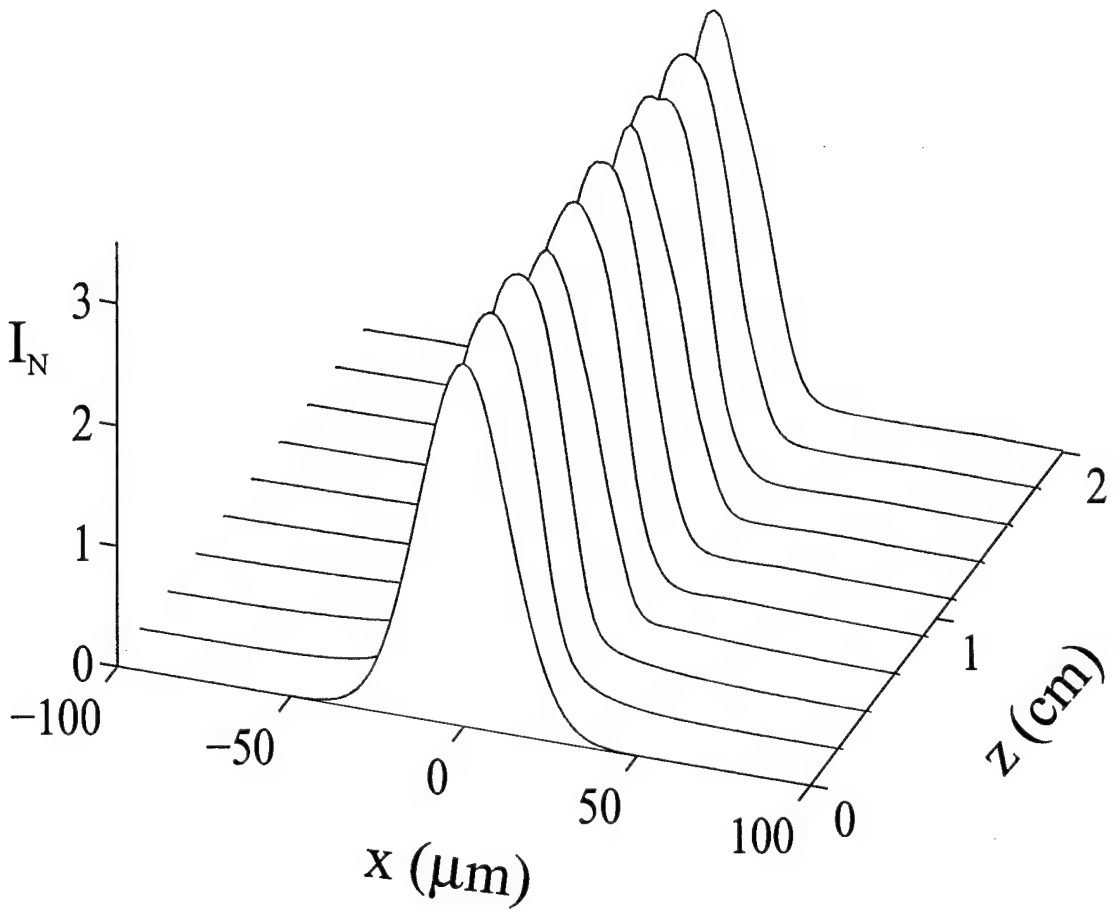


Figure 7.1: Propagation of bright incoherent quasi-soliton when *r=3* and at a bias of *550 V*.

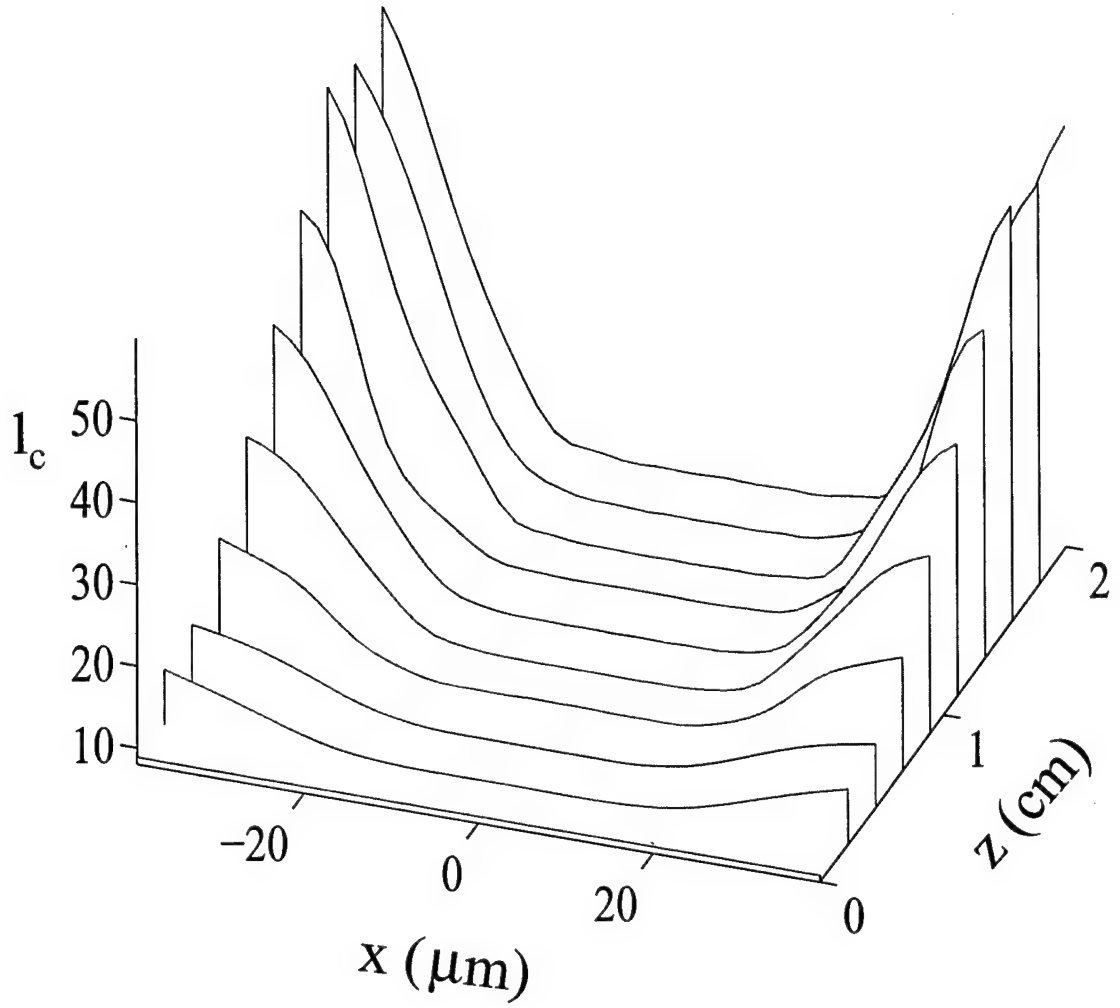


Figure 7.2: The coherence length $l_c$ of the bright soliton shown in Fig.7.1 as a function of distance.

With the application of $\sim -300\ V$, after a certain distance of propagation, an initially odd beam becomes a gray-like incoherent quasi-soliton whose FWHM and grayness oscillate around constant values. The intensity and the coherence length of this incoherent beam is depicted in Figures 7.3 and 7.4. Fig.7.3 shows that even though the beam itself exhibits a somewhat oscillatory behavior, its spatial FWHM varies between 9 $\mu m$ and 5.6 $\mu m$ and its grayness between 56 % and 31 % over a distance of 2 $cm$. Furthermore, its coherence length, Fig.7.4, becomes higher (by $\sim$ 20 %) within the dark notch with a mild depression at the center. Note that a gray-like fundamental incoherent dark quasi-soliton was also suggested by Hasegawa [85],[86],[87] by averaging the phase of all the quasi-particles involved in the Vlasov transport equation. Our analysis on the other hand, shows that the phase is extremely important (even more than the normalized intensity $\rho$), i.e. a single dark incoherent soliton is only possible provided that initially a $\pi$-phase shift is imposed on the wavefront. Fig.7.5 shows, what happens to this beam if we increase the bias voltage to $-550\ V$. In this case, the odd incoherent dark beam leads to a triplet. This differs from coherent triplets [9],[34],[108] since the central soliton is gray-like. Fig.7.6 shows that the coherence length increases again by $\sim$ 20 % around the soliton regions. If the incoherent beam at the input is even, a gray soliton doublet occurs. Our simulation shown in Fig.7.7, demonstrates that this is true when the bias voltage is $-550\ V$, the intensity FWHM is initially 10 $\mu m$

and $\epsilon^2 \ll 1$. Fig.7.8 shows the correlation length associated with these incoherent doublets.

Depending on the initial conditions, an even or odd number of incoherent dark-like structures can appear at higher voltage values. From these 1-D results one may speculate that 2-D incoherent vortex solitons may also be possible in photorefractives and in other non-instantaneous nonlinear media. Furthermore, we emphasize that the behavior of these bright/dark incoherent quasi-solitons is fundamentally different from that of their coherent counterparts. For example, unlike a coherent gray soliton, the fundamental incoherent dark soliton does not exhibit a transverse velocity in spite of its grayness.

## 7.4 Conclusions

In conclusion, we have shown that under appropriate initial conditions, bright as well as dark-like incoherent quasi-solitons can form in biased photorefractives. Using numerical simulations we have found that incoherent gray soliton pairs as well as triplets are possible under even or odd initial conditions. The coherence properties of these beams were found to be signi cantly affected during propagation by the photorefractive nonlinearity. Relevant examples have been provided.

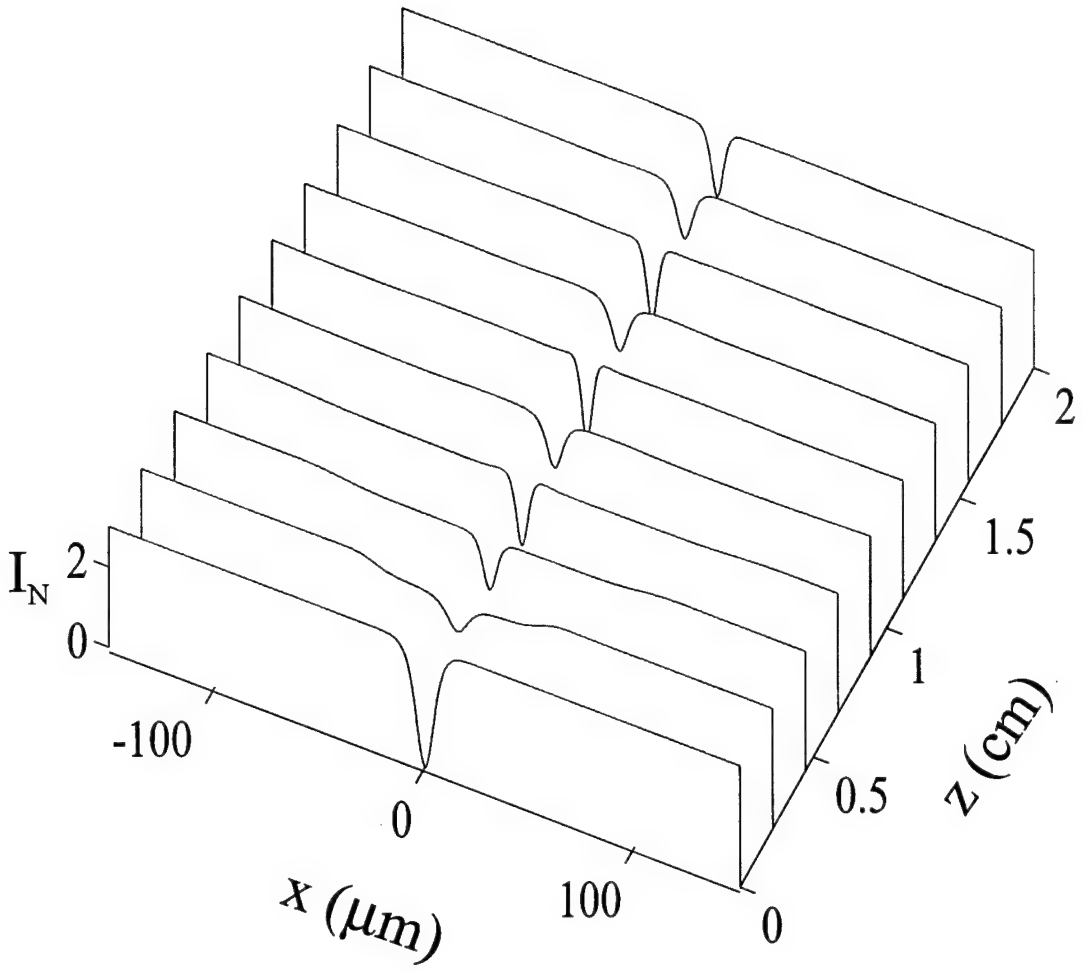


Figure 7.3: Intensity profile of a dark-like incoherent soliton when $\rho=3$ and the bias is *-300 V*.

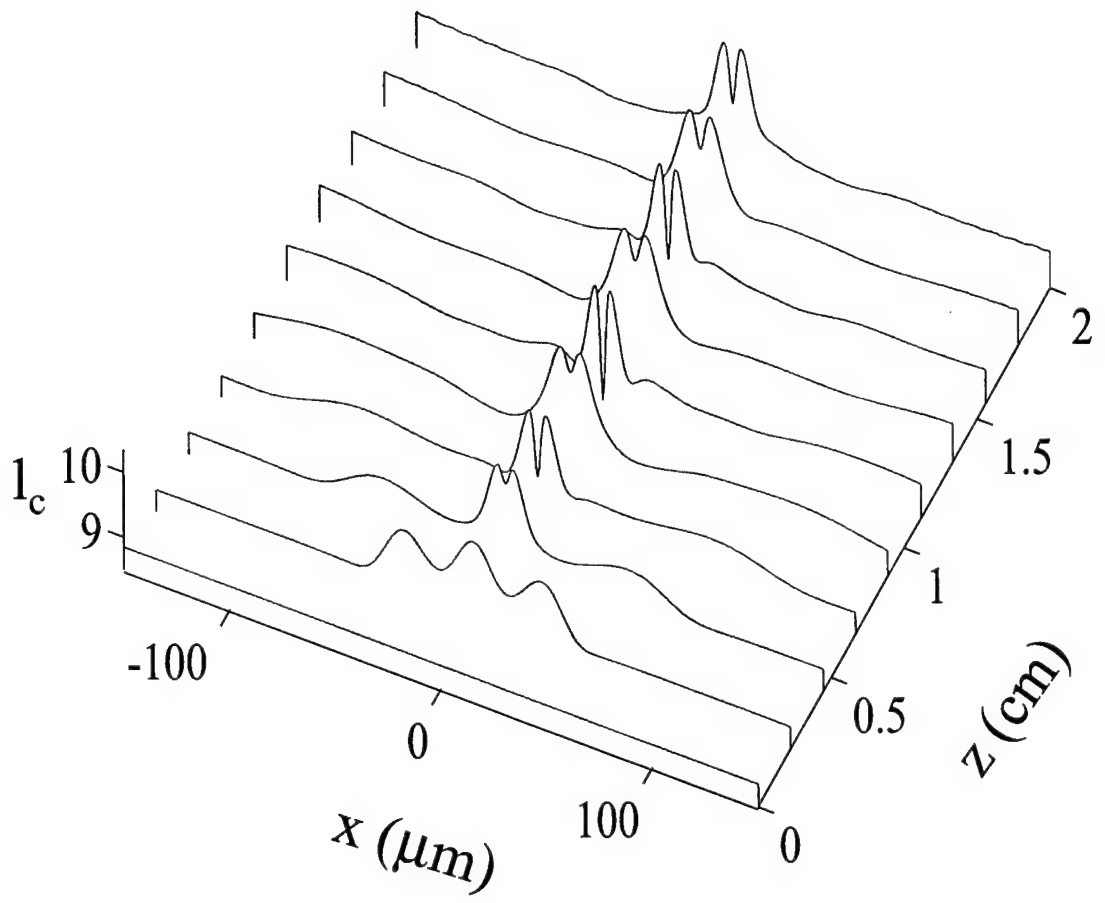


Figure 7.4: Coherence length $l_c$ of the dark soliton shown in Fig.7.3.

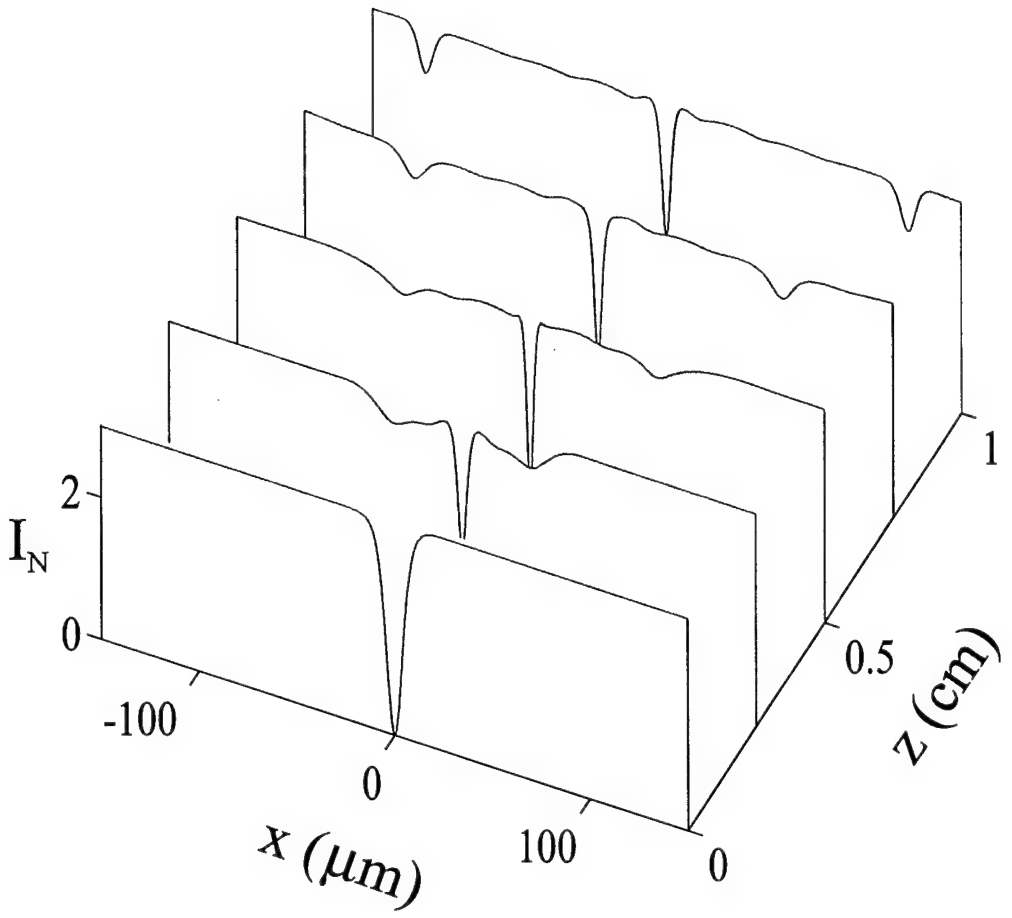


Figure 7.5: Formation of an incoherent soliton triplet when $\rho=3$ and the bias is *-550 V*.

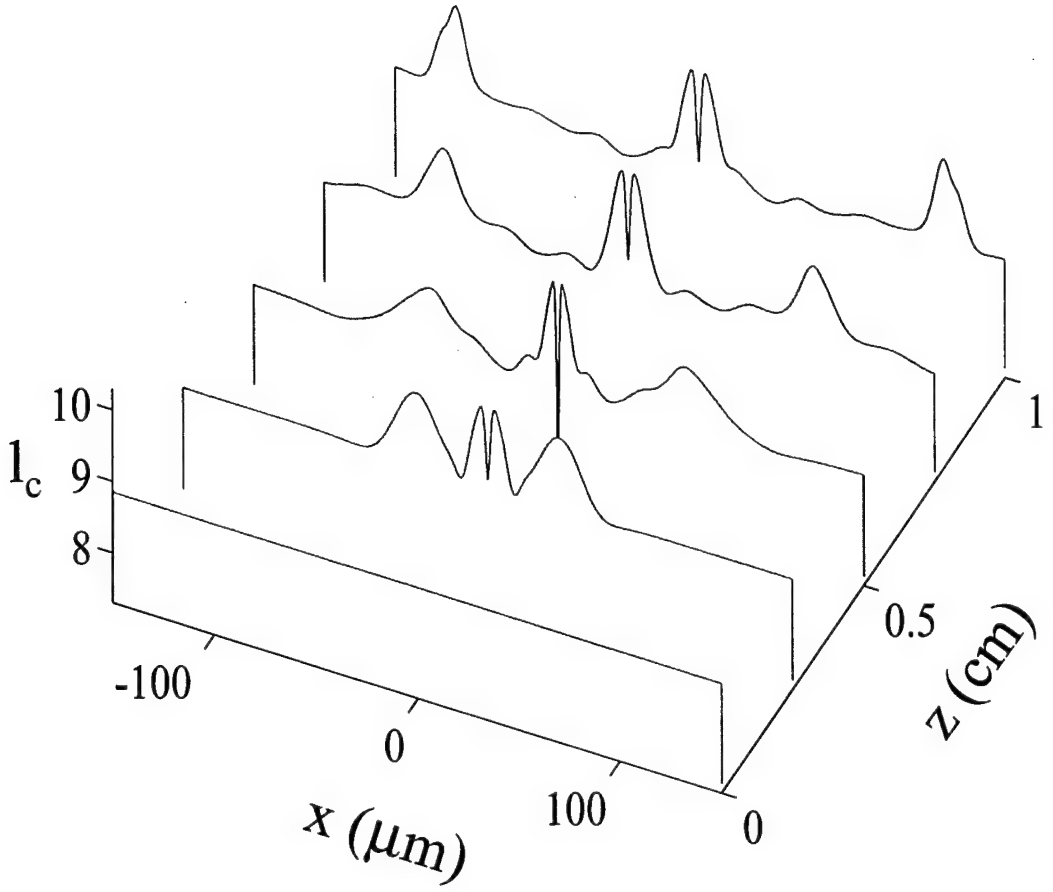


Figure 7.6: The coherence length $l_c$ of the triplet shown in Fig.7.5 as a function of distance.

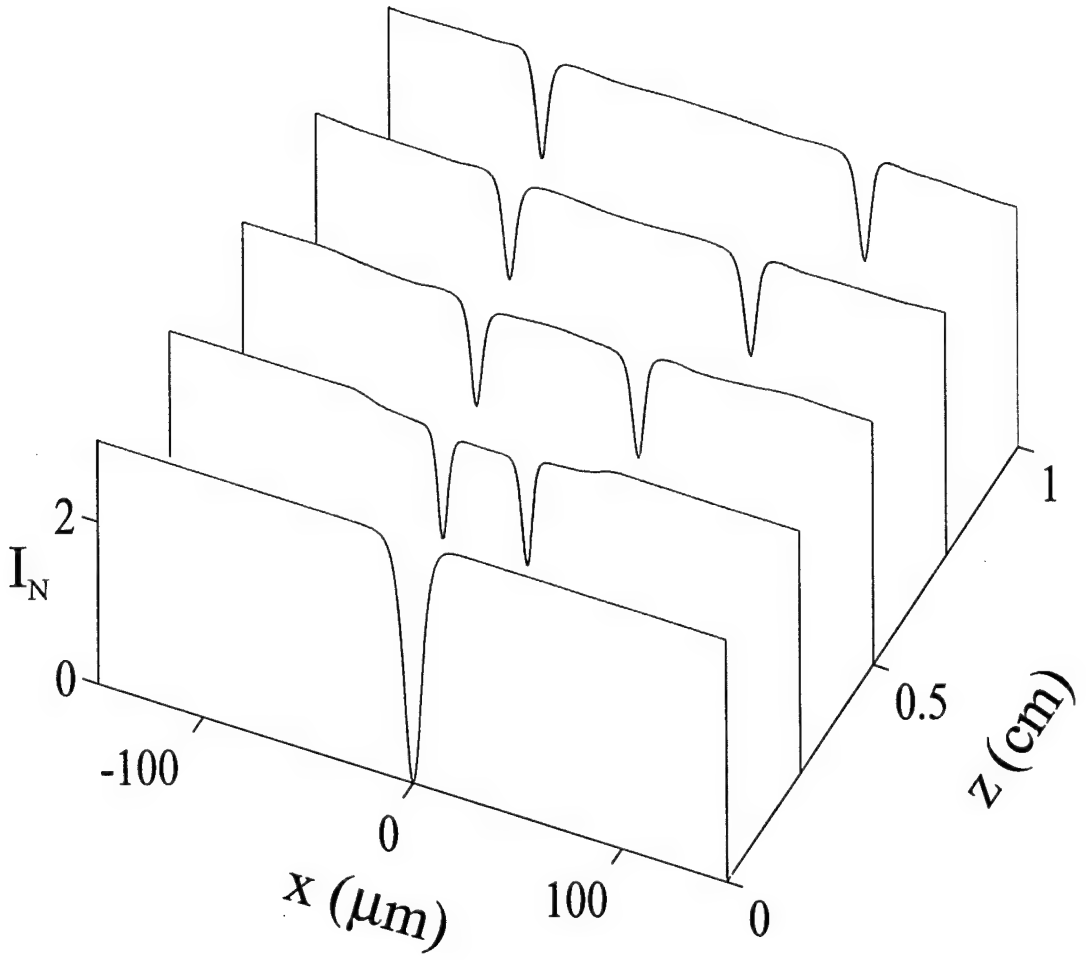


Figure 7.7: An incoherent gray soliton pair from even initial conditions.

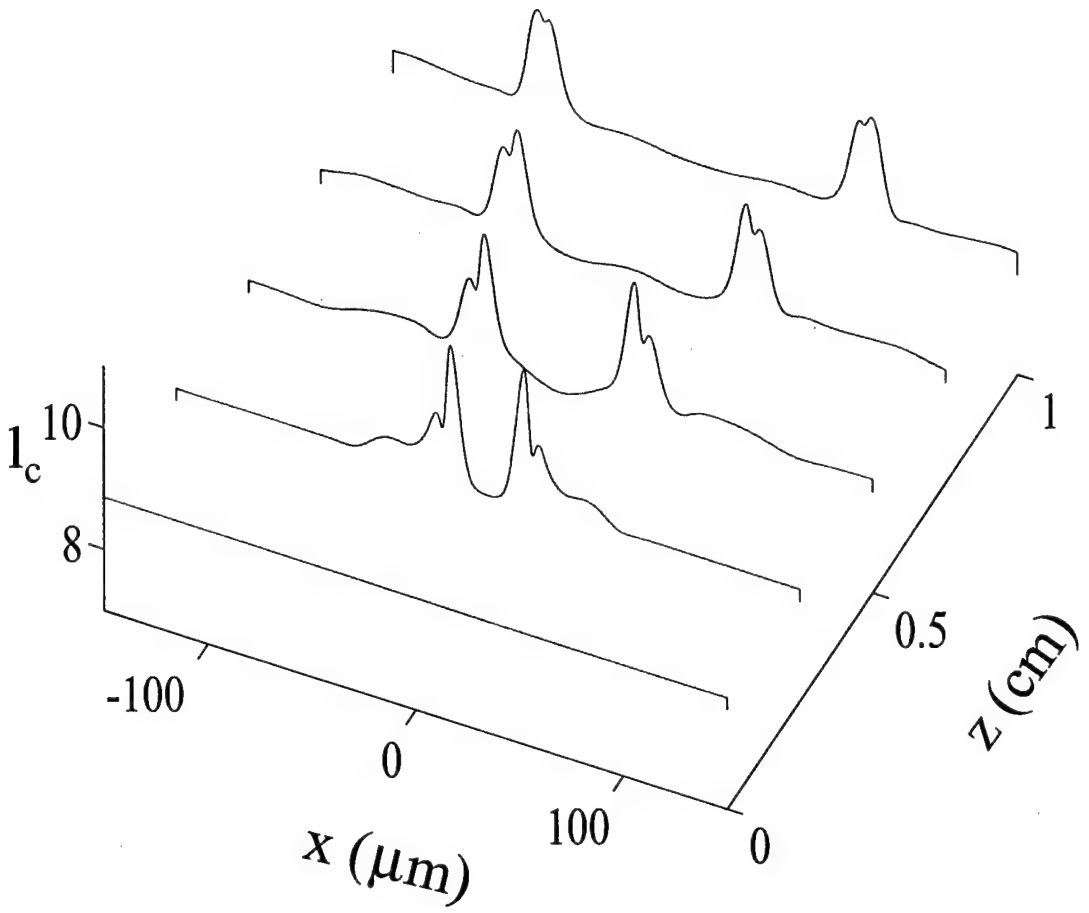


Figure 7.8: The coherence length $l_c$ associated with the pair shown in Fig.7.7.

# Chapter 8

# Dark incoherent soliton splitting and phase-memory effects

In this chapter, the effects of incoherence on the evolution of incoherent dark soliton doublets are investigated both theoretically and experimentally. We show that the dynamics of these incoherent self-trapped entities are associated with strong phase-memory effects which are otherwise absent in the linear regime.

## 8.1 Introduction

In the last chapter, we have shown that incoherent dark solitons may be possible in biased photorefractives [109]. Based on this prediction, incoherent dark planar and 2-D dark solitons ( vortices ) were observed in a SBN:60 crystal [110]. This was achieved by employing the photorefractive self-defocusing nonlinearity associated with screening solitons [23],[24]. As predicted in [109], the incoherent dark solitons were found to be gray. Moreover, these dark incoherent solitons were efficiently excited provided that an initial $\pi$-phase flip was imposed on the incoherent wavefront. Incoherent Y-soliton splitting was also predicted in the last chapter. Nevertheless, thus far we did not consider the behavior of these incoherent soliton doublets, for different degrees of coherence.

In this chapter, we report the first experimental observation of dark incoherent soliton Y-splitting in a noninstantaneous self-defocusing nonlinear medium as predicted in Chapter 7. The evolution of these incoherent soliton doublets is then systematically investigated as a function of their coherence, both theoretically and experimentally. Surprisingly, we find that over a wide range of parameters, the Y-splitting is approximately the same irrespective of coherence. Moreover, we show that the dynamical behavior of this incoherent Y-splitting process is associated with strong phase-memory effects which are otherwise absent in the linear regime. In other words, we show that dark incoherent self-trapped entities (dark incoherent

solitons) are characterized by a strong memory effect that lasts throughout propagation and governs their propagation behavior (single soliton versus Y-soliton splitting, etc.). This is in sharp contrast to all known so far about linear propagation of incoherent beams, in which all phase information is fully washed out after a nite distance [111],[112].

## 8.2 Coherent and incoherent Y-juntion solitons

### 8.2.1 Diffraction of coherent and incoherent beams

Our experiments were carried out in SBN:60 crystals. For this reason, here we use the (1+1) D saturable nonlinearity of the form $1/(1+I)$ [23], [24] so as to make direct comparisons with experiment. We emphasize, however, that our results hold for any noninstantaneous nonlinearity that can give rise to dark solitons. In this material system (photorefractives), the normalized intensity $I_N = I/I_d$ (where $I_d$ is the dark irradiance) of the incoherent dark beam evolves according to following normalized nonlinear integro-differential equation [79],[82],[109]:

$$i\left(\frac{\partial f}{\partial \zeta}+\alpha\frac{\partial f}{\partial s}\right)+\frac{1}{2}\frac{\partial^2 f}{\partial s^2}+\beta\frac{f}{1+I_N(s,\zeta)}=0 \tag{8.1}$$

where

$$I_N(s,\zeta)=\int_{-\infty}^{+\infty}|f(s,\zeta,\theta)|^2\,d\theta \tag{8.2}$$

and at $\zeta = 0$, the coherent density $f$ is given by

$$f(\zeta = 0, s, \theta) = \rho^{1/2} G_N^{1/2}(\theta)\, \phi_0(s) \quad . \tag{8.3}$$

In the above equations, we have used the following normalized coordinates: $\zeta = z/(kx_0^2)$ and $s = x/x_0$ where $x_0$ is an arbitrary spatial scale associated with the intensity FWHM of the beam. Moreover, $\alpha = kx_0\theta$, $\beta = (k^2x_0^2/2)\, n_e^2 r_{33} |E_0| (1+\rho)$ where $\theta$ represents an angle (in radians) with respect to the $z$ axis, $k = k_0 n_e$ is the wavenumber, $k_0 = 2\pi/\lambda_0$, $n_e$ is the extraordinary refractive index of the material, and $r_{33}$ is the electrooptic coefficient involved. $E_0 = -V/W$ is the value of the space charge eld at $x \to \pm\infty$ where $V$ is the reverse applied bias and $W$ the $x$-width of the crystal. $G_N(\theta)$ is the normalized angular power spectrum of the incoherent source and $\phi_0(s)$ is the input complex spatial modulation function. In this study, $G_N(\theta)$ is assumed to be Gaussian, i.e. $G_N(\theta) = (\pi^{1/2}\theta_0)^{-1} \exp(-\theta^2/\theta_0^2)$ where $\theta_0$ is associated with the width of angular power spectrum. Finally, $\rho$ is the normalized intensity of the dark beam at $x \to \pm\infty$. Here, as usual, we assume that, the beam at the input obeys a stationary random process. In general, the coherence properties of these beams can be followed using a version of the Van Cittert-Zernike theorem as in the last chapter. The coherence length of the beam at $z = 0$ can be readily obtained from $G_N(\theta)$ and it is given by $l_c = \sqrt{2\pi}/(k\theta_0)$. When the beam is fully coherent ($\theta_0 = 0$), the coherence length of the beam becomes in nite, i.e. $l_c \to \infty$. In this case, the system of Eqs. 8.1 and 8.2 collapse to a standard single differential

equation given in Chapter 2 [23],[24].

Before we present our experimental results, it may prove bene cial to rst discuss the behavior of such incoherent dark beams from a theoretical point of view. As in the experiment, let us consider a biased SBN:60 crystal with $n_e = 2.3$, $r_{33} = 250$ $pm/V$, $\lambda_0 = 514$ $nm$, $W = 5.3$ $mm$ [110]. We let the spatial modulation function at the input be $\phi_0(x) = \tanh(x/x_0)$ under odd initial conditions, and $\phi_0(x) = [1 - \epsilon^2 \operatorname{sec} h^2(x/x_0)]^{1/2}$ under even. The quantity $\epsilon^2$ de nes the beam s grayness. Throughout this work, we assume that at $z = 0$, $\epsilon^2 \approx 1$ (almost black even dark beams). The input intensity FWHM of the even and odd dark beams is taken here to be 25 $\mu m$ as shown in Fig.8.1(a). Moreover, the normalized background intensity is $\rho = 3$. First, we consider linear diffraction of coherent and incoherent dark-beams under odd and even initial conditions. Figs.8.1(b) and (c) show the diffracted intensity pro les of coherent odd and even dark beams respectively after $\sim 12$ $mm$ of propagation. In this case, the intensity FWHM of the odd dark beam at the output is $\sim 42$ $\mu m$ whereas that of the even is $\sim 76$ $\mu m$. It is important to note that after diffraction, the intensity of the odd coherent beam is always zero at the center whereas that of the even is gray-like. Fig. 8.1(d), on the other hand, demonstrates how an odd or even incoherent dark beam will diffract after 12 $mm$ of propagation when at the input $\theta_0 \simeq 5$ $mrads$ or $l_c = 17$ $\mu m$. This latter gure shows that, the intensity pro les of the odd and even incoherent dark beams are almost

identical with an output FWHM of $\sim 100\ \mu m$. Simulations suggest that the same also applies for the $l_c(x)$ curves corresponding to these two cases as shown in Fig. 8.1(e). Thus, from diffraction data alone, it is extremely difficult to distinguish an odd dark beam from an even one. In other words, the randomly changing speckled structure of an incoherent beam leads to a loss of phase memory. Therefore, as a result of this phase washing effect, a sufficiently incoherent dark beam diffracts approximately the same way regardless of the phase information initially imposed on it. An important distinction between diffraction of a coherent and an incoherent dark beam comes from the structure of their background. Figure 8.1 clearly demonstrates that a diffracted coherent dark beam involves intensity ripples in its background. These oscillations tend to disappear in the case of an incoherent beam as a result of its speckled structure.

When on the other hand the nonlinearity is activated, the dynamics of these incoherent beams depend on initial phase information. As previously predicted, generation of a single incoherent dark (which is in reality gray) beam or a higher-order triplet requires a $\pi$-phase shift. Conversely, starting from even initial conditions, an incoherent gray soliton pair or Y-soliton splitting can be obtained [109]. In other words, in the presence of nonlinearity, an incoherent dark beam tends to remember its origins and identity, i.e. a phase-memory effect is established. Thus, the beam starts to behave in a quasi-coherent fashion [34].

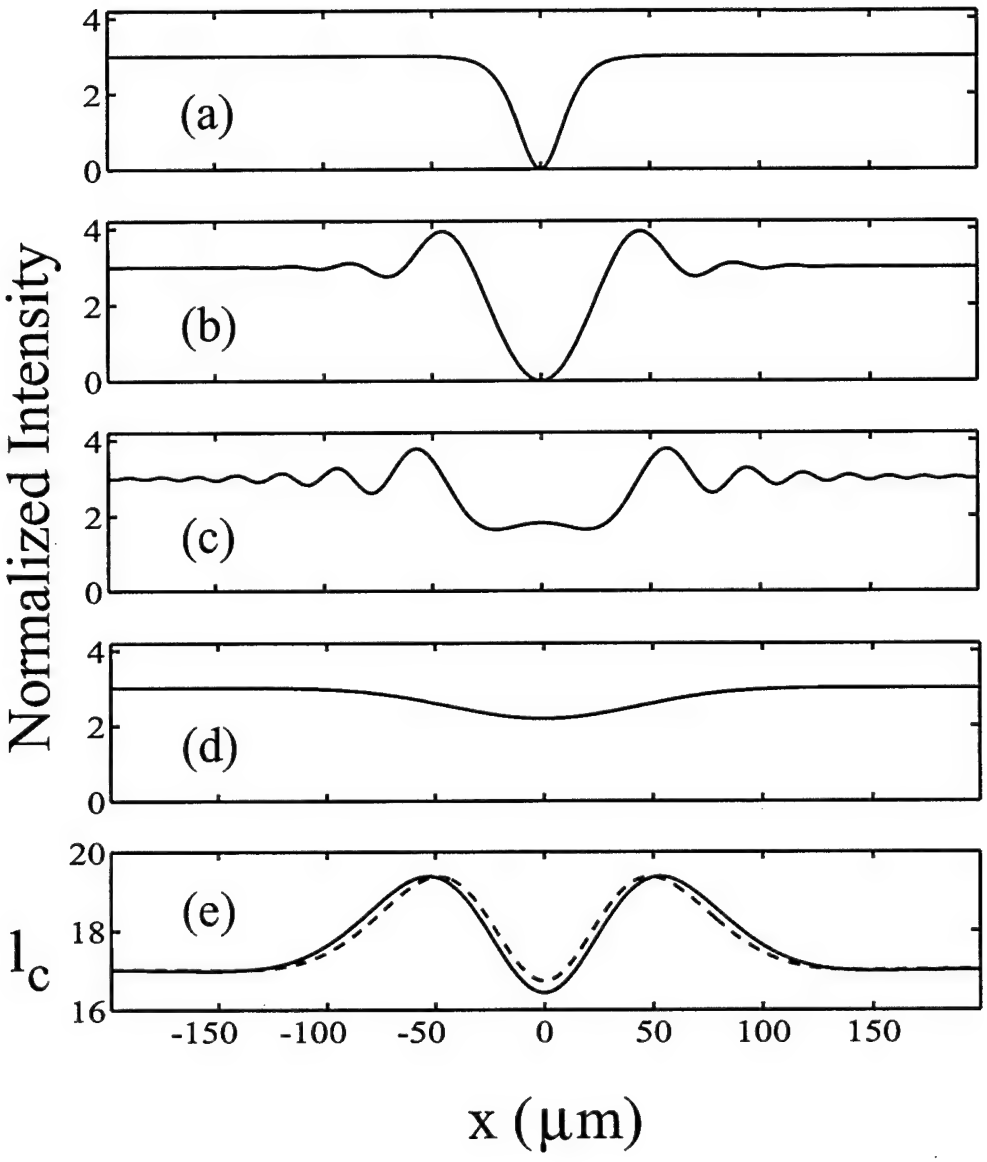


Figure 8.1: (a) Intensity profile of a *25 μm* odd or even dark beam at the input. Diffraction of an (b) odd coherent dark beam, (c) even coherent dark beam, (d) incoherent odd or even dark beam with $l_c$ = 7.3 *μm* after *12 mm* of propagation. (e) $l_c$ in *μm* as a function of *x* for the odd (dashed curve) and even (solid curve) diffracted incoherent dark beam shown in (d).

### 8.2.2 Experiment results

Experiments with an amplitude notch (even initial conditions) are performed by using both coherent and spatially incoherent light sources for comparison. Details regarding the coherent dark soliton experiments can be found in Ref. [34]. The laser used is a Ar ion laser ($\lambda_0 = 514\ nm$). An arti cial background dark irradiance is provided by uniformly illuminating the entrance face of the crystal (SBN:60) along the ordinary axis. The maximum intensity ratio (at the tails) of the dark beam with respect to dark irradiance is approximately 1.5. The dark beam is also broad enough to cover entire input face of the crystal. For the incoherent case, a rotating diffuser is employed to provide random phase uctuations across the beam [35],[36],[110]. In this case, we generate a dark notch on a broad partially spatially incoherent beam with controllable degree of coherence. The experimental arrangement is the same as that in Ref. [110], except that the phase mask is now replaced by an amplitude mask. Incoherent Y-junction solitons are generated and then compared with the coherent ones. Fig.8.2 shows typical experimental results. When the dark beam is coherent, it diffracts from a FWHM of 25 $\mu m$ (left) to about 58 $\mu m$ after $\sim 12\ mm$ of propagation (middle) when no nonlinearity is present. Note that, with the exception of the dark notch FWHM (which from simulations is expected to be $\sim 76\ \mu m$), its intensity structure is in agreement with Fig.8.1(c). The discrepancy in FWHM is attributed to the fact that the re ection from the metallic wire introduces a

quadratic phase which is not accounted in our simulations. After applying a voltage of $-350V$ (negative relative to the c-axis), the dark amplitude notch evolves into a pair of gray solitons (right). The second and third rows of this gure depict the same data when the dark beam is incoherent. The right column of the gure was obtained at $V = -350\ V$ and with an input FWHM of 25 $\mu m$. As seen in Fig.8.2, the grayness of the soliton pair increases as the incoherence of the beam increases. Nevertheless, the spacing of these two solitons at the crystal output face is about the same for a varying degree of coherence.

### 8.2.3 Simulation results

These experimental results are now compared with numerical simulations. By keeping in mind that in the experiment, the input speckle size of the incoherent beams is 30 $\mu m$ for Fig.8.2(b) and 15 $\mu m$ for Fig.8.2(c) and by considering their diffraction behavior, we estimate that the width of the angular power spectrum in these two cases is $\sim 3.5\ mrads$ and $5.2\ mrads$ respectively. The simulation shown in Fig.8.3(a) demonstrates how a coherent soliton doublet forms from a 25 $\mu m$ even dark beam after 12 $mm$ of propagation when $V = -450\ V$. For the same bias voltage and initial beam width, the intensity pro le of an incoherent doublet after 12 $mm$ of propagation is shown in Fig.8.3(b) when $\theta_0 = 3.5\ mrads$ or $l_c = 25\ \mu m$. Fig. 8.3(c) depicts similar data when $\theta_0 = 5.2\ mrads$ ($l_c = 17\ \mu m$) and again $V = -450\ V$.

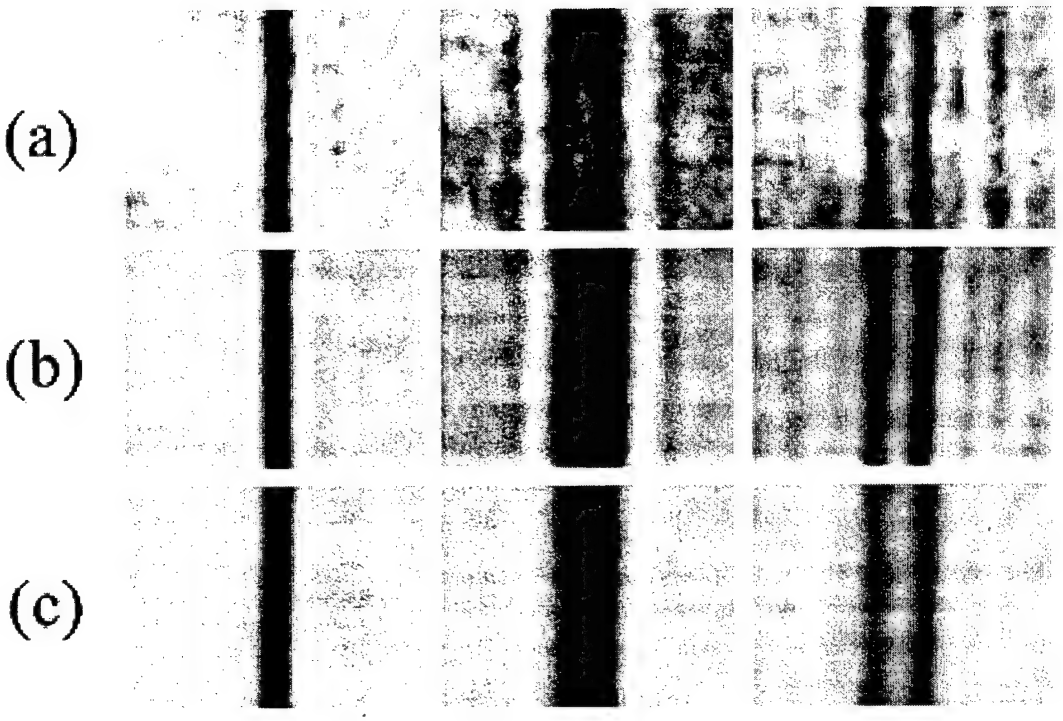


Figure 8.2: Experimental observation of coherent and incoherent Y-splitting: (a) coherent dark beam; (b) (c) incoherent dark beam with an average speckle size of *30 μm* and *15 μm* respectively. The first column depicts the input intensity, the second one diffraction data, and the third one Y-splitting at *-350 V*. In all the cases the intensity FWHM of the beam at the input is *25 μm*.

Both gures, 8.3(b) and (c), were obtained by numerically solving Eqs. 8.1-8.3 as done in previous chapters. In agreement with the experiment, Fig.8.3 demonstrates that the doublet becomes grayer as the incoherency increases. Surprisingly, for this range of parameters, both theory (Fig.8.3) and experiment (Fig.8.2) suggest that the Y-splitting angle or the doublet separation does not depend strongly on the degree of coherence. To further understand this Y-splitting process, we carried out another set of simulations. In this latter set, the intensity FWHM of the even dark beam was chosen to be 10 $\mu m$ (in order to accelerate splitting process) and $l_c$ varied from $\infty$ down to 3.4 $\mu m$. Figs.8.4(a)-(c) were obtained for the same initial conditions and bias voltage ($V = -2400\ V$) after 12 $mm$ of propagation for different degrees of coherence. Even in this case, the splitting is relatively insensitive to $\theta_0$. This is by itself very interesting considering the range in which $l_c$ varies. This is another manifestation of the phase memory effect discussed earlier. As the incoherency of the dark beam increases, a higher bias voltage is required to establish a doublet. Fig.8.4(d) shows Y-splitting of a 10 $\mu m$ even incoherent dark beam after 12 $mm$, when $V = -4000\ V$ and $l_c = 3.4\ \mu m$. Finally, at lower $l_c$ s, the doublet practically disappears (because of its grayness) and the splitting angle is further reduced.

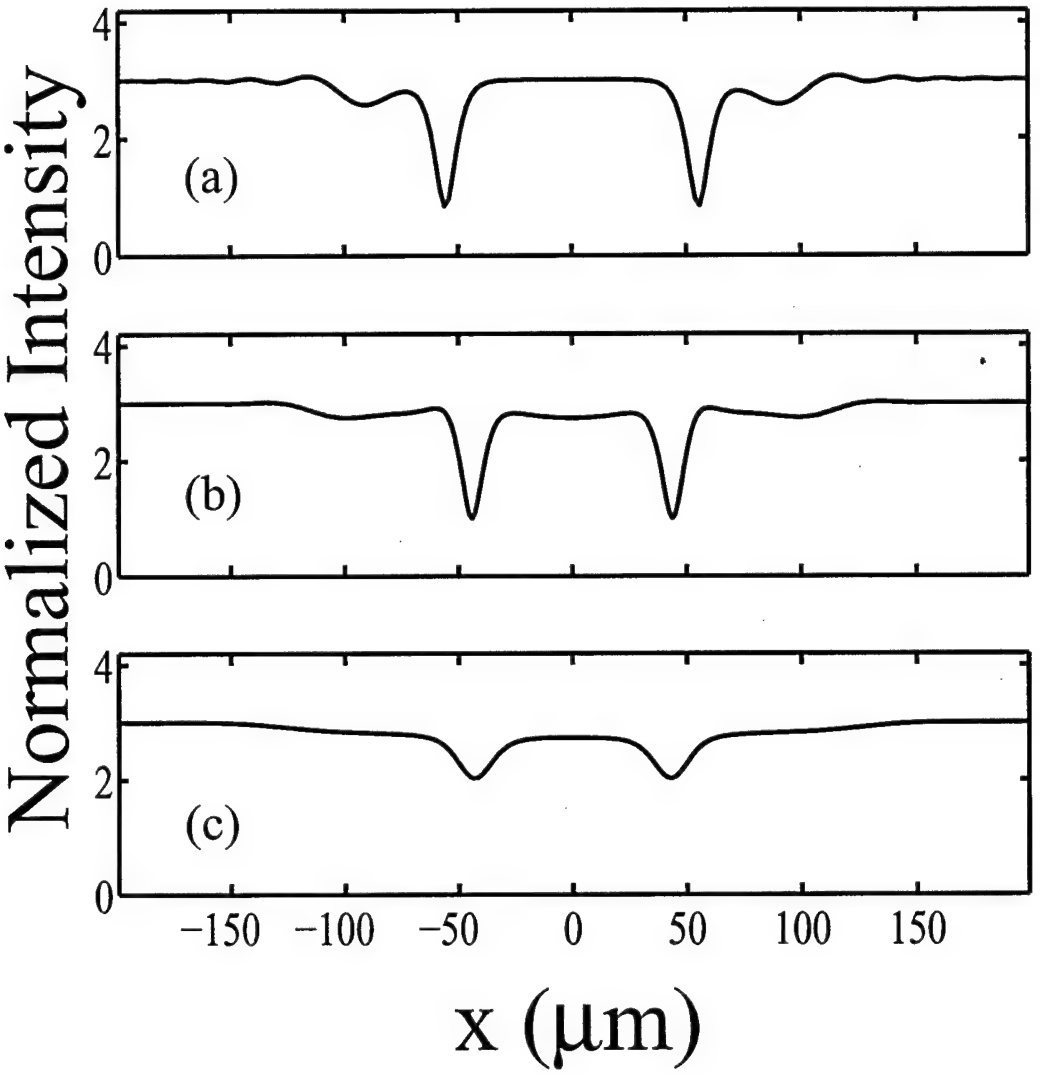


Figure 8.3: Intensity profile of a soliton doublet at $z = 12\ mm$ when the external bias is $-450\ V$ and the beam is (a) coherent or incoherent with (b) $l_c = 25\ \mu m$, (c) $l_c = 17\ \mu m$. In all cases the initial intensity FWHM of the beam is $25\ \mu m$.

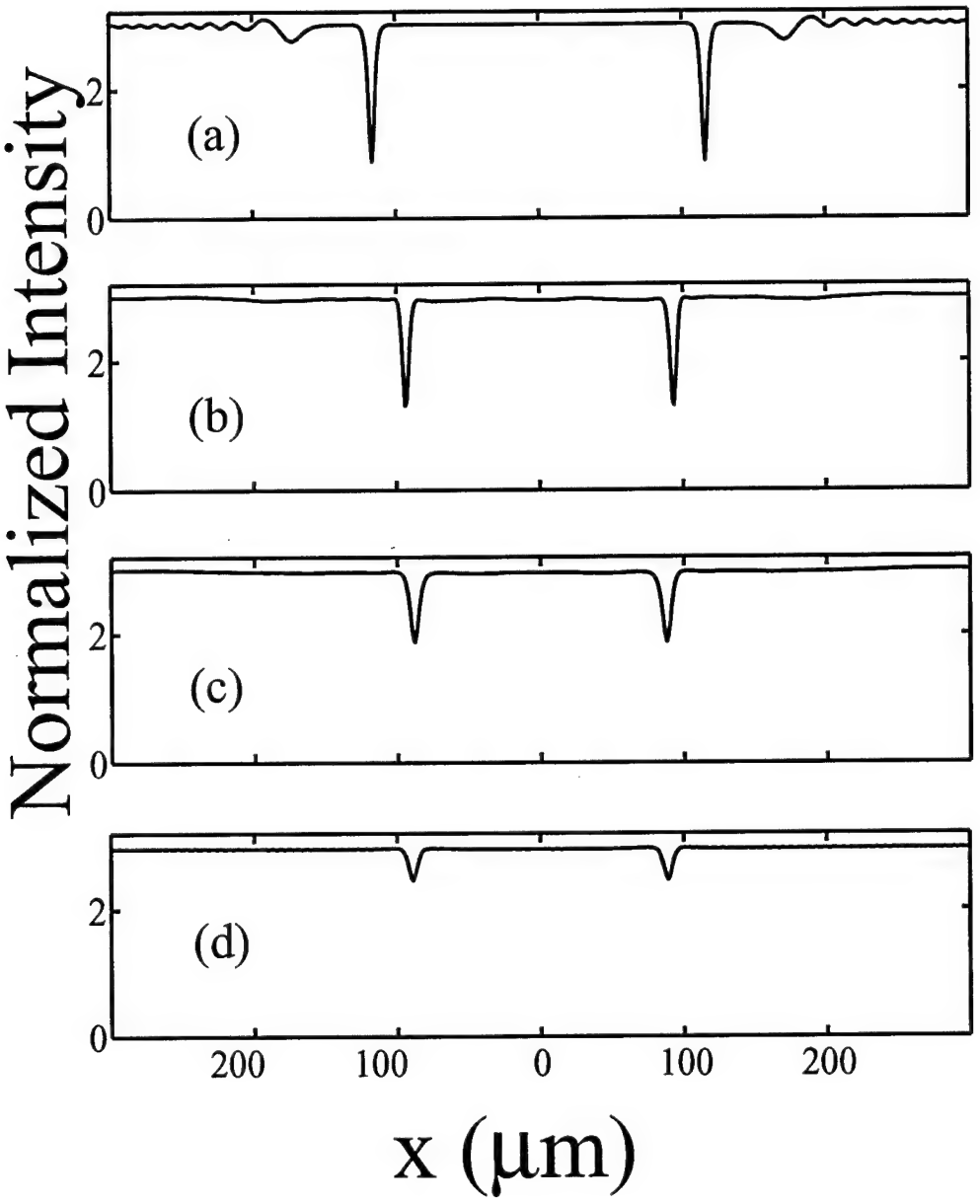


Figure 8.4: Intensity profile of a soliton doublet at $z = 12\ mm$ when the external bias is $-2400\ V$ and the beam is (a) coherent or incoherent with (b) $l_c = 9.3\ \mu m$, (c) $l_c = 7.3\ \mu m$. Same information when the external bias is $-4000\ V$ and $l_c = 3.4\ \mu m$. In all cases the initial intensity FWHM of the beam is $10\ \mu m$.

## 8.3 Conclusions

In conclusion, incoherent dark soliton Y-splitting has been demonstrated experimentally. Using the coherent density approach we have shown that the evolution of incoherent dark solitons in non-instantaneous nonlinear media is associated with strong phase-memory effects which are otherwise absent in the linear regime. The higher-order behavior of these dark beams has been compared under the same initial conditions but for different degrees of coherence. It was found that over a wide range of parameters, the Y-splitting is approximately the same irrespective of spatial coherence. Experimental observations are in good agreement with theoretical predictions.

# Chapter 9

# Theory of Incoherent Dark Solitons

In this chapter, we formulate the theory of incoherent dark spatial solitons in non-instantaneous self-defocusing nonlinear media. We find that the basic modal constituents of these incoherent dark soliton entities are radiation modes as well as bound states. Our results explain for the first time why incoherent dark solitons are in fact gray and why a transverse $\pi$-phase flip can facilitate their observation.

## 9.1 Introduction

The numerical results of Chapter 7 suggested that incoherent dark quasi-solitons can be effectively excited in self-defocusing (reverse biased) photorefractive crystals, provided that at the origin, a $\pi$ phase jump is imposed on the incoherent wavefront [109]. Even more importantly, unlike their coherent counterparts [113], these dark incoherent solitons were always found to be gray! The gray character of these solutions is in qualitative agreement with some earlier predictions of random-phase envelope solitons made by Hasegawa two decades ago within the context of plasma physics [85],[86],[87]. In that early work, the average dynamics of all the random quasi-particles involved were treated using a Vlasov transport equation.

Subsequently, incoherent dark-stripe and dark-hole (vortex) solitons were experimentally demonstrated in a biased photorefractive crystal [110]. In all cases, these self-trapped incoherent beams carried the characteristic signature of dark incoherent soliton structures [85],[86],[87],[109], i.e., they were found to be gray. Moreover, in agreement with predictions of Chapter 7 [109], the incoherent dark solitons were experimentally observed when an appropriate phase pro le was imposed on the wavefront. Yet, at this point, several important questions remain unanswered. First of all, are there truly stationary incoherent dark solitons and why are they gray? Furthermore, why is the $\pi$-phase jump necessary for their excitation and how is

it possible for this initial phase imprint to survive in the midst of random phase-uctuations? The answers to the above questions can not be obtained from the coherent density method (because of its inherent complexity) nor from the approximate Vlasov approach. These issues can only be resolved by identifying the modal composition of these dark incoherent soliton states, as was done in the case of their bright soliton counterparts [83],[114]-[116].

In this chapter, by means of an exact solution, we demonstrate that stationary incoherent dark solitons can exist in nonlinear self-defocusing media. These solitons, involve in general, a belt of radiation modes (both odd and even) as well as bound states. The presence of even radiation and bound modes explains why these structures are in fact gray. Moreover, we nd that the odd radiation modes dominate within the dark region of the beam, which justi es the $\pi$-phase shift required to excite these dark incoherent soliton states. The coherence properties of these solitons are also considered and they are found to be in good agreement with the results of Chapter 7.

## 9.2 Theoretical formulation

Let us consider a self-defocusing nonlinear medium of the Kerr type, i.e. $n^2 = n_0^2 - n_2 I$, where $n_0$ is the linear refractive index of the material, $n_2$ is the Kerr coefficient and $I$ the optical intensity. We also make the important assumption

that the nonlinearity responds much slower than the characteristic phase uctuation time across the beam so as to avoid beam breakup due to speckle instabilities [74],[83]. Thus in this regime, the material will experience only the time-averaged beam intensity. Such non-instantaneous Kerr-like media include for example, biased photorefractives at low intensity ratios and materials with appreciable thermal nonlinearities [23],[24], [92],[93]. For example, a typical phase uctuation time is 1 $\mu s$, whereas a photorefractive crystal responds within 0.1 $s$ [110]. Let the time-averaged intensity pro le of this planar dark incoherent soliton be of the form

$$I_s = I_0 \left[1 - \varepsilon^2 \mathrm{sech}^2 \left(x/x_0\right)\right] \tag{9.1}$$

where the parameter $\varepsilon^2 \leq 1$ is associated with its grayness and $x_0$ is related to its spatial extent. The partially-spatially incoherent dark beam is quasi-monochromatic and it propagates along $z$. Furthermore, let the electric eld of all the modes comprising this beam be written as $E = U(x)\exp(i\beta z)$ where $\beta$ is the mode propagation constant. Using Eq. 9.1, the modal function $U$ is then found to obey the following Helmholtz equation:

$$\frac{d^2U}{ds^2} + \left(g + f\mathrm{sech}^2(s)\right)U = 0 \tag{9.2}$$

where $s = x/x_0$, $g = [k_0^2(n_0^2 - n_2 I_0) - \beta^2]x_0^2$ and $f = k_0^2 x_0^2 \varepsilon^2 n_2 I_0$. In the spirit of Ref. [83], the next task will be to identify an appropriate modal composition such that the time averaged intensity $I_s$ gives rise to a nonlinear index change which is self-consistent [98] with the composition assumed in the very beginning. In

general, Eq. 9.2 exhibits two types of eigenfunctions: radiation modes and bound modes. As shown schematically in Fig.9.1, bound states are possible whenever $g = -q^2$ or $\beta^2 > k_0^2(n_0^2 - n_2 I_0)$, whereas radiation modes require that $g = +Q^2$ or $\beta^2 < k_0^2(n_0^2 - n_2 I_0)$.

At this point, let us first assume that the waveguide induced by this dark beam can only support one bound mode. This latter requirement can be met provided that the coefficient of the $\mathrm{sech}^2(s)$ potential is set equal to two, i.e. $f = 2$ or $x_0^2 = 2/(k_0^2 \varepsilon^2 n_2 I_0)$ [117],[118]. In this case, all possible modes allowed by Eq. 9.2 are given by (see Appendix F) [119]:

$$U_b = \mathrm{sech}(s) \tag{9.3}$$

$$U_{r,e} = Q\cos(Qs) - \tanh(s)\sin(Qs) \tag{9.4}$$

$$U_{r,o} = Q\sin(Qs) + \tanh(s)\cos(Qs) \tag{9.5}$$

For $f = 2$, $U_b$ is the only allowed bound state (at $q^2 = 1$) and the two degenerate eigenfunctions $U_{r,e}$ and $U_{r,o}$ are part of the radiation mode continuum. It is important to note that $U_{r,e}$ is an even radiation mode whereas $U_{r,o}$ is odd. Following these results, the total electric field is given by [117],[118]

$$\begin{aligned} E &= c_b U_b(s)\exp(i\beta_b z) \\ &\quad + \int_0^\infty dQ\,[\tilde{c}_e(Q)U_{r,e}(s,Q) + \tilde{c}_o(Q)U_{r,o}(s,Q)]\exp[i\beta_r(Q)z] \end{aligned} \tag{9.6}$$

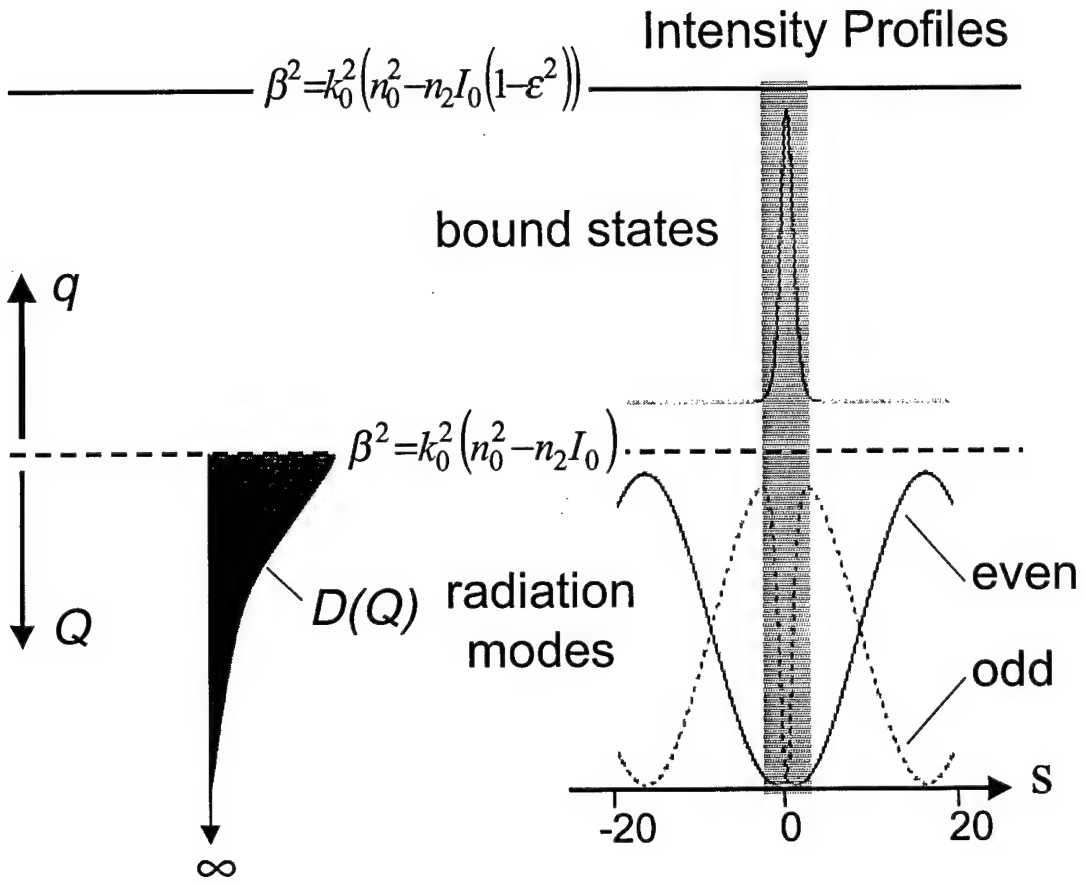


Figure 9.1: Eigenvalue diagram associated with a first-order incoherent dark soliton. The bound state intensity as well as the intensities of the even and odd radiation modes (at $Q = 0.1$) are also depicted. The dark stripe on the right shows the spatial extent of the soliton induced waveguide when $\varepsilon^2 = 0.5$.

where $c_b$ and $\widetilde{c}_{e,o}$ are modal eld coefficients that in general vary randomly in time [83],[114]-[116]. In Eq. 9.6, the upper limit of the integral is taken at in nity. As we will see, $Q$ is typically in the neighborhood of $Q \approx 0$, far away from $Q_{\max} = k_o(n_0^2 - n_2 I_0)^{1/2}$, which in turn justi es the upper limit of this integral. Under incoherent excitation, the following relationships hold true: $\left\langle c_{b,m} c_{b,n}^* \right\rangle \propto \delta_{mn}$, $\left\langle c_b \widetilde{c}_{e,o}^* \right\rangle = 0$, $\langle \widetilde{c}_o \widetilde{c}_e^* \rangle = 0$ and $\langle \widetilde{c}_e(Q) \widetilde{c}_e^*(Q') \rangle = \langle \widetilde{c}_o(Q) \widetilde{c}_o^*(Q') \rangle \propto D(Q)\delta(Q - Q')$. In other words, the statistical time expectation value of the $c$- eld coefficients is zero between different bound modes and the same applies between bound modes and radiation modes (odd or even). Furthermore, the odd and even radiation modes are always uncorrelated. Among the even radiation modes, the $\widetilde{c}_e$ coefficients correlate only for the same value of $Q$ and this is also true for the odd radiation elds. The last relationship also implies that the odd and even radiation modes are equally excited at the same $Q$ (with strength $D(Q)$). This is because the random source shows no preference to either odd or even radiation modes. The positive function $D(Q)$ represents a radiation mode distribution.

By utilizing these latter relationships, the intensity $I \propto \langle E(s,z) E^*(s,z) \rangle$ can then be obtained from Eq. 9.6, i.e.,

$$I = A^2 \mathrm{sech}^2(s) + \int_0^\infty D(Q) \left[ Q^2 + \tanh^2(s) \right] dQ \tag{9.7}$$

where in Eq. 9.7 we made use of the fact that $|U_{r,e}|^2 + |U_{r,o}|^2 = Q^2 + \tanh^2(s)$ and $\left\langle |c_b|^2 \right\rangle \propto A^2$. The rst term in Eq. 9.7 arises from the bound mode whereas

the second one from the combined intensity of odd and even radiation modes. For self-consistency, it is required that the intensity given by Eq. 9.7 is identical to $I_s$ of Eq. 9.1. This is satis ed provided that,

$$I_0 = \int_0^\infty D(Q)(Q^2+1)dQ \tag{9.8}$$

$$A^2 = \int_0^\infty D(Q)\left[1-\varepsilon^2(Q^2+1)\right]dQ \quad . \tag{9.9}$$

The analytical solution given by Eqs. 9.8 and 9.9 clearly demonstrates that stationary incoherent dark solitons indeed exist. This is the rst time we know of, that a soliton was found to involve a continuum of radiation modes as well as bound states. Even more importantly, this new class of solitons is gray because of the presence of even bound and radiation modes. It is evident from Eqs. 9.8 and 9.9 that the radiation mode distribution function $D(Q)$ is by no means unique. In fact, in nitely many self-consistent solutions can be obtained, depending on the particular choice of $D(Q)$.

To further illustrate our results, let $D(Q)$ be Boltzmann-like, i.e. $D(Q) = D_0 \exp(-Q/Q_0)$ where $Q_0$ represents the $Q$-width of this distribution. The exponentially decreasing character of $D(Q)$ can be justi ed whenever the angular power spectrum of the incoherent source decreases with the launch angle [79],[82],[109]. As a result, more power is expected to be coupled into small-angle ($Q \approx 0$) radiation modes than in those at higher $Q$ s. For this speci c choice of $D(Q)$, one quickly

nds that $D_0 = (I_0/Q_0)(2Q_0^2+1)^{-1}$ and that $A^2 = I_0\left[1-\varepsilon^2(2Q_0^2+1)\right](2Q_0^2+1)^{-1}$. Thus, $I_s = I_b + I_r$ where

$$I_b = \frac{I_0}{2Q_0^2+1}\left[1-\varepsilon^2(2Q_0^2+1)\right]\mathrm{sech}^2(s) \tag{9.10}$$

$$I_r = \frac{I_0}{2Q_0^2+1}\left[2Q_0^2+1-\mathrm{sech}^2(s)\right] \tag{9.11}$$

In Eqs. 9.10 and 9.11, $I_b$ is the bound-mode intensity component of the dark incoherent soliton and $I_r$ is the intensity pro le of the radiation-mode belt. It is also clear from Eq. 9.10 that this soliton exists provided that $\varepsilon^2(2Q_0^2+1) \leq 1$. The complex coherence factor $\mu_{1,2}(s_1,s_2)$ [69] of this incoherent soliton can then be obtained from Eq. 9.6, by evaluating the quantity

$$\begin{aligned}\langle E(s_1,z)E^*(s_2,z)\rangle \;\propto\; & A^2\mathrm{sech}(s_1)\mathrm{sech}(s_2) \\ & + \int_0^\infty D(Q)\left[U_{r,e}(s_1)U_{r,e}(s_2)+U_{r,o}(s_1)U_{r,o}(s_2)\right]dQ\end{aligned} \tag{9.12}$$

In turn, its correlation length can be found from $l_c(s) = x_0\int_{-\infty}^{\infty}\left|\mu_{1,2}(s,s+\delta)\right|^2 d\delta$ [109].

## 9.3 Results and discussion

Let us now physically interpret these results. From the $f = 2$ condition, one can deduce that for a given $n_2 I_0$, the width $x_0$ of the dark soliton increases with its grayness. Moreover, it is important to note that $Q_0$ de nes the correlation length

at the tails ($s \rightarrow \pm\infty$) of this dark incoherent soliton. In these regions, the bound states disappear and the soliton correlation length is determined by the width $Q_0$ of the radiation mode belt. At the tails, $l_c$ decreases as $Q_0$ increases and vice versa. In fact, $l_c$ in these regions coincides with the correlation length of the source. In the limit $Q_0 = 0$, $\varepsilon^2 = 1$, Eqs. 9.10 and 9.11 reduce to the well known coherent dark spatial soliton solution [113]. In this case, $I_b = 0$ and the soliton consists of an odd $tanh(s)$ mode at cut-off with $l_c = \infty$ everywhere. On the other hand, for $Q_0 = 0$ and $\varepsilon^2 \neq 1$, we obtain an incoherently-coupled dark-bright soliton pair, identical in nature to that previously considered in photorefractive crystals [50],[53]. From the condition $\varepsilon^2(2Q_0^2 + 1) \leq 1$, it is also clear that the dark soliton becomes more gray as its incoherence increases. Another interesting possibility arises in the limit $\varepsilon^2(2Q_0^2 + 1) = 1$. In this case the bound state is empty ($I_b = 0$) and thus the dark incoherent soliton consists of only radiation modes. As previously noted, the dark incoherent soliton is actually gray because of the presence of even radiation and even bound modes. To further illustrate these issues, let us consider a practical example. Let $n_0 = 2$, $\lambda_0 = 0.5\ \mu m$ and $n_2 I_0 = 10^{-3}$. Let the soliton grayness be 50% or $\varepsilon^2 = 0.5$. These parameters are in fact close to the those previously considered in photorefractives in Chapters 7 and 8 [109],[110]. In this case, $x_0 \simeq 5\ \mu m$ and this soliton exists for $Q_0 \leq 1/\sqrt{2}$. Figures 9.2(a) and (b) show the soliton intensity pro le and correlation length when $Q_0 = 0.4$. The correlation length of the source

$\approx 13.5\ \mu m$. The depression in $l_c$ at $s \approx 0$, is due to the presence of the bound mode. Figs.9.3(a) and (b) provide the same information when $Q_0 = 0.7$. This corresponds to a source correlation length of $\approx 5.3\ \mu m$ and in this case the bound mode is almost absent. For this reason, $l_c$ increases around the dark notch. Overall, the behavior of the $I_s$ and $l_c$ curves is in qualitative agreement with the ndings of previous chapters [109]. From the above results, it becomes apparent, that for our choice of $D(Q)$, the radiation modes are mostly con ned within a narrow belt around $Q \approx 0$. Because of this, the odd radiation modes dominate in the soliton-induced waveguide as shown schematically in Fig.9.1. This behavior can be easily understood by considering Eqs. 9.4 and 9.5 in the neighborhood of $s \approx 0$ when $Q \approx 0$. Thus, in order to effectively launch this dark incoherent soliton the phase must be properly manipulated so as at the center ($s = 0$), the eld distribution is mostly odd. This explains why a $\pi$-phase shift can greatly facilitate their observation [109],[110]. The even bound mode will subsequently appear as a result of evolution.

Similarly, higher-order dark incoherent solitons can be obtained for $f = 6, 12, 20, ...$ [117],[118], [119]. For example, if $f = 6$, the soliton-induced potential can support two bound states, i.e. $U'_{b1}$ =sech$^2(s)$ and $U'_{b2}$ =sech$(s)\tanh(s)$ at $q_1^2 = 4$ and $q_2^2 = 1$ respectively. In this case ($f = 6$), the radiation modes are given by

$$U'_{r,e} = \left[1 + Q^2 - 3\tanh^2(s)\right]\cos(Qs) - 3Q\tanh(s)\sin(Qs) \qquad (9.13)$$

$$U'_{r,o} = \left[1 + Q^2 - 3\tanh^2(s)\right]\sin(Qs) + 3Q\tanh(s)\cos(Qs) \quad . \qquad (9.14)$$

Thus $I_b' = B^2\text{sech}^4(s) + C^2\text{sech}^2(s)\tanh^2(s)$. As in the case of rst-order incoherent dark solitons, $D(Q)$ is not unique. If we choose however, $D(Q) = D_0' \exp(-Q/Q_0)$, we nd that $D_0' = (I_0/2Q_0)(12Q_0^4 + 5Q_0^2 + 2)^{-1}$,

$$B^2 = Q_0 D_0' \left[\left(3 + 6Q_0^2\right) - 2\varepsilon^2\left(12Q_0^4 + 5Q_0^2 + 2\right)\right]$$

and $C^2 = B^2 + 9Q_0 D_0'$. The intensity component of the radiation belt is given by

$$I_\tau' = D_0' Q_0 \left[2\left(12Q_0^4 + 5Q_0^2 + 2\right) + 9\text{sech}^4(s) - \left(12 + 6Q_0^2\right)\text{sech}^2(s)\right] \quad . \quad (9.15)$$

Again, $I_b' + I_\tau' = I_s$ where $I_s$ is given by Eq.9.1. From the above, $C > B$ and this soliton is possible provided that $B^2 \geq 0$. In the limit $B = 0$, the rst (even) bound mode is empty and the soliton involves only radiation modes and the next odd bound state. Furthermore, for a given degree of grayness and nonlinear index change, the $f = 6$ dark soliton is broader than the rst-order one by a factor of $\sqrt{3}$. Figs.9.4(a) and (b) depict the intensity pro le and correlation length of such a second-order incoherent dark soliton, under the same parameters used before when $Q_0 = 0.5$, $\varepsilon^2 = 0.49$ and $x_0 \simeq 8.8\ \mu m$. The source correlation length is 11 $\mu m$. As shown in Fig.9.4(b), the correlation length curve now exhibits a richer sub-structure within the local $l_c$ minimum around $s \approx 0$. This is due to the presence of the additional odd bound mode. Figs.9.2(b), 9.3(b), and 9.4(b) also suggest that what was found in the computational study of Chapter 7 was actually a dark incoherent soliton of the rst-order type. More speci cally, the $l_c$ curve of the dark quasi-soliton of

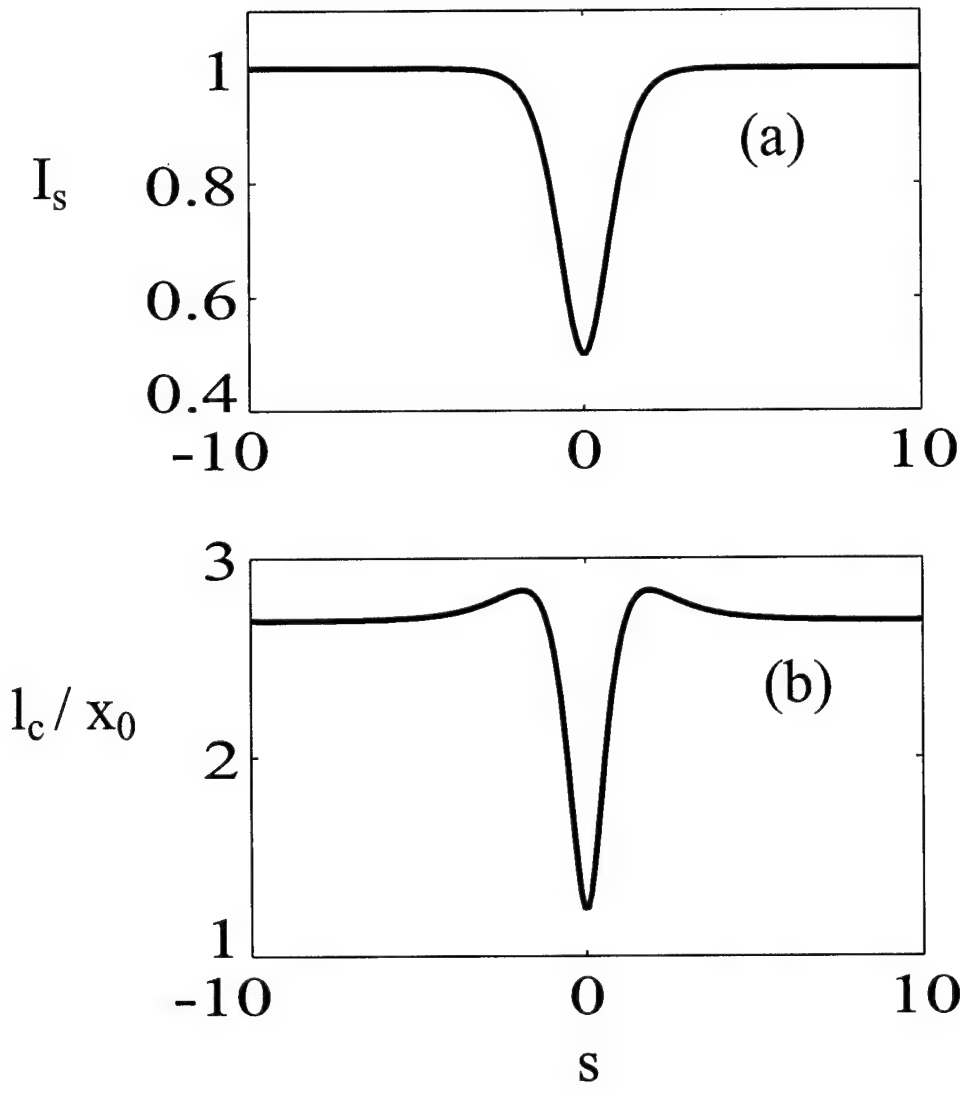


Figure 9.2: (a) Intensity profile and (b) corresponding correlation length curve of a first-order incoherent dark soliton when $\varepsilon^2 = 0.5$ and $Q_0 = 0.4$.

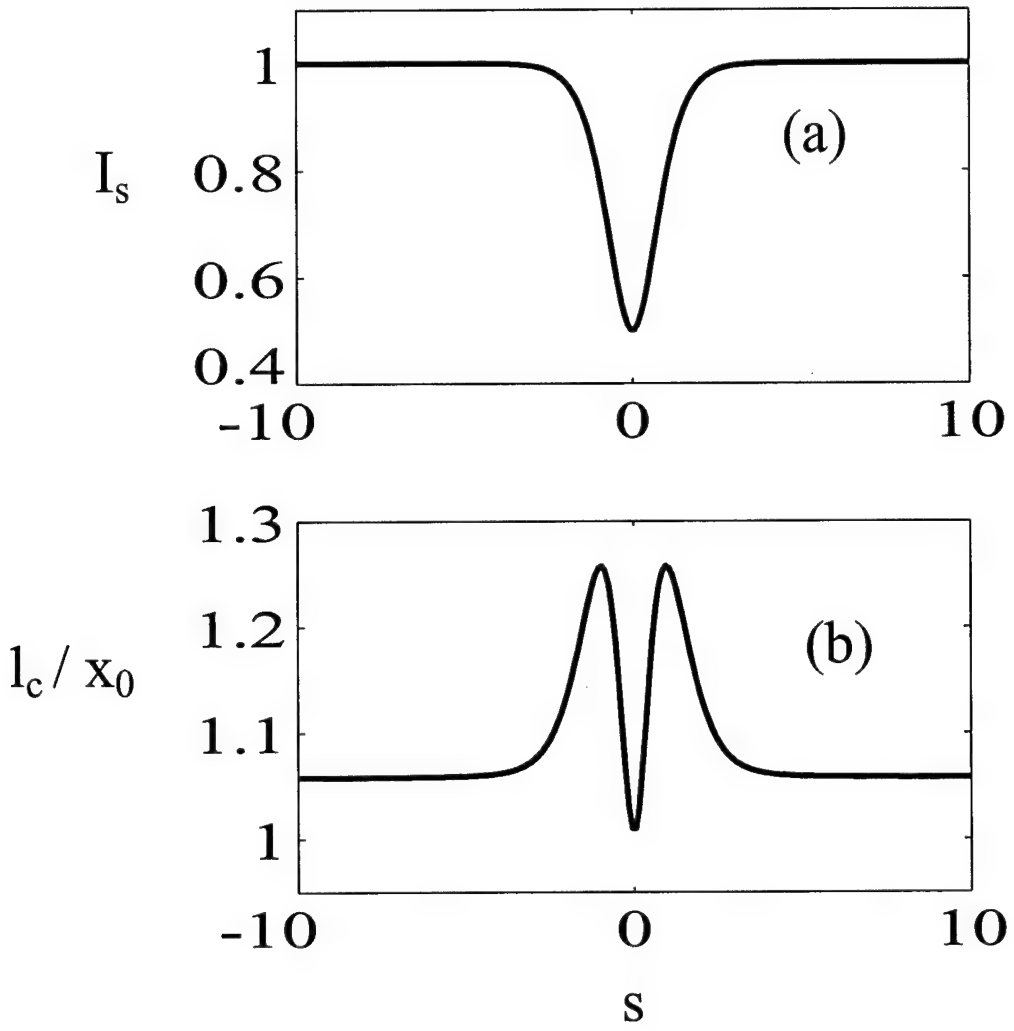


Figure 9.3: (a) Intensity profile and (b) corresponding correlation length curve of a first-order incoherent dark soliton when $\varepsilon^2 = 0.5$ and $Q_0 = 0.7$.

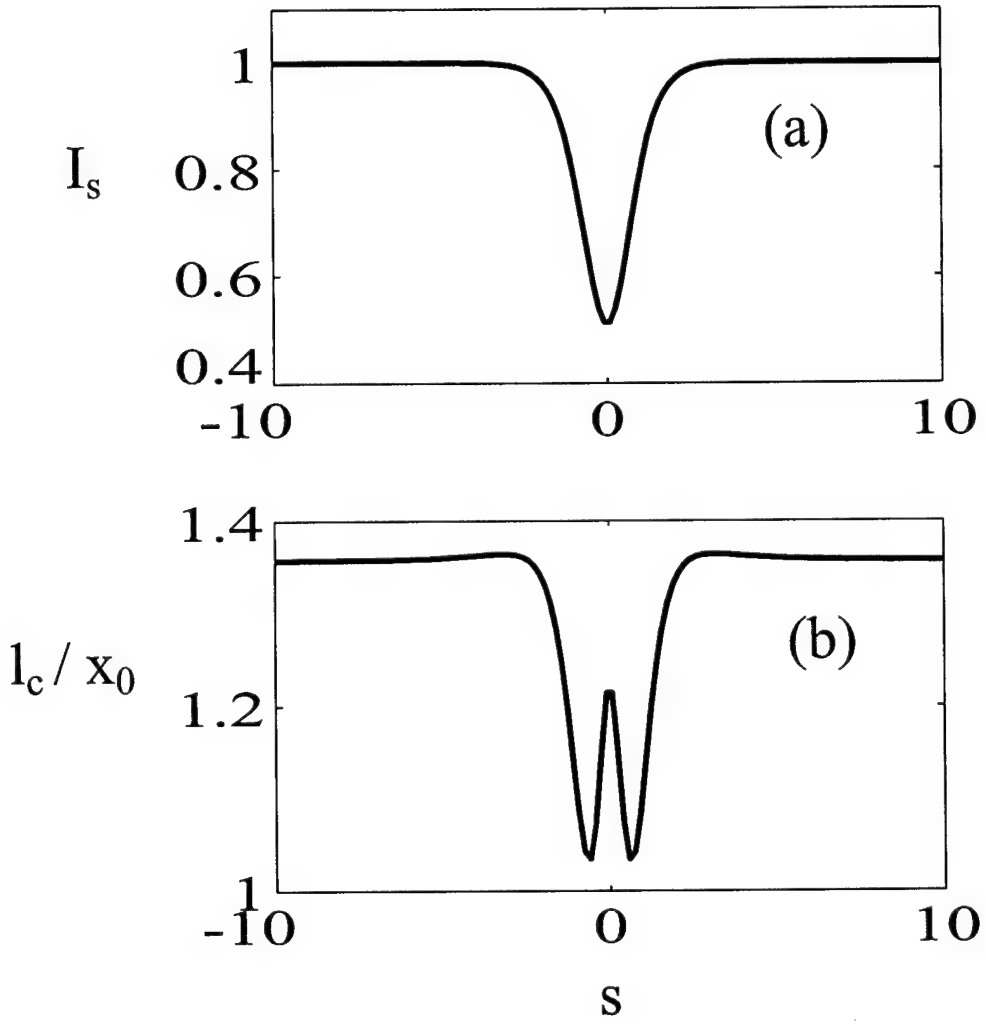


Figure 9.4: (a) Intensity profile and (b) corresponding correlation length curve of a second-order incoherent dark soliton when $\varepsilon^2 = 0.49$ and $Q_0 = 0.5$.

this chapter was very similar to that of Fig.9.3(b) and had no sub-structure around $s \approx 0$ which is characteristic of a higher-order dark soliton state. It is also very important to note, that in this latter case ($f = 6$), the narrow ($Q \approx 0$) radiation mode belt is dominated by even radiation modes within the waveguide region. On the other hand, our analysis shows that this second-order dark incoherent soliton has a strong contribution from the second odd bound state which by the way is never empty. Such higher order dark solitons can be launched by properly engineering the input beam in a manner similar to that of Ref. [120]. The modal composition of even higher-order dark incoherent solitons ($f = 12, 20, ...$) can be obtained in a similar fashion. These results are however more involved.

## 9.4 Conclusions

In conclusion we have theoretically demonstrated the existence of dark incoherent spatial solitons in non-instantaneous self-defocusing nonlinear media. These new dark soliton entities were found to involve radiation modes as well as bound states. Our results explain for the first time why these solitons are gray and why a $\pi$-phase shift tends to facilitate their experimental observation. Finally, we emphasize that our results can be in principle extended in two dimensions, i.e. in the description of two-dimensional dark incoherent solitons.

# Chapter 10

# Conclusions

In this thesis, we have investigated several issues regarding incoherent spatial solitons and their coherence properties. In particular, we have developed two complimentary approaches in order to explain the observed incoherent self-focusing behavior in biased photorefractive media. The first one is the so-called coherent density approach where the underlying evolution model takes the form of a nonlinear Schrödinger-like integro-differential equation provided that at the origin the coherent density is appropriately scaled with respect to the angular power spectrum of the incoherent source. The second one is essentially a self-consistent incoherent multimode approach. In brief, in this procedure, an incoherent spatial soliton is sought, which intensity-wise is a superposition of all the modes self-consistently guided in its nonlinearly induced waveguide. The numerical simulations resulting

from these theoretical approaches were found to be in good agreement with the experimental observations. We wish to emphasize that our theoretical approaches apply not only to photorefractive media but also to any other nonlinear system whose temporal response time is much bigger than the phase uctuation time of the incoherent beam.

We have shown that under appropriate initial conditions, bright as well as dark-like incoherent solitons are possible in biased photorefractive crystals. Our numerical simulations have demonstrated that the coherence properties of these beams are sig-ni cantly affected by the self-trapping process. More speci cally, in the case of a bright incoherent beam, we have found that coherence length remains approximately constant around the center of the beam, whereas it increases at the margins. The increase of the coherence length at the margins of the beam can be explained from the fact, that away from the center, only the higher order modes contribute to the coherence. Our numerical simulations also show that further increase of the bias voltage sets the bright beam into cycles of compression and expansion. In this latter case, the coherence length decreases at the center of the beam during compression and it increases when the beam expands. Our analysis has also demonstrated that a single dark incoherent soliton can be excited only if initially a $\pi$-phase shift is imposed on the incoherent wave front. Moreover, our simulations show that incoherent dark solitons are in fact gray. In this case, the coherence length was found to be higher

within the dark notch, with a depression at the center. Th dynamics of incoherent dark solitons have been studied under different initial conditions. Depending on the initial conditions, an even or an odd number of incoherent dark-like structures can be obtained in self-defocusing media. It is important to note that the behavior of bright/dark incoherent solitons is fundamentally different from that of their coherent counterparts. For example, unlike a coherent gray soliton, an incoherent dark soliton does not exhibit a transverse velocity in spite of its grayness. Furthermore, we have shown that the evolution of incoherent dark solitons in non-instantaneous nonlinear media is associated with strong phase-memory effects which are otherwise absent in the linear regime. The higher-order behavior of these dark beams have been compared under the same initial conditions but for different degrees of coherence. It was found that over a wide range of parameters, the Y-splitting is approximately the same irrespective of the initial spatial coherence. Experimental observations are in good agreement with our theoretical predictions.

In addition to bright solitons in photorefractive media, we have shown that partially incoherent spatial solitons are also possible in other saturable nonlinear media. An exact Gaussian solution was obtained in the case where the nonlinearity is of the logarithmic type. We found that these incoherent Gaussian solitons can exist as long as their spatial width is appropriately interrelated with the strength of the nonlinearity and the width of the incoherent angular power spectrum of the source.

The behavior of these beams above and below this limit was also investigated using computer simulations. By using the self-consistent multimode approach, we have shown that incoherent spatial solitons in logarithmically saturable nonlinear media are multimoded. These solitons can exist as long as their mode-occupancy function obeys a Poisson distribution. We have found that two approaches, that is the dynamic coherent density description as well as the self-consistent multimode method lead in this case to exactly the same results. Even though the saturable logarithmic nonlinearity differs from the photorefractive, it provides nevertheless a platform (perhaps the only platform) upon which the equivalence of the two previously mentioned approaches can be established in closed form. In the same vein, we have shown that two dimensional incoherent Gaussian solitons can also exist in this nonlinear system. Moreover, these incoherent solitons can be elliptical or circular depending on whether the angular power spectrum of the incoherent source is symmetric or not. The possibility of generating two dimensional elliptical solitons in isotropic nonlinear media seems to be unique to incoherent multimode solitons, since it has been shown that their elliptical coherent counterparts change their widths periodically during propagation.

We have also shown that multimode incoherent spatial solitons are possible in non-instantaneous Kerr-like media. Closed form solutions were obtained using the self-consistency method provided that their intensity pro le is of the $\mathrm{sech}^2(x/x_0)$

type. The coherence properties of these incoherent soliton states were also investigated in detail and explained by means of their modal composition. Note that the cross-sections of the complex coherence factor $\mu_{12}$ were very different in character from those found in the case of logarithmically saturable nonlinear media. In Log systems, the statistical process is everywhere stationary, i.e. $\mu_{12}$ depends only on $\delta$ and it is Gaussian in nature. For the Kerr case, the coherence curves depend also on the position $\eta$ and do not always go to zero as $\delta \rightarrow \pm\infty$. This feature was also encountered in saturable Kerr media of the type $I/(1+I)$. This important difference is due to the nite number of modes associated with the Kerr incoherent solitons. In particular, the induced waveguides in Kerr and Kerr-saturable media exhibit cutoffs ( nite number of modes) whereas the logarithmic one does not.

Finally, we have theoretically demonstrated the existence of dark incoherent spatial solitons in non-instantaneous self-defocusing nonlinear media of the Kerr type. These dark soliton entities were found to involve radiation modes as well as bound states. The presence of even radiation and bound modes explains why these structures are in fact gray. Moreover, we have found that the odd radiation modes dominate within the dark region of the beam (for rst-order incoherent dark beams), which justi es the $\pi$-phase shift required to excite these dark incoherent soliton states. Thus, in order to effectively launch dark incoherent solitons the phase must be properly manipulated so as at the center, the eld distribution is

mostly odd. The even bound mode subsequently appears as a result of evolution The coherence properties of these solitons were also considered and they were found to be in good agreement with the results of numerical simulations in the case of photorefractive nonlinearity. The existence of such incoherent dark solitons was later veri ed experimentally.

In closing, we would like to note that other issues may also merit further investigation. For example, as in the coherent case, the dynamics of two dimensional Log type incoherent bright solitons can be described in closed form. Furthermore, our results for one dimensional incoherent dark solitons can be in principle extended in two dimensions to analyze two-dimensional dark incoherent solitons. Detailed investigations of coherent and incoherent soliton collisions might be another interesting avenue for future studies. The outcome of collisions from incoherent beams is expected to be more involved since incoherent beams are multimoded. It also remains to be seen how one can control the coherence of an optical beam by using incoherent beams.

# Bibliography


[1] M. Ablowitz and H. Segur, *Solitons and the Inverse Scattering Transforms* (Siam, Philadelphia, 1981).

[2] F. Calogero and A. Degasperis, *Spectral Transform and Solitons I* (North Holland, Amsterdam, 1982).

[3] G. P. Agrawal and R. W. Boyd, *Contemprorary Nonlinear Optics* (Academic Press, Boston, 1992).

[4] A. Hasegawa, *Optical Solitons in Fibers* (Springer-Verlag, New York, 1989).

[5] G. P. Agrawal, *Nonlinear Fiber Optics* (Academic Press, San Diego, 1995).

[6] D.N. Christodoulides and R. I. Joseph, Phys. Rev. Lett. 62, 1746 (1989).

[7] R. Y. Chiao, E. Garmire and C. H. Townes, Phys. Rev. Lett. 13, 479 (1964).

[8] V. E. Zakharov and A. B. Shabat, Sov. Phys. JETP 34, 62 (1972).

[9] V. E. Zakharov and A. B. Shabat, Sov. Phys. JETP 37, 823 (1973).

[10] A. Barthelemy, S. Maneuf and C. Froehly, Opt. Comm. 55, 201 (1985).

[11] J.S. Aitchison, A.M. Weiner, Y. Silberberg, M. K. Oliver, J. L. Jackel, D. E. Leaird, E. M. Vogel and P. W. Smith, Opt. Lett. 15, 471 (1990)

[12] Y. R. Shen, *Principles of Nonlinear Optics* (John Wiley & Sons, New York, 1984).

[13] P. L. Kelley, Phys. Rev. Lett. 15, 1005 (1965).

[14] V. N. Vlasov, I. A. Petrishchev, and V. I. Talanov, Quantum Electron. Radiophys. 14, 1062 (1974).

[15] M. Segev, B. Crosignani, A. Yariv and B. Fischer, Phys. Rev. Lett. 68, 923 (1992).

[16] B. Crosignani, M. Segev, D. Engin, P. DiPorto, A. Yariv and G. Salamo, J. Opt. Soc. Am. B-10, 449 (1993).

[17] P. Gunter and J. P. Huignard, eds. *Photorefractive Materials and Applications I and II* (Springer-Verlag, Berlin, 1988).

[18] P. Yeh, *Photorefractive Nonlinear Optics* (Wiley, New York, 1993).

[19] G. Duree, J. L. Shultz, G. Salamo, M. Segev, A. Yariv, B. Crosignani, P. Di Porto, E. Sharp, and R. Neurgaonkar, Phys. Rev. Lett. 71, 533 (1993).

[20] G. Duree, M. Morin, G. Salamo, M. Segev, A. Yariv, B. Crosignani, P. Di Porto, and E. Sharp, Phys. Rev. Lett. 74, 1978 (1995).

[21] M. Segev, A. Yariv, G. Salamo, G. Duree, J. Shultz, B. Crosignani, P. Di Porto and E. Sharp, Opt. & Phot. News 4, 8 (1993).

[22] M. Segev, G. Salamo, G. Duree, M. Morin, B. Crosignani, P. DiPorto, and A. Yariv, Opt. & Phot. News 5, 9 (1994).

[23] M. Segev, G. C. Valley, B. Crosignani, P. DiPorto, and A. Yariv, Phys. Rev. Lett. 73, 3211 (1994).

[24] D. N. Christodoulides and M. I. Carvalho, J. Opt. Soc. Am. B 12, 1628 (1995).

[25] M. Shih, M. Segev, G. C. Valley, G. Salamo, B. Crosignani, and P. DiPorto, Elect. Lett. 31, 826 (1995).

[26] M. Shih, P. Leach, M. Segev, M. Garrett, G. Salamo, and G. C. Valley, Opt. Lett. 21, 324 (1996).

[27] G. C. Valley, M. Segev, B. Crosignani, A. Yariv, M. M. Fejer, and M. Bashaw, Phys. Rev. A 50, Rapid Comm., R4457 (1994).

[28] M. Taya, M. Bashaw, M. M. Fejer, M. Segev, and G. C. Valley, Phys. Rev. A 52, 3095 (1995).

[29] M. Taya, M. Bashaw, M. Fejer, M. Segev, and G. Valley, Opt. Lett. 21, 943 (1996).

[30] W. E. Torruelas, Z. Wang, D. J. Hagan, E. W. Van Stryland, G. I. Stegeman, L. Torner, and C. R. Menyuk, Phys. Rev. Lett. 74, 5036 (1995).

[31] M. Morin, G. Duree, G. Salamo, and M. Segev, Opt. Lett. 20, 2066 (1995).

[32] Z. Chen, M. Mitchell, M. Shih, M. Segev, M. H. Garret, and G. C. Valley, Opt. Lett. 21, 629 (1996).

[33] Z. Chen, M. Mitchell, and M. Segev, Opt. Lett. 21, 716 (1996).

[34] Z. Chen, M. Segev, S. R. Singh, T. H. Coskun, and D. N. Christodoulides, J. Opt. Soc. Am. B 14, 1407 (1997).

[35] M. Mitchell, Z. Chen, M. Shih, and M. Segev, Phys. Rev. Lett. 77, 490 (1996).

[36] M. Mitchell and M. Segev, Nature 387, 880 (1997).

[37] S. R. Singh and D. N. Christodoulides, Opt. Comm. 118, 569 (1995).

[38] M. I. Carvalho, S. R. Singh, and D. N. Christodoulides, Opt. Comm. 120, 311 (1995).

[39] S. R. Singh, M. I. Carvalho, and D. N. Christodoulides, Opt. Comm. 130, 288 (1996).

[40] M. Shih, M. Segev, and G. Salamo, Opt. Lett. 21, 931 (1996).

[41] M. D. Iturbe-Castillo, P. A. Marquez-Aguilar, J. J. Sanchez-Mondragon, S. Stepanov, and V. Vysloukh, Appl. Phys. Lett. 64, 408 (1994).

[42] M. Iturbe-Castillo, M. Torres-Cisneros, J. Mondragon, S. Cerda, S. Stepanov, V. Vysloukh, and G. Torres-Cisneras, Opt. Lett. 20, 1853 (1995).

[43] M. D. Iturbe-Castillo, J. J. Sanchez-Mondragon, S. Stepanov, M. B. Klein, and B. A. Weshsler, Opt. Comm. 118, 515 (1995).

[44] M. I. Carvalho, S. R. Singh, and D. N. Christodoulides, Opt. Comm. 126, 167 (1996).

[45] S. R. Singh and D. N. Christodoulides, J. Opt. Soc. Am. B. 13, 719 (1996).

[46] W. Krolikowski, N. N. Akhmediev, D. R. Anderson, and B. Luther-Davies, Opt. Comm. 132, 179 (1996).

[47] M. Segev, G. C. Valley, S. R. Singh M. I. Carvalho, and D. N. Christodoulides, Opt. Lett. 20, 1764 (1995).

[48] S. R. Singh, M. I. Carvalho, and D. N. Christodoulides, Opt. Lett. 20, 2177 (1995).

[49] M. I. Carvalho, S. R. Singh, D. N. Christodoulides, and R. I. Joseph, Phys. Rev. E 53, R53 (1996).

[50] D. N. Christodoulides, S. R. Singh, M. I. Carvalho, and M. Segev, Appl. Phys. Lett. 68, 1763 (1996).

[51] Z. Chen, M. Segev, T. H. Coskun, and D. N. Christodoulides, Opt. Lett. 21, 1436 (1996).

[52] Z. Chen, M. Segev, T. H. Coskun, D. N. Christodoulides, Y. S. Kivshar, and V. V. Afanasjev, Opt. Lett.,21, 821 (1996)

[53] Z. Chen, M. Segev, T. H. Coskun, D. N. Christodoulides, and Y. S. Kivshar, J. Opt. Soc. Am. B. 14, 3066 (1997).

[54] M. Shih and M. Segev, Opt. Lett. 21, 1538 (1996).

[55] M. Shih, Z. Chen, M. Segev, T. H. Coskun, and D. N. Christodoulides, App. Phys. Lett. 69, 4151 (1996).

[56] M. Shih, M. Segev, and G. Salamo, Phys. Rev. Lett. 78, 2551 (1997).

[57] M. Chauvet, S. A. Hawkins, G. J. Salamo, M. Segev, D. F. Bliss, and G. Bryant, Opt. Lett. 21, 1333 (1996).

[58] M. Chauvet, S. Hawkins, G. J. Salamo, M. Segev, D. Bliss, and G. Bryant, Appl. Phys. Lett. 70,2499 (1997).

[59] M. Segev, M. Shih, and G. C. Valley, J. Opt. Soc. Am. B. 13, 706 (1996).

[60] G. Duree, G. Salamo, M. Segev, A. Yariv, B. Crosignani, P. Di Porto, and E. Sharp, Opt. Lett. 19, 1195 (1994).

[61] M. Segev, A. Yariv, B. Crosignani, P. Di Porto, G. Duree, G. Salamo, and E. Sharp, Opt. Lett. 19, 1296 (1994).

[62] D. N. Christodoulides and M. I. Carvalho, Opt. Lett. 19, 1714 (1994).

[63] S. Gatz and J. Herrman, J. Opt. Soc. Am. B 8, 2296 (1991).

[64] Z. Chen, M. Segev, D. Wilson, R. Muller, and P. D. Maker, Phys. Rev. Lett. 78, 2948 (1997).

[65] A. Ashkin, G. D. Boyd, J. M. Dziedric, R. G. Smooth, A. A. Ballman, J. J. Levinstein, and K. Nassau, Appl. Phys. Lett. 9, 72 (1966).

[66] V. L. Vinetskii and N. Kukhtarev, Sov. Phys. 16, 2414 (1975).

[67] N. Kukhtarev, V. B. Markov, S. G. Odulov, M. S. Soskin, and V. L. Vinetskii, Ferroelectrics 22, 949 (1979).

[68] M. P. Petrov, S. I. Stepanov, and A. V. Khomenko, *Photorefractive Crystals in Coherent Optical Systems* (Springer-Verlag, Berlin, 1991).

[69] L. Mandel and Wolf, Optical Coherence and Quantum Optics (Cambridge University Press, New York, 1995).

[70] J. Goodman, *Statistical Optics* (John Wiley & Sons, New York, 1985).

[71] R. DeSalvo, D. J. Hagan, M. Sheik-Bahae, G. Stegeman, and E. W. Van Stryland, Opt. Lett. 17, 28 (1992).

[72] W. E. Torruellas, Z. Wang, D. J. Hagan, E. W. Van Stryland, G. I. Stegeman, L. Torner, and C. R. Menyuk, Phys. Rev. Lett. 74, 5036 (1995).

[73] M. D. Castillo, P. A. Aguilar, J. J. Mondragon, and S. Stepanov, Appl. Phys. Lett. 64, 408 (1994).

[74] B. Ya. Zel dovich, N. F. Pilipetsky, and V. V. Shkunov, *Principles of Phase Conjunction* (Springer-Verlag, Berlin, 1985).

[75] B. Crosignani, B. Daino, and P. DiPorto, J. Appl. Phys. 42, 399 (1971).

[76] A. Papoulis, *Probability, Random Variables, and Stochastic Process* (McGraw-Hill, New York, 1965).

[77] H. H. Hopkins, J. Opt. Soc. Am. 47, 508 (1957).

[78] D. Marcuse, Appl. Opt. 19, 1653 (1980).

[79] D. N. Christodoulides, T. H. Coskun, M. Mitchell, and M. Segev, Phys. Rev. Lett. 78, 646 (1997).

[80] A. W. Snyder and J. D. Mitchell, Opt. Lett. 22, 16 (1997).

[81] L. I. Schiff, *Quantum Mechanics*, 3rd ed. (McGraw-Hill, New York, 1968).

[82] D. N. Christodoulides, T. H. Coskun, and R.I. Joseph, Opt. Lett. 22, 1080 (1997).

[83] M. Mitchell, M. Segev, T. H. Coskun, and D. N. Christodoulides, Phys. Rev. Lett. 79, 4990 (1997).

[84] A. W. Snyder and D. J. Mitchell, Phys. Rev. Lett. 80, 1422 (1998).

[85] A. Hasegawa, Phys. Fluids 18, 77 (1975).

[86] A. Hasegawa, Phys. Fluids 20, 2155 (1977).

[87] A. Hasegawa, Opt. Lett. 5, 416 (1980). In this paper, incoherent temporal solitons in multimode bers have been suggested. These occur when several transverse modes excited by a coherent light pulse lock together and propagate at the same velocity. Strictly speaking, these are not incoherent solitons since they are not excited by an incoherent source where the relative phase among modes is totally random.

[88] D. N. Christodoulides and R. I. Joseph, Opt. Lett. 13, 53 (1988).

[89] V. A. Vysloukh, V. Kutuzov, V. M. Petnikova, and V. V. Shuvalov, Quantum Electronics 27, 843 (1997).

[90] V. Kutuzov, V. M. Petnikova, V. V. Shuvalov, and V. A. Vysloukh, Phys. Rev. E 57, 6056 (1998).

[91] B. Ya. Zel dovich, A. V. Mamaev, and V. V. Shkunov, *Speckle-Wave Interactions in Applications to Holography and Nonlinear Optics* (CRC, Boca Raton, 1995).

[92] J. P. Gordon *et al.*, J. Appl. Phys. 36, 3 (1965).

[93] S. A. Akhmanov *et al.*, JETP Letters 6, 38 (1967).

[94] G. Askar yan, Sov. Phys. JETP 15, 1088 (1962).

[95] A. W. Snyder, D. J. Mitchell, L. Poladian, and F. Ladouceur, Opt. Lett. 16, 21 (1991).

[96] A. W. Snyder and D. J. Mitchell, Opt. Lett. 18, 101 (1993).

[97] A. W. Snyder, S. J. Hewlett, and D. J. Mitchell, Phys. Rev. Lett. 72, 1012 (1994).

[98] A. W. Snyder, D.J. Mitchell, and Y. S. Kivshar, Mod. Phys. Lett. B 9, 1479 (1995).

[99] M. Abramowitz and I. A. Stegun, *Handbook of Mathematical Functions* (Dover Publications, New York, 1970).

[100] N. N. Akhmediev and A. Ankiewicz, *Solitons-Nonlinear Pulses and Beams* (Chapman and Hall, London, 1997).

[101] A. W. Snyder and D.J. Mitchell, Science 276, 1538 (1997).

[102] Y. R. Shen, Science 276, 1520 (1997).

[103] A. Yariv, *Quantum Electronics* (John Wiley & Sons, New York, 1989).

[104] A. W. Snyder and C. Pask, J. Opt. Soc. Am. 63, 806 (1973).

[105] The Poisson modal composition of Gaussian Schell-model sources was rst obtained by F. Gori, Opt. Commun. 34, 301 (1980), and further elaborated on by A. Starikov and E. Wolf, J. Opt. Soc. Am. 72, 923 (1982).

[106] A. Erdelyi, W. Magnus, F. Oberhettinger, and F. Tricomi, *Higher Transcendental Functions*, vol. 2 (McGraw-Hill, New York, 1953).

[107] S. Piazzola and P. Spano, Optics Commun. 43, 175 (1982).

[108] K. J. Blow and N. J. Doran, Phys. Lett. A 107, 55 (1985).

[109] T. H. Coskun, D. N. Christodoulides, M. Mitchell, Z. Chen, and M. Segev, Opt. Lett. 23, 418 (1998).

[110] Z. Chen, M. Mitchell, M. Segev, T. H. Coskun, and D. N. Christodoulides, Science 280, 889 (1998).

[111] P. H. Van Cittert, Physica 1, 201 (1934).

[112] F. Zernike, Physica 5, 785 (1938).

[113] Y. S. Kivshar and B. Luther-Davies, Phys. Rep. 298, 81 (1998).

[114] D. N. Christodoulides, T. H. Coskun, M. Mitchell, and M. Segev, Phys. Rev. Lett. 80, 2310 (1998).

[115] V. V. Shkunov and D. Z. Anderson, Phys. Rev. Lett. 81, 2683 (1998).

[116] M. I. Carvalho, T. H. Coskun, D. N. Christodoulides, M. Mitchell, and M. Segev, Phys. Rev. E 59, 1193 (1999).

[117] A. W. Snyder and J. D. Love, *Optical Waveguide Theory* (Chapmen and Hall, New York, 1983).

[118] T. Tamir, *Guided-Wave Optoelectronics* (Springer-Verlag, Berlin, 1990).

[119] G. L. Lamb, *Elements of Soliton Theory* (John Wiley, New York, 1980).

[120] M. Mitchell, M. Segev, and D. N. Christodoulides, Phys. Rev. Lett. 80, 4657 (1998).

# Appendix A

# Normalized mode functions

In this Appendix we provide the normalized mode functions $\widetilde{u}_n^m(\eta)$. Here we de ne $T = \tanh(\eta)$ and $S = \mathrm{sech}(\eta)$. The $\widetilde{u}_n^m(\eta)$ functions appear in accord to their modal order (lowest order mode rst).

For $n = 1$:

$$\widetilde{u}_1^1(\eta) = S \tag{A.1}$$

For $n = 2$:

$$\widetilde{u}_2^2(\eta) = S^2 \tag{A.2}$$

$$\widetilde{u}_2^1(\eta) = ST \tag{A.3}$$

For $n = 3$:

$$\widetilde{u}_3^3(\eta) = \sqrt{15/16}S^3 \tag{A.4}$$

$$\widetilde{u}_3^2(\eta) = \sqrt{5/2}S^2T \tag{A.5}$$

$$\widetilde{u}_3^1(\eta) = (1/4)\,S\left(4 - 5S^2\right) \tag{A.6}$$

For $n = 4$:

$$\widetilde{u}_4^4(\eta) = \sqrt{7/8}S^4 \tag{A.7}$$

$$\widetilde{u}_4^3(\eta) = (3/4)\sqrt{7}S^3T \tag{A.8}$$

$$\widetilde{u}_4^2(\eta) = \left(\sqrt{2}/4\right)S^2\left(6 - 7S^2\right) \tag{A.9}$$

$$\widetilde{u}_4^1(\eta) = (1/4)\,ST\left(4 - 7S^2\right) \tag{A.10}$$

For $n = 5$:

$$\widetilde{u}_5^5(\eta) = \left(\sqrt{210}/16\right)S^5 \tag{A.11}$$

$$\widetilde{u}_5^4(\eta) = (1/2)\sqrt{21}S^4T \tag{A.12}$$

$$\widetilde{u}_5^3(\eta) = \left(\sqrt{42}/16\right)S^3\left(8 - 9S^2\right) \tag{A.13}$$

$$\widetilde{u}_5^2(\eta) = \left(\sqrt{7}/2\right)S^2T\left(2 - 3S^2\right) \tag{A.14}$$

$$\widetilde{u}_5^1(\eta) = (1/8)\,S\left(8 - 28S^2 + 21S^4\right) \tag{A.15}$$

For $n = 6$:

$$\widetilde{u}_6^6(\eta) = (3/16)\sqrt{22}S^6 \tag{A.16}$$

$$\widetilde{u}_6^5(\eta) = (5/16)\sqrt{66}S^5T \tag{A.17}$$

$$\widetilde{u}_6^4(\eta) = \left(\sqrt{3}/4\right)S^4\left(10 - 11S^2\right) \tag{A.18}$$

$$\widetilde{u}_6^3(\eta) = (3/16)\sqrt{10}S^3T\left(8 - 11S^2\right) \tag{A.19}$$

$$\widetilde{u}_6^2(\eta) = \left(\sqrt{10}/16\right)S^2\left(16 - 48S^2 + 33S^4\right) \tag{A.20}$$

$$\widetilde{u}_6^1(\eta) = (1/8)\, ST\left(8 - 36S^2 + 33S^4\right) \tag{A.21}$$

# Appendix B

# Complex coherence factors

In this Appendix, the functional form of the complex coherence factors $\mu_{12}$ is provided up to $n = 5$. Again we have de ned $T(\eta) = \tanh(\eta)$ and $S(\eta) = \mathrm{sech}(\eta)$.

For $n = 1$:

$$\mu_{12}(\eta, \eta + \delta) = 1 \tag{B.1}$$

For $n = 2$:

$$\mu_{12}(\eta, \eta + \delta) = T(\eta) T(\eta + \delta) + S(\eta) S(\eta + \delta) \tag{B.2}$$

For $n = 3$:

$$\mu_{12}(\eta, \eta + \delta) = 1 + (5/2) \{S(\eta) S(\eta + \delta) \tag{B.3}$$

$$\times \left[T(\eta)T(\eta+\delta)+S(\eta)S(\eta+\delta)\right] \tag{B.4}$$
$$-(1/2)\left[S^2(\eta)+S^2(\eta+\delta)\right]\}$$

For $n=4$:

$$\mu_{12}(\eta,\eta+\delta) = T(\eta)T(\eta+\delta)\left\{\begin{array}{c}1-(7/4)\left[S^2(\eta)+S^2(\eta+\delta)\right]\\ +7S^2(\eta)S^2(\eta+\delta)\end{array}\right\} \tag{B.5}$$
$$+S(\eta)S(\eta+\delta)\left\{\begin{array}{c}9/2-(21/4)\left[S^2(\eta)+S^2(\eta+\delta)\right]\\ +7S^2(\eta)S^2(\eta+\delta)\end{array}\right\}$$

For $n=5$:

$$\mu_{12}(\eta,\eta+\delta) = 1+7\{T(\eta)T(\eta+\delta)S(\eta)S(\eta+\delta) \tag{B.6}$$
$$\times\left[1-(3/2)\left(S^2(\eta)+S^2(\eta+\delta)\right)+3S^2(\eta)S^2(\eta+\delta)\right]$$
$$-(1/2)\left(S^2(\eta)+S^2(\eta+\delta)\right)+(3/8)\left(S^4(\eta)+S^4(\eta+\delta)\right)$$
$$+S^2(\eta)S^2(\eta+\delta)\left[\begin{array}{c}13/4-3\left(S^2(\eta)+S^2(\eta+\delta)\right)\\ +3S^2(\eta)S^2(\eta+\delta)\end{array}\right]\}$$

# Appendix C

# Diffraction equations of Gauss-Hermite beams

This Appendix details the steps that lead to the diffraction equation of Gauss-Hermite beams.

An optical beam propagates in a linear material by obeying the following differential equation:

$$i\frac{\partial U}{\partial \xi} + \frac{1}{2}\frac{\partial^2 U}{\partial s^2} = 0 \tag{C.1}$$

where the normalized coordinates are $\xi = z/kx_0$, $s = x/x_0$, and $k = k_0 n_0$ is the wavenumber in this material. Let as assume that at $\xi = 0$ the optical field is given by $u_m = A_0 \exp\{-s^2/2\} H_m(s)$ where $H_m$ are Hermite functions. Now, let the

diffraction solution be

$$u_m = A(\xi)\exp\left\{-s^2/2\omega^2(\xi)\right\} H_m\left(s/\omega(\xi)\right)\exp\left\{i\left[\theta(\xi)+F(\xi)s^2\right]\right\} \tag{C.2}$$

where $A$, $\omega$, $\theta$, $F$ are real functions. Substituting this solution into Equation C.1 gives

$$\begin{aligned} 0 \;=\; & i\dot{A}H_m\left(\frac{s}{\omega}\right) + AH_m\left(\frac{s}{\omega}\right)\left[i\frac{s^2}{\omega^3}\dot{\omega} - \dot{\theta} - \dot{F}s^2\right] - iA\frac{\dot{\omega}}{\omega^2}sH'_m\left(\frac{s}{\omega}\right) \\ & + \left\{\frac{A}{2}\left[\frac{s^2}{\omega^4} - 4F^2s^2 - i\frac{4Fs^2}{\omega^2} - \frac{1}{\omega^2} + i2F\right]H_m\left(\frac{s}{\omega}\right)\right. \\ & \left. + \frac{2}{\omega}\left[-\frac{s}{\omega^2} + i2Fs\right]H'_m\left(\frac{s}{\omega}\right) + \frac{1}{\omega^2}H''_m\left(\frac{s}{\omega}\right)\right\} \end{aligned} \tag{C.3}$$

where $\dot{A} = dA/d\xi$, etc., $H'_m(\eta) = dH_m/d\eta$, $H''_m(\eta) = d^2H_m/d\eta^2$ where $\eta = s/\omega$. From the imaginary part of this equation we get

$$\left[\dot{A} + FA\right]H_m + \left[2\frac{F}{\omega} - \frac{\dot{\omega}}{\omega^2}\right]AH'_m s - \left[2\frac{F}{\omega^2} - \frac{\dot{\omega}}{\omega^3}\right]AH_m s^2 = 0 \tag{C.4}$$

By equating the coefficients of the $s$-polynomial to zero we get

$$\dot{A} + FA = 0 \tag{C.5}$$

and

$$\frac{\dot{\omega}}{\omega} = 2F \tag{C.6}$$

From the real part of Equation C.3 we obtain

$$-AH_m\left(\dot{\theta} + \dot{F}s^2\right) + \left[\frac{A}{2\omega^4}s^2 - 2AF^2s^2 - \frac{A}{2\omega^2}\right]H_m - \frac{A}{2\omega^2}\left[H''_m - \frac{2s}{\omega}H'_m\right] = 0 \tag{C.7}$$

This relation can be further simplified by using the following definition

$$\frac{d^2 H_m}{d\eta^2} - 2\eta \frac{dH_m}{d\eta} = -2mH_m \tag{C.8}$$

and we end up with

$$-\left(\dot{\theta} + \dot{F}s^2\right) AH_m + \left[\frac{1}{2\omega^4}s^2 - 2F^2 s^2 - \frac{1}{2\omega^2}\right] AH_m - \frac{1}{\omega^2} mAH_m = 0 \; . \tag{C.9}$$

Thus

$$\dot{\theta} = -\frac{1}{2\omega^2}(1 + 2m) \tag{C.10}$$

$$\dot{F} + 2F^2 - \frac{1}{2\omega^4} = 0 \tag{C.11}$$

$$A^2\omega = \text{constant} = A_0^2 \tag{C.12}$$

where we assume that the initial spot size $\omega_0$ is equal to 1, i.e. $\omega(\xi = 0) = 1$. Eq.C.6 can be written in the following form

$$F = \frac{1}{4\omega^2}\frac{d}{d\xi}\left(\omega^2\right) \; . \tag{C.13}$$

Substituting this result into Equation C.11, we obtain the following relationship

$$\ddot{\omega} = \frac{1}{\omega^3} \; . \tag{C.14}$$

From this equation one can solve for $\omega$. This is given by

$$\omega(\xi) = \left(1 + \xi^2\right)^{1/2} \tag{C.15}$$

Furthermore, using this solution in Eq.C.10, one may calculate the phase accumulated $\theta(\xi)$:

$$\theta(\xi) = -\frac{2m+1}{2}\tan^{-1}(\xi) + \theta_0 \tag{C.16}$$

where $\theta_0$ is the initial value of the phase associated with this beam. Again substituting Eq.C.15 into Eq.C.12 one directly finds the amplitude of the diffracting mode which is given by

$$A(\xi) = \frac{A_0}{\omega(\xi)^{1/2}} = \frac{A_0}{\left(1+\xi^2\right)^{1/4}} \tag{C.17}$$

One can also find the function $F(\xi)$ by substituting Eq. C.15 into Eq. F.11 to get

$$F(\xi) = \frac{\xi}{2\left(1+\xi^2\right)} \tag{C.18}$$

Substituting $A$, $\omega$, $\theta$, $F$ into Eq. C.2 and taking the absolute value square, the intensity of a diffracting Gauss-Hermite beam is given by:

$$|u_m(\xi)|^2 = \frac{A_0}{\left(1+\xi^2\right)^{1/2}} \exp\left\{-\frac{s^2}{1+\xi^2}\right\} H_m^2\left(\frac{s}{\left(1+\xi^2\right)^{1/2}}\right) . \tag{C.19}$$

In general, if the initial value of the spot size is not unity, i.e. $\omega \neq \omega_0$ at $\xi = 0$, Eqs.C.15 takes the following form

$$\omega(\xi) = \omega_0\left(1+\xi^2/\omega_0^4\right)^{1/2} \tag{C.20}$$

and the diffracting beam is given by

$$|u_m(\xi)|^2 = \frac{A_0}{\left(1+\xi^2/\omega_0^4\right)^{1/2}} \exp\left\{-\frac{s^2}{\omega_0^2\left(1+\xi^2/\omega_0^4\right)}\right\} H_m^2\left(\frac{s}{\omega_0\left(1+\xi^2/\omega_0^4\right)^{1/2}}\right) \tag{C.21}$$

# Appendix D

# Intensity and coherence function of incoherent Gaussian beams

In this Appendix, by using modal description, we compute the time-averaged intensity and complex coherence function of an incoherent Gaussian beam during diffraction.

The optical field of an incoherent Gaussian beam can be expressed through superposition, i.e., $U = \sum_{m=0}^{\infty} c_m u_m$. Here the Gauss-Hermite modes at $\xi = 0$ are given by

$$u_m = H_m\left(\alpha^{1/2} s\right) \exp\left(-\alpha s^2/2\right) \tag{D.1}$$

at $\xi = 0$ whereas they are

$$u_m = \frac{1}{\left(1+\alpha^2\xi^2\right)^{1/4}} \exp\left\{-\frac{\alpha}{2}\frac{s^2}{\left[1+\alpha^2\xi^2\right]}\right\} \tag{D.2}$$
$$\times H_m\left(\frac{\alpha^{1/2}s}{\left(1+\alpha^2\xi^2\right)^{1/2}}\right) \exp\left\{i\left[\theta(\xi) + \frac{\alpha^2\xi}{2\left[1+\alpha^2\xi^2\right]}s^2\right]\right\}$$

at $\xi \neq 0$ from Appendix C. Furthermore, $c_m$ are the mode-occupancy coefficients that vary randomly in time and let the mode-occupancy be described by a Poisson distribution, that is $\left\langle |c_m|^2 \right\rangle = \hat{r}\exp(-p/2)(p/2)^m/m!$ where $p$ is the Poisson parameter and $\hat{r} = r(1-p^2)\exp -p/2$ is a constant. The time-average intensity of this beam can then be obtained from

$$I_D = \left\langle |U|^2 \right\rangle = \sum_{m=0}^{\infty} \left\langle |c_m|^2 \right\rangle |u_m|^2 \tag{D.3}$$

where we made use of the fact that the time average of the cross-interference terms is zero ($\left\langle c_i c_j^* \right\rangle \delta_{ij}$) under incoherent excitation. Therefore, the time-average intensity of this multimoded beam during linear diffraction is given by

$$I_D = \hat{r}\exp\left(-\frac{p}{2}\right)\sum_{m=0}^{\infty}\frac{(p/2)^m}{m!}\frac{1}{\left(1+\alpha^2\xi^2\right)^{1/2}} \tag{D.4}$$
$$\times \exp\left\{-\frac{\alpha s^2}{\left[1+\alpha^2\xi^2\right]}\right\} H_m^2\left(\frac{\alpha^{1/2}s}{\left(1+\alpha^2\xi^2\right)^{1/2}}\right) \tag{D.5}$$

This expression can be simpli ed, by using Mehler s formula:

$$\sum_{m=0}^{\infty}\frac{(t/2)^m}{m!}H_m^2(x) = \frac{1}{(1-t^2)^{1/2}}\exp\left\{\frac{2tx^2 - 2t^2x^2}{1-t^2}\right\} \tag{D.6}$$

where $t < 1$. Thus as a result one nds

$$I_D = \frac{r}{\left(1+\alpha^2\xi^2\right)^{1/2}} \exp\left\{-\frac{\alpha s^2}{\left[1+\alpha^2\xi^2\right]}\left[1-\frac{2p}{1+p}\right]\right\} \tag{D.7}$$

Knowing that $\alpha(1-p)/(1+p) = 1$, we further simplify Eq.D.7 which gives

$$I_D = \frac{r}{\left(1+\alpha^2\xi^2\right)^{1/2}} \exp\left\{-\frac{s^2}{\left[1+\alpha^2\xi^2\right]}\right\} . \tag{D.8}$$

The coherence function is de ned as follows:

$$\mu_{12}(s_1, s_2, \xi) = \frac{\langle U(s_1,\xi)\, U^*(s_2,\xi)\rangle}{\left[I_D(s_1,\xi)\, I_D(s_2,\xi)\right]^{1/2}} \tag{D.9}$$

Therefore, in our case

$$\begin{aligned} \langle U(s_1,\xi)\, U^*(s_2,\xi)\rangle &= \left\langle \sum_{m=0}^{\infty} c_m u_m(s_1,\xi) \sum_{n=0}^{\infty} c_n^* u_n^*(s_2,\xi) \right\rangle \\ &= \sum_{m=0}^{\infty} \left\langle |c_m|^2 \right\rangle u_m(s_1,\xi)\, u_m^*(s_2,\xi) \end{aligned} \tag{D.10}$$

since the time average of the cross-interference terms is zero. Substituting the functional form of $u_m(s_1,\xi)$ and $u_m^*(s_2,\xi)$ into above equations, and by using again Mehler s Formula, and after some simpli cation, we obtain the following complex coherence function

$$\mu_{12}(s,\delta,\xi) = \exp\left\{-\frac{p\delta^2}{(1-p)^2\left(1+\alpha^2\xi^2\right)}\right\} \exp\left\{-i\frac{\alpha^2\left(\delta^2+2s\delta\right)\xi}{2\left(1+\alpha^2\xi^2\right)}\right\} \tag{D.11}$$

where $s = s_1$ and $\delta = s_2 - s_1$.

# Appendix E

# Diffraction of an incoherent Gaussian beam

In this Appendix, by using coherent density approach, we analyze the diffraction of an incoherent Gaussian beam.

The diffraction equation in normalized coordinates and quantities is given by:

$$i\left[\frac{\partial f}{\partial \xi}+\alpha\frac{\partial f}{\partial s}\right]+\frac{1}{2}\frac{\partial^2 f}{\partial s^2}=0 \tag{E.1}$$

where $s=x/x_0$, $\xi=z/kx_0$, $k=k_0n_0$, and $\alpha=kx_0\theta$. Now let $\xi=\zeta$ and $\eta=s-\alpha\xi$. After this transformation, the above equation takes the following form

$$i\frac{\partial f}{\partial \zeta}+\frac{1}{2}\frac{\partial^2 f}{\partial \eta^2}=0 \tag{E.2}$$

Let at the input, the coherent density function be given by

$$f(\zeta=0,\eta)=r^{1/2}\exp\left(-\eta^2/2\right)\left(\sqrt{\pi}\theta_0\right)^{-1/2}\exp\left(-\theta^2/2\theta_0^2\right)\ .$$

Therefore at $\zeta \neq 0$, the intensity of this function evolves according to following expression

$$|f(\zeta,\eta)|^2=\frac{r}{\sqrt{\pi}\theta_0\left(1+\zeta^2\right)^{1/2}}\exp\left(-\frac{\eta^2}{1+\zeta^2}\right) \tag{E.3}$$

or

$$|f(\xi,s,\theta)|^2=\frac{r}{\sqrt{\pi}\theta_0\left(1+\xi^2\right)^{1/2}}\exp\left(-\frac{(s-\alpha\xi)^2}{1+\xi^2}\right) \tag{E.4}$$

The total intensity of the incoherent beam can be calculated from $I_D=|U|^2=\int_{-\infty}^{\infty}|f(s,\xi,\theta)|^2\,d\theta$. Substituting Eq.E.4 into this latter equation gives

$$I_D=\frac{r\exp\left[-s^2/\left(1+\xi^2\right)\right]}{\sqrt{\pi}\left(1+\xi^2\right)^{1/2}}\int_{-\infty}^{+\infty}d\lambda\exp\left\{-\lambda^2\left(\frac{1+(1+V^2)\,\xi^2}{1+\xi^2}\right)+\lambda\frac{2sV\xi}{1+\xi^2}\right\} \tag{E.5}$$

where $V=kx_0\theta_0$ and $\lambda=\theta/\theta_0$. The integral of the above expression can be simpli ed by using $\int_{-\infty}^{\infty}\exp\left(-a^2x^2+bx\right)=\pi^{1/2}/a\exp\left(b^2/4a^2\right)$. Therefore, the total intensity of a incoherent Gaussian beam during diffraction is given by

$$I_D=\frac{r}{\left[1+(1+V^2)\,\xi^2\right]^{1/2}}\exp\left\{-\frac{s^2}{\left[1+(1+V^2)\,\xi^2\right]}\right\} \tag{E.6}$$

# Appendix F

# Radiation modes

In this Appendix, we compute the radiation modes of the Helmholtz equation when the potential is of the $sech^2(s)$ type.

In this case, the Helmholtz equation is given by

$$\frac{d^2U}{ds^2} + \left[g + f\,\mathrm{sec\,h}^2(s)\right]U = 0 \tag{F.1}$$

where $g$ is required to be a positive number, i.e. $g = Q^2$, for radiation modes. We assume that the induced waveguide can support only one bound mode, i.e. $f = 2$. In that case this equation takes the following form

$$\frac{d^2U}{ds^2} + \left[Q^2 + 2\,\mathrm{sec\,h}^2(s)\right]U = 0\ . \tag{F.2}$$

To find the odd radiation modes, let us assume that

$$U = U_o = F(s)\cos(Qs) + G(s)\sin(Qs) \tag{F.3}$$

After substituting this solution into Equation F.2 and by selecting the $cos\,(Qs)$ terms we nd

$$\ddot{F} + 2Q\dot{G} + 2\,\mathrm{sec\,h}^2\,(s)\,F = 0 \tag{F.4}$$

whereas by selecting $sin\,(Qs)$ terms we get

$$\ddot{G} - 2Q\dot{F} + 2\,\mathrm{sec\,h}^2\,(s)\,G = 0 \tag{F.5}$$

Let $G = G_0$ is a constant. Therefore Eqs.F.5 and F.4 can be simpli ed to give

$$\ddot{F} + 2\,\mathrm{sec\,h}^2\,(s)\,F = 0 \tag{F.6}$$

$$G_0 = \frac{Q\dot{F}}{\mathrm{sec\,h}^2\,(s)} \tag{F.7}$$

or

$$\mathrm{sec\,h}^2\,(s) = \frac{Q\dot{F}}{G_0} \tag{F.8}$$

Substituting Eq.F.8 into Eq.F.6 results with the following relation

$$\ddot{F} + \frac{2QF}{G_0}\dot{F} = 0 \tag{F.9}$$

Integrating the last equation once yields

$$\dot{F} + \frac{Q}{G_0}F^2 = C \tag{F.10}$$

Moreover, from its asymptotic behavior we know that $F\,(s \to \pm\infty) = \pm 1$ and $\dot{F}\,(s \to \pm\infty) = 0$. The constant $C$ can be found by using these boundary conditions and letting $G_0 = Q$ and it is $C = 1$. Now, Eq.F.10 can be integrated one

more time to nd $F(s)$ which is given by

$$F(s) = \tanh(s) \ . \tag{F.11}$$

Finally, substituting the functional form of $F(s)$ and constant value of $G = Q$ into Eq.F.3 yields

$$U_o = Q\sin(Qs) + \tanh(s)\cos(Qs) \ . \tag{F.12}$$

The even radiation modes can be generated from the odd one by letting $U_e = \nu U_o$ and by using variation of parameters. By doing so, we nd

$$U_e = U_o \int \frac{ds}{U_o^2} \text{ or } \nu = \int \frac{ds}{U_o^2} \tag{F.13}$$

and

$$U_e = [Q\sin(Qs) + \tanh(s)\cos(Qs)] \int \frac{ds}{[Q\sin(Qs) + \tanh(s)\cos(Qs)]^2} \tag{F.14}$$

Therefore the even radiation modes are given by

$$U_e = Q\cos(Qs) - \tanh(s)\sin(Qs) \tag{F.15}$$

Since $U_o\dot{U}_e - \dot{U}_o U_e = -Q^2 - Q \neq 0$ these two degenerate modes are linearly independent. Moreover $U_o^2 + U_e^2 = Q^2 + 1$, i.e. constant, at $s \to \pm\infty$.

# Vita

Tamer Coskun was born in Beysehir, Konya, Turkey on the 27th of October, 1967. He is the oldest son of Hasan and Mumine Coskun. He received his BS and MS degrees from the Department of Electrical Engineering at Dokuz Eylul University, Izmir, Turkey in 1989 and in 1993, respectively. He joined Lehigh University in August 1994 to pursue his Ph.D. degree. He is married to Hacer and has two children, Bukre Cenan and Hasan Bera.

**Publications:**

1. T. H. Coskun, D. N. Christodoulides, Z. Chen, and M. Segev, Dark incoherent soliton splitting and phase-memory effects: Theory and experiment , Physical Review E (May issue, 1999).

2. M. I. Carvalho, T. H. Coskun, D. N. Christodoulides, M. Mitchell, and M. Segev, Coherence properties of multimode incoherent spatial solitons in noninstantaneous Kerr media , Physical Review E, vol. 59, pp. 1193, 1999.

3. Z. Chen, M. Mitchell, M. Segev, T. H. Coskun, and D. N. Christodoulides, Self-trapping of incoherent dark beams , Optics and Photonics News, vol. 9, pp. 48, 1998.

4. D. N. Christodoulides, T. H. Coskun, M. Mitchell, Z. Chen, and M. Segev, Theory of incoherent dark solitons , Physical Review Letters, vol. 80, pp. 5113, 1998.

5. M. Mitchell, Z. Chen, M. Segev, T. H. Coskun, and D. N. Christodoulides, Self-trapping of incoherent bright and dark beams , Asian Journal of Physics, invited paper, October, 1998.

6. Z. Chen, M. Mitchell, M. Segev, T. H. Coskun, and D. N. Christodoulides, Self-trapping of dark incoherent light beams , Science, vol. 280, pp. 889, 1998.

7. T. H. Coskun, D. N. Christodoulides, M. Mitchell, Z. Chen, and M. Segev, Dynamics of incoherent bright and dark self-trapped beams and their coherence properties in photorefractive crystals , Optics Letters, vol. 23, pp. 418, 1998.

8. D. N. Christodoulides, T. H. Coskun, M. Mitchell, and M. Segev, Multimode incoherent spatial solitons in logarithmically saturable nonlinear media , Physical Review Letters, vol. 80, pp. 2310, 1998.

9. Z. Chen, M. Segev, S. R. Singh, T. H. Coskun, and D. N. Christodoulides, Sequential formation of higher-order dark photorefractive spatial solitons: Experiments and theory , Journal of the Optical Society of America B, vol. 14, pp. 1407, 1997.

10. D. N. Christodoulides, T. H. Coskun, M. Mitchell, and M. Segev, Theory of incoherent self-focusing in biased photorefractive media , Physical Review Letters, vol. 78, pp. 646, 1997.

11. D. N. Christodoulides, T. H. Coskun, and R. I. Joseph, Incoherent spatial solitons in saturable nonlinear media , Optics Letters, vol. 22, pp. 1080, 1997.

12. Z. Chen, M. Segev, T. H. Coskun, D. N. Christodoulides, and Y. S. Kivshar, Coupled photorefractive spatial soliton pairs , Journal of the Optical Society of America B, vol. 14, pp. 3066, 1997.

13. M. Mitchell, M. Segev, T. H. Coskun, and D. N. Christodoulides, Theory of self-trapped spatially incoherent light beams , Physical Review Letters, vol. 79, pp. 4990, 1997.

14. D. N. Christodoulides and T. H. Coskun, Self-bouncing optical beams in photorefractive waveguides , Optics Letters, vol. 21, pp. 1220, 1996.

15. Z. Chen, M. Segev, T. H. Coskun, and D. N. Christodoulides, Observation

of incoherently coupled photorefractive spatial soliton pairs , Optics Letters, vol. 21, pp. 1436, 1996.

16. D. N. Christodoulides and T. H. Coskun, Diffraction-free planar beams in unbiased photorefractive media , Optics Letters, vol. 21, pp. 1460, 1996.

17. Z. Chen, M. Segev, T. H. Coskun, D. N. Christodoulides, Y. S. Kivshar, and V. V. Afanasjev, Incoherently coupled dark-bright photorefractive solitons , Optics Letters, vol. 21, pp. 1821, 1996.

18. M. Shih, Z. Chen, M. Segev, T. H. Coskun, and D. N. Christodoulides, Incoherent collisions between one-dimensional steady-state photorefractive screening solitons , Applied Physics Letters, vol. 69, pp. 4151, 1996.

**Conference Presentations:**

1. T. H. Coskun, D. N. Christodoulides, M. Mitchell, Z. Chen, and M. Segev, Incoherent dark quasi-solitons in biased photorefractive media , paper NThC4, Nonlinear Guided Waves and their Applications98, Victoria, Canada, April 1-3, 1998.

2. Z. Chen, M. Mitchell, M. Segev, T. H. Coskun, D. N. Christodoulides, Self-trapping of partially spatially incoherent dark beams , invited paper QMB2, IQEC98, San Francisco, California, May 3-8, 1998.

3. Z. Chen, M. Mitchell, M. Segev, T. H. Coskun, D. N. Christodoulides, Self-trapping of dark incoherent light beams , Nonlinear Guided Waves and their Applications98, paper NThC5, Victoria, Canada, April 1-3, 1998.

4. M. Mitchell, M. Segev, T. H. Coskun, and D. N. Christodoulides, Theory of incoherent solitons: Self-trapped spatially incoherent light beams , paper QME3, IQEC98, San Francisco, California, May 3-8, 1998.

5. T. H. Coskun, D. N. Christodoulides, M. Mitchell, and M. Segev, Theory of incoherent self-focusing in biased photorefractive media , CLEO/QELS, paper QThG50, Baltimore, Maryland, May 18-23, 1997.

6. Z. Chen, M. Segev, T. H. Coskun, D. N. Christodoulides, Y. S. Kivshar, and V. V. Afanasjev, Incoherently coupled photorefractive spatial soliton pairs , CLEO/QELS, invited paper, paper QThF1, Baltimore, Maryland, May 18-23, 1997.

7. M. Mitchell, M. Segev, T. H. Coskun, and D. Christodoulides, Self-trapping of incoherent white light beams , Sixth Topical Meeting on Photorefractive Materials, Effects and Devices (PR 97), paper TB4, Chiba, Japan, June 11-13, 997.

8. Z. Chen, M. Segev, T. H. Coskun, D. Christodoulides, Y. Kivshar, and V. Afanasjev, Incoherently coupled photorefractive spatial soliton pairs , Sixth

Topical Meeting on Photorefractive Materials, Effects, and Devices (PR 97), paper FP07, Chiba, Japan, June 11-13, 1997.

9. Z. Chen, M. Segev, T. H. Coskun, and D. N. Christodoulides, Coupled photorefractive spatial soliton pairs in bulk SBN , OSA Annual Meeting, paper TuDD5, Rochester, New York, October 20-24, 1996.